Mathematisch-Naturwissenschaftliche Fakultät
Wegelerstr. 10
53115 Bonn

Rearranged DNA

in mitochondrial DNA maintenance disorders

Dissertation
zur
Erlangung des Doktorgrades (Dr. rer. nat.)
der
Mathematisch-Naturwissenschaftlichen Fakultät
der
Rheinischen Friedrich-Wilhelms-Universität Bonn

vorgelegt von

Viktoriya Milanova Peeva

aus

Bulgarien

Bonn, 2014

Angefertigt mit Genehmigung der Mathematisch-Naturwissenschaftlichen Fakultät der
Rheinischen Friedrich-Wilhelms-Universität Bonn

1. Gutachter Prof. Dr. Wolfram S. Kunz

2. Gutachter Prof. Dr. Dieter O. Fürst

Tag der Promotion: 25.08.2014

Erscheinungsjahr: 2015

Table of Contents:

Acknowledgements

My graduate education at the University of Bonn has been a wonderful journey, which would not have become true without the help and support of many people, to whom I would like to give my special gratitude.

Foremost, I would like to express my special appreciation and thanks to my advisor Prof. Dr. Wolfram S. Kunz for giving me the great opportunity to work in his lab, with his wonderful team, which became my small family during these almost five years of work together and also for his continuous support during my PhD study and research, for the given security, patience and motivation. Prof. Kunz is an exceptional scientist, excited over so many and different scientific topics, always ready to grasp opportunities with great enthusiasm. His immense knowledge has always astonished me and I could not be prouder of my academic roots and hope that in our future work together I will be able to return the research values and research dreams that he has given to me. Thank you also for giving me the chance to join and participate in the best acknowledged mitochondrial and bioenergetics conferences and meetings, which gave me an opportunity to meet great researchers from all over the world.

A special thank you goes to my direct supervisor, Dr. Gabor Zsurka, together with Prof. Dr. WS Kunz you have been tremendous mentors for me as a junior member of academia and gave me great freedom to pursue independent work and be creative.

Dr. Zsurka is one of the most intelligent and cordial people I have ever known, working with him gave me chance not only to learn a lot, but also provided a stimulating and fun filled work environment. Gabor, thank you for all the patience and detailed explanation of each point of view over the millions of different challenges, which I faced during my PhD research, thank you for being not only a great supervisor, with so many different ideas over my work and thesis, but also a good friend, who always encouraged me and gave me advise necessary for me to proceed and complete my dissertation.

I would also like to extend my gratitude to the rest of my committee members, Prof. Dr. phil. Dieter O. Fürst, Prof. Dr. Walter Witke and Prof. Dr. Wolfgang Voos for their fast response and support and with their presence letting my upcoming defense look as an enjoyable moment filled with great discussions.

I want to thank also to Dr. Cornelia Kornblum, without whom the whole project over the MGME1 patients would not be possible, she is unique physician devoted to her work in all aspects, who always showed great interest to our research findings and supported me kindly all these years, she showed me how research and medicine can benefit from each other in a great way.

The members of Kunz group have contributed immensely to my personal and professional time. I am especially grateful to the technical assistant in our lab Susanne Beyer, for introducing me to the lab work and being always there when I needed help, and making our work so easy and perfectly organized.

Special thanks to Dr. Sandra Knabe, my closest friend and a wonderful colleague, who always believed in me, encouraged me and supported me in all difficult moments.

I want to thank specially to my partner, Artur Motza, who patiently and with great understanding stood next to me until my graduation, who listened each presentation and smiled to each agarose gel picture, at which I was staring with excitement, and inspired me in every step of my studies.

Finally, I would like to extend my sincerest appreciation to my family and friends for their unwavering support. I am eternally grateful to my parents, without their permanent sacrifice, motivation and inspiration I would never have made it till here. Мамо и татко, благодаря ви от цялото си сърце за подкрепата, неуморното въодушевление и вярата в мен, по целият неравен път до тук. Вие сте моята муза и опора от дете и до сега. Благодаря!

Summary

Mitochondrial genetics has been changing its focus during the last decade. Originally limited to describing effects of mutations of the mitochondrial DNA (mtDNA) research at present aims to understand circumstances of mutation generation and propagation in the context of mitochondrial genome maintenance. Key players of the mitochondrial DNA synthesis machinery have been thoroughly investigated by many research groups. However, little is known about the influence of other processes that are crucial for mtDNA maintenance. During my PhD study, I have been working on projects that seek to shed light on specific aspects of disturbances in mtDNA maintenance. (i) Investigating three families with an mtDNA maintenance disorder, we discovered a novel gene MGME1 that can process single stranded DNA molecules and flap structures, shows 5'-exonuclease activity, and probably plays a role in the process of replication and turn-over of replication intermediates, such as 7S DNA.

(ii) Different factors that affect mitochondrial biogenesis in general might also influence mtDNA maintenance. Mitofusin 2 is one of these factors playing a crucial role in fusion of mitochondria, and thus in achieving an appropriate balance of mitochondrial dynamics. Pathogenic mutations in the *MFN*2 gene lead to mitochondrial fragmentation. We were able to show that alteration of mitochondrial dynamic leads to respiratory deficiency through a disturbed mtDNA replication.

(iii) Our group developed techniques to investigate complex mixtures of large mtDNA deletions that are known to be involved in several human diseases, such as Parkinson's and Alzheimer's, as well as, in normal aging. We demonstrate that TLE with AHS, a rather common neurological disorder, is also associated with pathological changes in the mitochondrial genome. Analyzing detailed spectra of deletions we are able to investigate alterations of deletion patterns that might provide hints about different mechanisms leading to deletion generation.

List of Tables:

List of Figures:

List of Abbreviations:

AD	area dentate
ADP	adenosine diphosphate
adPEO	autosomal dominant progressive external ophthalmoplegia
AHS	Ammon's horn sclerosis
ALS	amyotrophic lateral sclerosis
APS	ammonium persulfate
ATP	adenosine-5'-triphosphate
BER	base excision repair
BL	blood
BSA	bovine serum albumin
CA1	cornu Ammonis 1
CA3	cornu Ammonis 3
CCCs	covalently closed circles
CMT1A	Charcot–Marie–Tooth Neuropathy Type 1A
CMT2A	Charcot–Marie–Tooth Neuropathy Type 2A
CoA	coenzyme A
COX	cytochrome *c* oxidase
CPEO	chronic progressive external ophthalmoplegia
CRAC	calsium release activated channel
CSB	conserved sequence blocks
Ct_{mito}	Ct value of mtDNA fragment
Ct_{nuc}	Ct value of reference gene
CYTb	cytochrome b
ddC	2', 3'-dideoxycytidine
ddH_2O	double-distilled water
D-loop	displacement loop
DMEM	Dulbecco's Modified Eagle's Medium
DMSO	dimethyl sulfoxide
DNA2	DNA replication helicase/nuclease 2
dNTP	deoxyribonucleotide triphosphate
DR	direct repeat
dRP	deoxyribose phosphate
DRP1	dynamin related protein 1
DSB	double-strand break
DSBR	double-strand break repair
dsDNA	double-stranded DNA
EDTA	ethylenediaminetetraacetic acid
EM	electron microscopy
ER	endoplasmic reticulum
EtBr	ethidium bromide
F	forward primer
FB	fibroblasts
FBS	fetal bovine serum
FEN1	flap structure specific endonuclease 1
FIS1	fission 1
FRDA	Friedrich's ataxia
FW	forward primer
GTP	guanosine-5'-triphosphate
HEK	human embryonic kidney
HEPES	hydroxyethyl piperazineethanesulfonic acid
HMG-box	high mobility group box

HR2 domain	heptad repeat domain 2
HSP	heavy strand promoter
H-strand	heavy strand
IMM	inner mitochondrial membrane
IMS	inner membrane space
Kir4.1	ATP-sensitive inward rectifier potassium channel 10
KSS	Kearn-Sayre syndrome
LHON	Leber's Hereditary Optic Neuropathy
LIG3	ligase 3
LMP	ligation-mediated PCR primer
LM-PCR	Ligation-Mediated PCR
LR-PCR	Long-range PCR
LP-BER	long patch base excision repair
LSP	light strand promoter
L-strand	light strand
M	muscle
MAP	microtubule associated protein
MB	muscle biopsy
MDS	mtDNA depletion syndromes
MEF	mouse embryonic fibroblasts
MELAS	mitochondrial encephalomyopathy, lactic acidosis and stroke like episodes
MERRF	myoclonic epilepsy and ragged red fibers
MFN1	mitofusin 1
MFN2	mitofusin 2
MGME1	mitochondrial genome maintenance exonuclease 1
MMD	mtDNA maintenance disorders
MMR	mismatch repair
MP	morbus Parkinson
mtDNA	mitochondrial DNA
MTERF1	mitochondrial transcription termination factor 1
mtSSB	mitochondrial single strand DNA binding protein
MuB	Mung Bean nuclease
NADH	nicotinamide adenine nucleotide
NARP	neuropathy, ataxia, and retinitis pigmentosa
ND	nicotinamide adenine nucleotide dehydrogenase
NHEJ	non-homologous end-joining
NTP	nucleotide triphosphate
OD	optical density
O_H	heavy strand origin of replication
O_L	light strand origin of replication
OMM	outer mitochondrial membrane
OPA1	optic atrophy 1
OXPHOS	oxidative phosphorylation system
P	patient
PAGE	polyacrylamide gel electrophoresis
PBS	phosphate buffered saline
PCR	polymerase chain reaction
PEO	progressive external ophthalmoplegia
PH	parahippocampus
POLG	polymerase gamma
POLRMT	mitochondrial RNA polymerase
PS	Pearson syndrome
QBK	quick blunting kit
qPCR	quantitative Real-Time PCR

R	reverse primer
RC	respiratory control
RITOLS	ribonucleotide incorporation throughout the lagging strand
Rnase H1	ribonuclease H1
ROI	region of interest
ROS	reactive oxygen species
RRF	ragged red fibers
RW	reverse primer
SDH	succinate dehydrogenase
smLM-PCR	single-molecule ligation-mediated PCR
smPCR	single-molecule PCR
SN-BER	single nucleotide base excision repair
SPMS	secondary progressive multiple sclerosis
SSB	single strand break
ssDNA	single stranded DNA
STIM1	stromal interaction molecule 1
T4	T4 polymerase
TAS	termination associated sequence
TBE	tris borate EDTA
TCA cycle	tricarboxylic acid cycle
TE	tris EDTA
TEMED	tetramethylethylenediamine
TERM	mitochondrial transcription termination sequence
TFAM	mitochondrial transcription factor A
TK2	thymidine kinase
TLE	temporal lobe epilepsy
TM	TaqMann probe
TPR	tetratrico-peptide repeats
TWINKLE	T7-like mitochondrial DNA helicase
UR	urine sediment
wt	wild-type
y	years old

1. Introduction

1. 1 Brief history of mitochondria

Mitochondria were first described by Richard Altmann in 1890; he called them 'bioblasts' and assumed that they are ubiquitous 'elementary organisms' living inside the cells (Altmann, 1890), having the properties of free-living microbes. The name 'mitochondrion' was given by Benda in 1898, based on their appearance during spermatogenesis, from the Greek 'mitos' (thread) and 'chondros' (granule) (Benda, 1898; Ernster and Schatz, 1981). In 1900, Michaelis has visualized mitochondria actively engaged in cellular respiration, by Janus Green B staining, which was the single method used to stain mitochondria until their first electron micrographs (Palade, 1952) (Figure 1). Fifty years after Michaelis finding, Lazarow and Cooperstein have proven that the Janus Green B staining is possible due to reoxidizing of the dye by mitochondrial cytochrome oxidase (Lazarow and Cooperstein, 1953).

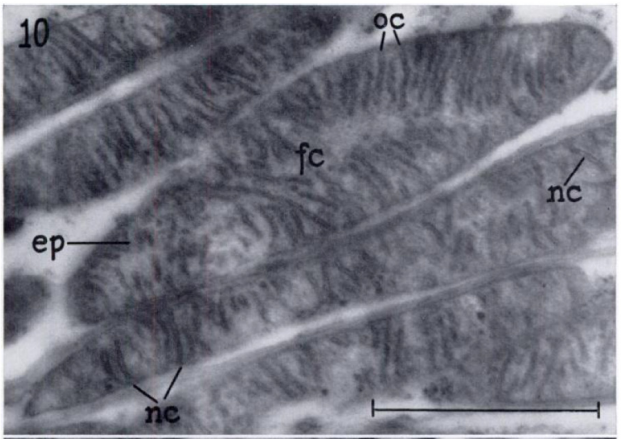

Figure 1 Micrograph image of mitochondria from rat kidney. Made by Palade in 1953 (adapted from Palade, 1953); 'ep', ellipsoidal profile; 'fc', free channel; 'nc' cristae showing three-layered structure; 'oc', christae showing dimmed three-layered structure. The bar indicates 0.1µm.

Since the mitochondria were discovered, there is a vivid dispute over their origin. The researches of the Russian botanist Konstantin Mereschkowsky (1905) and the previous discoveries of Sachs (Sachs, 1882) and Altmann (Altmann, 1890) have given rise to the "serial endosymbiotic theory" of repeated discrete endosymbiotic events which led to the formation of the eukaryotic cells. Its recent active populizer was Lynn Margulis who was strongly criticized by the research community for standing against the basic assumptions about evolution. Together with Dorion Sagan they stated: "Life did not take over the globe by combat, but by networking. Life forms multiplied and complexified by co-opting others, not by killing them" (Margulis and Sagan, 2001). In 1927, Ivan Wallin broadened the serial

endosymbiotic theory to mitochondria. According to it, mitochondria are result of a symbiotic relationship between primitive prokaryotic cell, able to perform oxidative phosphorylation (proteobacteria and for chloroplasts, cyanobacteria) and a proto-eukaryotic cell (Scheffler, 2008). And indeed, phylogenetic analyses have accumulated evidences suggesting that mitochondria share a common ancestor, the α-proteobacterium, with the obligate intracellular parasite Rickettsia prowazekii (Andersson *et al.*, 1998; Andersson *et al.*, 2003; Emelyanov, 2003; Gray, 2001).

Eukaryotes missing mitochondria (from the kingdom of Archezoa) (Cavalier-Smith, 1981), such as trichomonads, cilliates and chytrid fungi (Embley *et al.*, 2003, Broers *et al.* 1993; Fenchel and Finlay 1995; Roger and Silberman 2002) were shown to contain ancestral mitochondria-like organelles such as hydrogenosomes and mitosomes, or remnant mitochondria (Müller, 1993; Williams *et al.*, 2002; Tovar *et al.*, 1999; Zubáčová *et al.*, 2013; Hjort *et al.*, 2010; Shiflett and Johnson, 2010). These organelles are surrounded by a double membrane; in most cases they have lost their DNA and oxidative phosphorylation function, but have kept other biochemical functions of the mitochondria (Honigberg *et al.*, 1984); for example, the hydrogenosomes can perform fermentative metabolism of pyruvate and ATP synthesis through substrate-level phosphorylation, creating molecular hydrogen as a by-product (Lindmark and Müller, 1973; Hjort *et al.*, 2010).

1. 2 Structure and morphology of mitochondria

The structure of mitochondria can be observed in detail by electron microscopy (EM). A traditional view on the inner structure of mitochondria is shown on Figure 2. Each mitochondrion has two separate membranes, the outer membrane, which draws the smooth boundaries of the mitochondrion and the inner membrane, which forms many invaginations and tubes spanning the mitochondrial lumen, called cristae. The inner membrane and the lamellar structures are connected by narrow tube-like connections, called the cristae junctions (Scheffler, 2008). The inner and the outer membrane have completely different protein content and are functionally distinct (Lodish *et al.*, 2012). The most abundant protein of the outer mitochondrial membrane (OMM) is the protein porin. Ions and small molecules can pass easily through the pore of this transmembrane channel protein (Benz, 1985; Benz, 1990). Mitochondrial porins have size of 30 to 35 kDa. The maximal molecular weight of uncharged molecules which can pass through the OMM porins is about 5 kDa (Benz, 1985; Benz, 1990; Shoshan-Barmatz and Mizrachi, 2012). The inner mitochondrial membrane (IMM), which has 76% protein content, more than any other cellular membrane (Gohil and Greenberg, 2009; Lodish *et al.*, 2012), is a tight permeability barrier, with functional consequences.

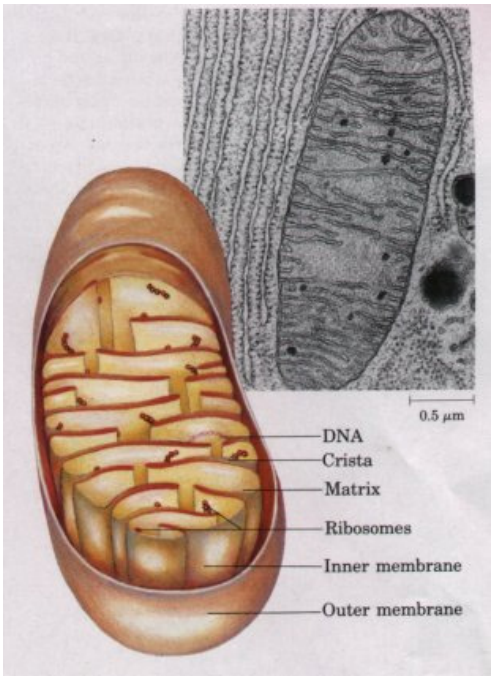

Figure 2 Schematic representation of mitochondrial structure (adapted from Nelson and Cox, Lehninger Principles of Biochemistry, 3rd edition, 2000).

The space closed between the outer and the inner mitochondrial membrane is named intermembrane space and the mitochondrial matrix is the lumen of the mitochondria, surrounded by the inner membrane. Due to its cristae the IMM has much larger surface area in comparison to the outer membrane. The cristae are containing the adenosine-5'-triphosphate (ATP) synthesis complexes, protruding from the inner membrane to the matrix. The cristae number and size varies between the cells, and it is thought to be dependent on the energy demand of the cell. The more surface area is formed by the cristae, the more ATP synthase complexes are present in the mitochondrion. For example, the inner membrane area of a muscle cell contains three times as many cristae as a liver cell, presumably due to the greater energy (ATP) demand of the cell (Lodish *et al.*, 2012).

1. 2. 1 Biochemical reactions in mitochondria

The biochemical reactions taking place in mitochondria are part of many metabolic pathways, that play central role in the cellular function. For example, the fatty acid oxidation (Lehninger, 1945) and the Krebs cycle, also known as the tricarboxylic acid cycle (TCA cycle) (Krebs and Johnson, 1937; Svirbely and Szent-Györgyi, 1933; Scheffler, 2008) are taking place in the mitochondria. The process of aerobic oxidation of glucose and fatty acids starts in the cytosol, where the glucose is being converted to pyruvate and the fatty acids to fatty acyl

coenzyme A (CoA). They then enter the mitochondrial matrix through the porin channels on the OMM and by transporters on the IMM. The pyruvate and the fatty acyl CoA are being converted to acetyl CoA and further oxidized until the release of CO_2. Nine sequential oxidative reactions are turning the acetyl group of acetyl CoA into CO_2, and they form the TCA cycle. The transfer of electrons from the coenzyme electron carriers to and between the complexes of the respiratory chain and the process of oxydative phosphorylation (OXPHOS) ends with reduction of O_2 and release of water. The functional enzyme complexes of the OXPHOS system are NADH: ubiquinone oxidoreductase (Complex I), succinate: ubiquinone oxidoreductase (Complex II, succinate dehydrogenase, SDH), ubiquinol: cytochrome *c* oxidoreductase (Complex III, cytochrome bc_1 complex), ferricytochrome *c*: oxygen oxidoreductase (Complex IV, COX) and the F_1F_0-ATPase (Complex V) (Chinnery and Schon, 2003; Hatefi, 1985; Saraste, 1999). The transport of electrons through the electron transport chain is used to pump protons into the innermembrane space and out of the matrix, which consequently creates an electrochemical gradient or protonmotive force (Jastroch *et al.*, 2010) used from the F_0F_1 complex, called ATP synthase to produce ATP from ADP and inorganic phosphate (P_i). This theory of ATP synthesis was proposed by Peter Mitchell in 1961 and is called the chemiosmotic theory (Mitchell P, 1961).

Mitochondria are involved also in other major pathways such as the urea cycle in which ammonia (NH_3) is converted to urea ($(NH_2)_2CO$) (Krebs and Henseleit, 1932 a, b, c); heme biosynthesis; partially, they participate in steroid, dolichol and ubiquitine biosynthesis, and in the synthesis of cardiolipin. Mitochondria are as well the origin of iron-sulphur (Fe-S) centers (Scheffler, 2008). They play a crucial role in maintenance of calcium homeostasis and programmed cellular death (Lee and Peng, 2008).

1. 3 Distribution, motility and dynamics of mitochondria

1. 3. 1 Mitochondrial distribution

In the cellular cytosol mitochondria are forming networks, which depending on the mitochondrial number, size and position differ in the different cell lines and tissues. Generally, the mitochondria network is most dense around the nucleus and scatters to the periphery of the cell (Frazier *et al.*, 2006). The cells can answer to their energy demands by inducing changes in mitochondria distribution. For example, mitochondria cluster in the presynaptic nerve terminal as result of local synaptogenic signals and play important role for the synapse formation by providing ATP needed for the actin cytoskeleton assembly of the presynapse (Lee and Peng, 2008; Peters *et al.*, 1991). The correct positioning of the mitochondria is involved as well in the mobilization of the synaptic vesicles (Verstreken *et al.*,

2005). Mitochondria were reported to be involved in the dendritic spine formation as well as in immunological response functions, such as podosome activations of the lymphocytes, and synapse formation in activated T-cells (Li *et al.*, 2004; Sung *et al.*, 2008; Campello *et al.*, 2006; Quintana *et al.*, 2007). The local calcium concentration may depend on calcium uptake from the mitochondria; thereafter, mitochondria are distributed not only in subcellular regions with high metabolic requirements, but also at such with Ca^{2+} accumulation (Werth and Thayer, 1994; Zucker, 1999).

1. 3. 2 Mitochondrial motility

Organelles are often transported far away from the place of their biosynthesis in the cytoplasm reaching a goal location, for example, the nerve cell axons may be more then a meter in length. The well defined tracks on which the organelles slide to these locations are formed by microtubules, which can load different types of 'cargo'. The microtubules are built up from αβ-tubulin dimers and are stabilized and aligned by different classes of microtubule associated proteins (MAPs). Such proteins characteristic for the neuronal cells are the tau protein and the MAP2 protein (Lodish *et al.*, 2012). The transportation of different loads takes different time, from very slow as fraction of mm a day (microfilaments, metabolic enzymes, clathrin complex – 2 to 8 mm a day; neurofilaments and microtubules – 0.2 to 1 mm a day), to very fast as 200 to 400 mm a day (small vesiculotubular structures, neurotransmitters, membrane proteins and lipids). The mitochondria are trafficked at medium speed down the axons to the synapses with 50 to 100 mm a day (Morfini *et al.*, 2012).

There are two main motor protein families responsible for the transportation of the different 'cargoes' along the microtubules, the kinesins and dyneins. The transport proceeding from the cellular body to the axons and the synapses is named anterograde axonal transport (Lodish *et al.*, 2012) and in the opposite direction, retrograde axonal transport (Figure 3). Along the microtubule network mitochondria are trafficked anterogradely by kinesin-1 (KIF5) or kinesin-3 (KIF1) (Nangaku *et al.*, 1994; Tanaka *et al.*, 1998) and retrogradely by cytoplasmic dynein, whose motor coordination is being supported by the binding of kinesin (Salinas *et al.*, 2008) and microtubule associated protein 1B (MAP1B).

Milton, Miro, syntabulin and a mitochondria specific isoforms of kinectin are protein adaptors serving as connection between mitochondria and kinesins (Salinas *et al.*, 2008). The microtubule based transport is used for long-range movements and actin-based transport for short-range movements (Morris and Hollenbeck *et al.*, 1995). Actin-based transport of mitochondria was suggested to participate in the docking of mitochondria (Sheng and Cai, 2012; Salinas *et al.*, 2008).

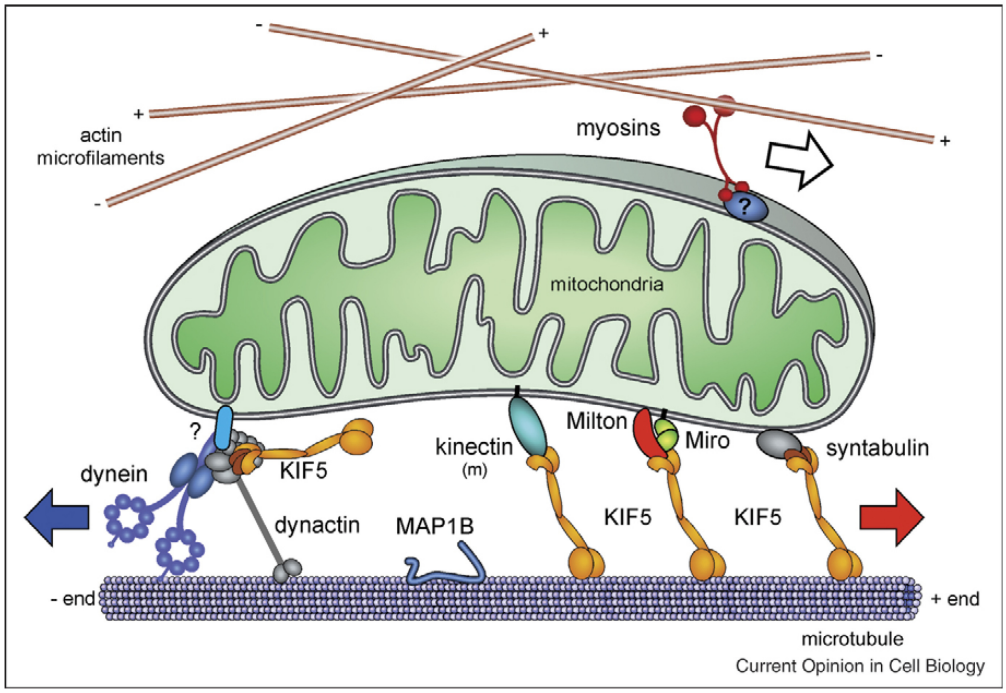

Figure 3 Anterograde and retrograde transport of mitochondria (adapted from Salinas *et al.*, 2008).

The Miro protein family includes mitochondrial Rho GTPases participating in mitochondrial transport. In mammals there are two known proteins belonging to it, Miro-1 and Miro-2 (Liu and Hajnóczky, 2009). Cells lacking active Miro are having disrupted mitochondrial motility and networking, and higher apoptosis rates (Liu and Hajnóczky, 2009; Fransson *et al.*, 2003).

Milton 1 and 2 are proteins associated with mitochondrial motility in *Drosophila melanogaster* (Stowers *et al.*, 2002). Their mammalian homologues are TRAK 1 and TRAK 2 (Brickley and Stephenson, 2011). Miro interacts with Milton protein, which simultaneously binds to kinesin-1 and in this way this Miro-Milton interaction can affect the recruitment of Milton to mitochondria (Glater *et al.*, 2006).

The mitofusins MFN1 and MFN2, involved in mitochondrial fusion and fission, also were proven to interact with the Miro-Milton complex. Dysfunction of MFN2 leads to slower mitochondrial transport in both retrograde and anterograde directions, but does not affect the transport of other organelles. A dysfunction of the OPA1, protein also involved in the fusion of the IMM does not affect the motility of mitochondria, which points to MFN2 as specific part of the mitochondrial transport machinery (Misko *et al.*, 2010).

1. 3. 3 Mitochondrial dynamics

Beside their constant movement mitochondria are undergoing process of active fusion and fission (Figure 4) (Chan, 2006). Mitochondrial fusion is controlled by the mitofusins: mitofusin 1 and mitofusin 2 (MFN1 and MFN2) for the OMM and by optic atrophy 1 protein (OPA1) involved in the IMM fusion (Hales and Fuller, 1997; Rojo *et al.*, 2002). The mitofusins belong to the GTPase protein family (Hales and Fuller, 1997). MFN1 and MFN2 differ in their functions, for example, in their interactions with other proteins such as OPA1 (Cipolat *et al.*, 2004). In the absence of MFN2, MFN1 together with OPA1 are enough to mediate efficient fusion (Cipolat *et al.*, 2004; Ishihara *et al.*, 2004).

Close to their N-terminal, the mitofusins have a GTPase domain and on their C-terminal a coiled-coil domain facing the cytosol and followed by two transmembrane spans and another coiled-coil domain (Figure 4). During the process of fusion, two mitochondria dock through the mitofusins anchored into their OMM. The mitofusins bind to other mitofusin molecules in like-attract-like fashion on closely placed mitochondria and tether them. Once the mitofusins are bound to each other a GTP hydrolysis takes place. It is still unclear how this process changes the shape of membranes and provides their merging (Chen *et al.*, 2003; Hales and Fuller, 1997; Hermann *et al.*, 1998) (Figure 4). MFN1 tethers more efficiently the mitochondrial membranes in comparison to MFN2 (Ishihara *et al.*, 2004) and recently, it was suggested that only MFN2 is involved in endoplasmic reticulum (ER) tethering, but not MFN1 (de Brito and Scorrano, 2008).

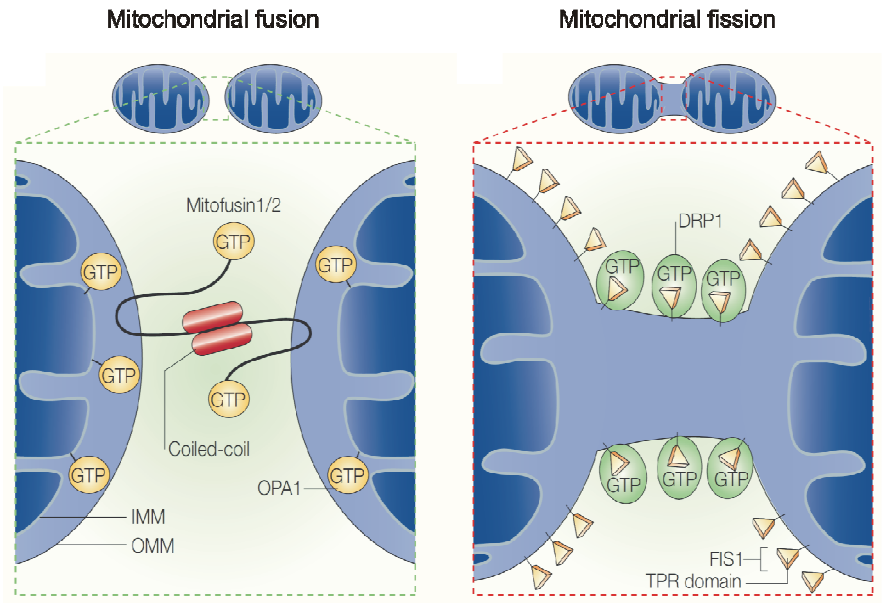

Figure 4 Mitochondrial fusion and fission (adapted from Youle and Karbowski, 2005).

The process of mitochondrial fission (Figure 4) is mediated by membrane-associated adaptor proteins fission 1 (FIS1), which recruits the large GTPase and dynamin homologue dynamin related protein 1 (DRP1) from the cytoplasm by using its tetratrico-peptide repeats (TPR). DRP1 participates at the final step of mitochondrial fission by forming spirals around constricted sites on mitochondria and pinching off the membrane stalk at the scission sites, between the two newly formed mitochondria (Youle and Karbowski, 2005; Koirala *et al.*, 2013). The mitochondria fission sites depend on the early interaction of mitochondria with the ER prior to DRP1 binding (Friedman *et al.*, 2011).

1. 4 Mitochondrial DNA

1. 4. 1 Structure

In 1963 Margit and Sylvan Nass have described for the first time the mitochondrial DNA (mtDNA) (Nass and Nass, 1963) and its circularity was discovered by electron microscope imaging by Nass, (1966). In mammals, mtDNA is a double-stranded circular molecule with size of approximately 16 kb (Figure 5), in human 16,569 base pairs (bp) (Anderson, 1981). On Figure 6 is shown the structure of the mtDNA. It has nucleotide composition with 44% (G+C) content. The mitochondrial strand with greater intrinsic buoyant density in alkaline cesium chloride gradients and respectively high content of guanine bases is called the heavy (H) strand (Figure 6, H-strand depicted in black) and its complementary strand, rich in cytosine is called the light (L) strand (Figure 6, L-strand depicted in gray) (Clayton, 1996).

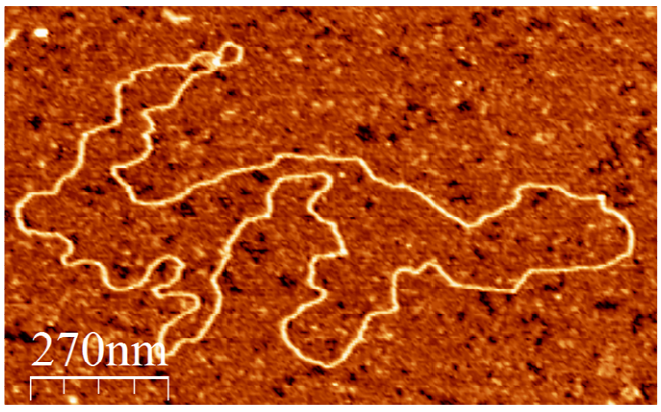

Figure 5 Circular mitochondrial DNA molecules by atomic force microscopy (provided from collaborative study with Prof. Kotlyar, George S Wise Faculty of Life Sciences, Tel Aviv, Ramat Aviv, Israel).

Animal mtDNA is intronless and most of the genes are located on the heavy strand. Altogether, it is encoding 37 genes, from which 13 are protein coding for respiratory chain

and ATPase subunits (Figure 6, in green), 22 transfer RNAs (tRNAs) (Figure 6, in blue, the letters stand for the corresponding amino acids) and two ribosomal RNAs (rRNAs) (Figure 6, in purple), all crucial for the process of oxidative phosphorylation (Shadel and Clayton, 1997). The two rRNAs, 12 mRNAs, and 14 tRNAs are encoded from the H-strand, whereas the L-strand encodes one mRNA and eight tRNAs (Figure 6). The genetic code of the mtDNA is different to the one in the nuclear DNA and it also varies between species (Lodish *et al.*, 2012). The process of replication and transcription of mtDNA is regulated by nuclearly encoded factors. Polymerase gamma (POLG), the only known polymerase located in mitochondria (Graziewicz *et al.*, 2004), is also encoded in the nucleus.

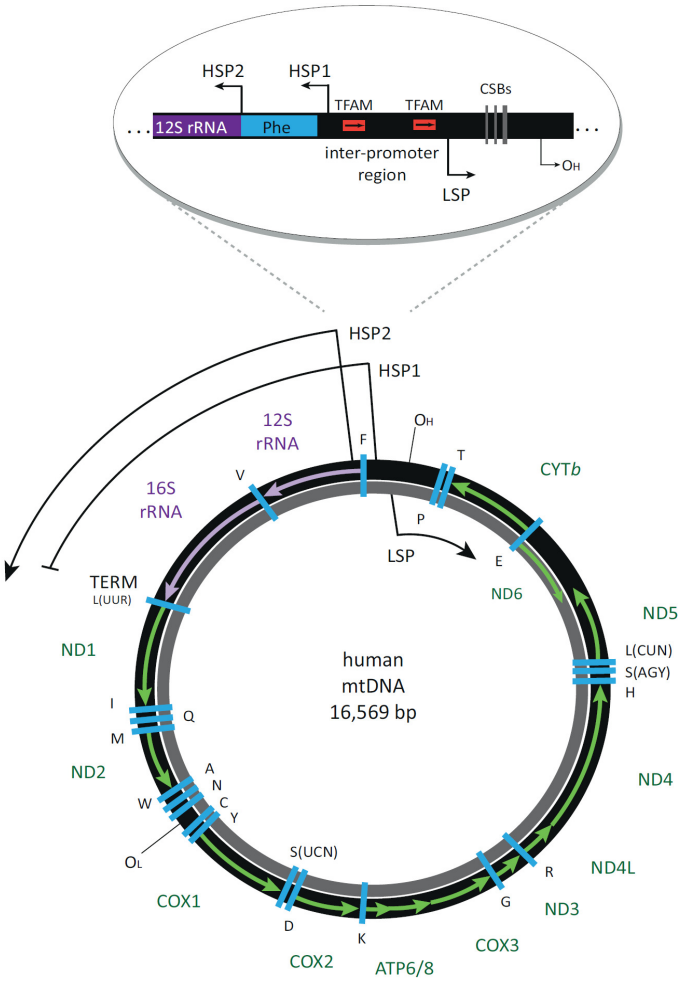

Figure 6 Scheme of the human mitochondrial genome (adapted from Bestwick and Shadel, 2013). The heavy H-strand in black and the light L-strand in gray encode for rRNAs (purple), mRNAs (green), and tRNAs (blue, letters mark allied amino acids). The H-strand genes are indicated outside and the L-strand genes inside the circle. ND, NADH dehydrogenase; COX, cytochrome c oxidase; ATP, ATP-synthase; CYTb, cytochrome b.

Since only 13 of the estimated proteins are encoded by the mtDNA, mitochondria are relying on the permanent interplay between the mtDNA and the nuclear DNA (Thorsness and

Weber, 1996). All but one protein complexes for the respiratory chain are encoded by both nuclear and mtDNA. The only enzyme complex exclusively encoded by nuclear DNA is the Complex II (Smeitink *et al.*, 2001). The mtDNA contains a D-loop region, which is non-coding and contains essential sites for replication and transcription initiation (Taylor and Turnbull, 2005) (shown expanded on Figure 6). It is called a displacement loop (D-loop) as the two strands are separated from each other, in a small stretch, by a third strand complementary to the light strand, called the 7S DNA (Doda *et al.*, 1981). The replication origins of both mtDNA strands are O_H and O_L, respectively for the heavy and the light strand (Figure 6).

The H-strand transcription initiates from H-strand promoter 1 (HSP1) and 2 (HSP2), with HSP1 transcripts terminating at a termination sequence (TERM), within the tRNA-Leu (UUR) gene, to which a mitochondrial termination factor (MTERF)1 binds. The TERM region is strongly protected from methylations assuring the frequent and highly specific binding of the MTERF1 (Rebelo *et al.*, 2009). The HSP2 transcripts are almost full length polycistronic transcripts. The L-strand transcription starts from an L-strand promoter site (LSP) that also generates near full-length polycistronic transcripts. Both transcripts from the H and the L-strand, and the tRNA are later on processed into mRNA (Bestwick and Shadel, 2013). Transcription initiated at the light strand promoter (LSP) is suggested to be responsible for the formation of the RNA primer needed for the heavy strand replication. One hypothesis is that the primers are formed by the action of RNA endonuclease, which is cleaving primary transcript starting from LSP (Lee and Clayton, 1997; 1998; Wanrooij *et al.*, 2010). Both LSP and HSP sites are protected as well from methylation (Rebelo *et al.*, 2009). Downstream of the LSP are located three conserved sequence blocks (CSB), that show low variability in mammals (CSB I, II, III), CSB II is considered to support the formation of RNA-DNA hybrids transition (Pham *et al.*, 2006).

The mtDNA is organized into protein-DNA complexes called nucleoids (the name is derived from the bacterial nucleoids, comprising their chromosomes) (Kukat and Larsson, 2013). The nucleoids have uniform mean size of approximately 100 nm in mammals. They are histone-free formations, containing prevalently single copies mtDNA (average of 1.4 mtDNA molecules per nucleoid). The nucleoids contain as well proteins of mtDNA replication and gene expression machinery, and the process of fission and new mitochondrial tubule formation occurs adjacent to the nucleoids (Figure 4) (Tauber *et al.*, 2013; Bogenhagen, 2012). It was suggested that the fission process helps to prevent the nucleoid clustering (Ban-Ishihara *et al*., 2013).

The nucleoids are packed by the mitochondrial transcription factor A (TFAM), belonging to the family of architectural high mobility group (HMG)-box proteins, binding to DNA. TFAM can bind, wrap and bend DNA without DNA sequence-specificity (Fisher *et al.*, 1992) and is fully coating the mtDNA in human (Alam *et al.*, 2003). Therefore, TFAM plays

important role in the nucleoid formation and mtDNA maintenance (Kukat *et al.*, 2011; Ngo *et al.*, 2011). *In vivo*, it is providing bending and looping of the mtDNA, which is shaping the nucleoids in spherical structures (Kaufman *et al.*, 2007). Crystallographic experiments suggest that TFAM induces a 180° U-turn of the mtDNA when bound to it (Ngo *et al.*, 2011). Knockout of TFAM in mice causes severe mtDNA depletion and is lethal to the fetus (Larsson *et al.*, 1998; Mao and Holt, 2009).

The mtDNA is a multicopy genome and its number varies between cells and tissues, and is dependent on the energy demands of the cells (Moraes, 2001). Usually, there are 10^2–10^4 copies of mtDNA per cell (Ruhanen *et al.*, 2011). Due to its polyploid nature, the mitochondrial genome can be homoplasmic, when all mtDNA copies are identical and heteroplasmic when two or more variants of the mtDNA exist together. A single mutation which affects all mtDNA copies is a homoplasmic mutation, and when it affects some mtDNA molecules it is a heteroplasmic mutation (Taylor and Turnbull, 2005). In difference to the homoplasmic mutations, which are transferred to all maternal offspring the transmission of a heteroplasmic mutations is much more complicated and depends on the mutation type and its segregation within the maternal tissues (Taylor and Turnbull, 2005).

All mtDNA encoded proteins are synthesized on ribosomes unique for the mitochondria, mitoribosomes, which are located in the mitochondrial matrix (Taanman, 1999). In rat hepatocytes there are less then 100 mitoribosomes per mitochondrion (Cantatore *et al.*, 1987). The mitoribosomes differ from the cytosolic ones; they have lower sedimentation coefficient and have lower RNA content. Their 12S and 16S rRNAs are encoded as well from the mtDNA (Attardi and Ojala, 1971). The process of translation is supported by 22 tRNAs that are also mitochondria specific, different from the cytosolic ones and encoded by the mtDNA. The genes encoding the mito tRNAs are highly prone to mutations and often are reason for different diseases and mitochondrial dysfunction (Suzuki *et al.*, 2011). The heavy strand tRNA loops share high sequence homology with the O_L loop. There is a suggestion that tRNA loops may serve as alternative origins of replication over the mtDNA (Seligmann, 2009).

1. 5 mtDNA replication

In 1968 Kirschner *et al.*, have proven for the first time that the mtDNA is self-replicating in the mitochondrion. The replication of mtDNA takes about one to two hours (Berk and Clayton, 1974; Clayton, 1982), it is independent from the cell cycle phase (Clayton, 1996) and happens at lower level in postmitotic cells (Magnusson *et al.*, 2003).

1. 5. 1 Strand displacement model of replication

The classical mtDNA replication model described in the literature is the strand displacement model, or the asynchronous replication model (Robberson *et al.*, 1972), (Figure 7). The model is called asynchronous as there is spatial and time asymmetric way of replication of both strands – the leading (H-strand) and lagging (L-strand) strand of replication (Brown and Clayton, 2006).

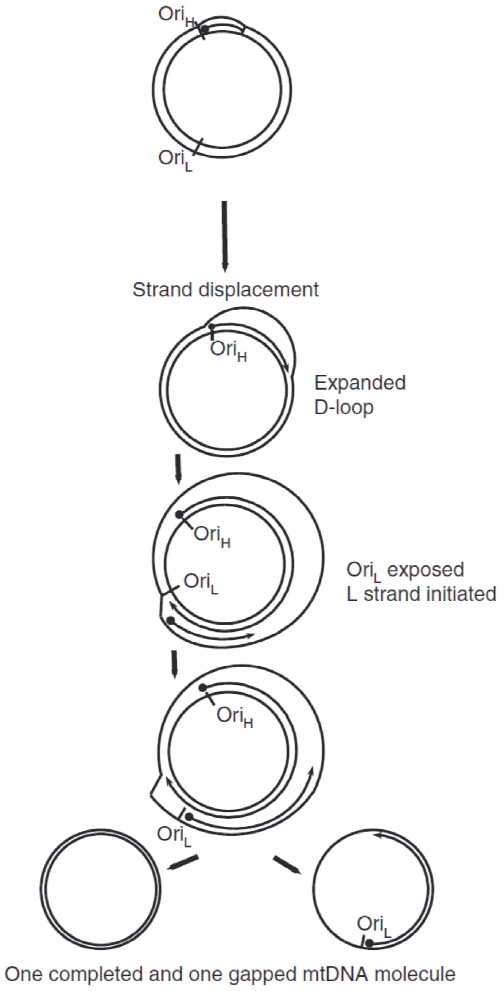

Figure 7 Asynchronous model of mtDNA replication (modified from Kasiviswanathan *et al.*, 2012).

According to Clayton (1996, 1982) in this model the replication begins at the H-strand origin of replication (O_H) and continues for about 450±80 nucleotides and stops (Kasamatsu *et al.*, 1971). The formed nascent H-strand fragment remains single stranded, bound to the light strand and displaces the parental H-strand, forming the D-loop. This fragment has a sedimentation coefficient of 7S and thereafter is called the 7S DNA. In this model, when the replication is to continue, the single stranded daughter H-strand is being synthesized and it displaces the parental H-strand unidirectionally (Berk and Clayton, 1974; Robberson and

Clayton, 1972). The formation of the 7S DNA fragment is a matter of dispute, it was suggested as well that it is formed as an end-step of the H-strand replication by the termination of the replication at the termination associated sequence (TAS) region (Chang and Clayton, 1985; Doda *et al*., 1981; Berk and Clayton, 1974).

The replication of the mtDNA is coupled with the process of transcription, which is initiated from a single promoter on the light strand – LSP (Figure 6). The synthesized transcript forms RNA-DNA hybrid. RNaseMRP is an enzyme which processes the hybrid, by cutting the RNA into pieces that afterwards are being used as replication primers at the O_H, by POLG (Brown and Clayton, 2002; Shadel and Clayton, 1997).

After the H-strand replication has proceeded to two thirds of its total length, the L-origin of replication (O_L) becomes exposed and the replication of the L-strand begins from it (Wanrooij and Falkenberg, 2010; Wong and Clayton, 1985). O_L is approximately 30 nucleotides in size, it is highly conserved in vertebrates (Wanrooij *et al.*, 2012), it is flanked by tRNA genes and has the potential of forming a stable stem-loop structure when being single stranded (Fusté *et al*., 2010; Clayton, 1996). The O_L is being exposed to the action of a mitochondrial RNA polymerase called POLRMT, able to recognize it and initiate priming from a poly-dT stretch in the single-stranded loop region and to begin DNA synthesis (Clayton, 1996; Fusté *et al*., 2010). The primer for L-strand replication is an RNA sequence complementary to the T-rich loop structure of the O_L and the switch from RNA to DNA synthesis is happening after about 25 nt near the base of the stem (Fusté *et al*., 2010; Wong and Clayton, 1985).

The asynchronous replication of the two mitochondrial strands leads to the synthesis of two daughter molecules (Berk and Clayton, 1974). The newly synthesized mtDNA daughter molecules are having relaxed shape for about an hour and afterwards they pass into a super-coiled state with approximately 100 negative super turns (Bogenhagen and Clayton, 1977). The synthesis of new D-loop completes the replication cycle (Clayton, 1996). It has been suggested that the 7S DNA serves to relax the super helical turns of the super coiled mtDNA and might have role in the exposure of the parental H-strand (Clayton, 2003; Tapper and Clayton, 1981; Kang *et al*., 1997; Kasamatsu *et al.*, 1971). The turnover of the 7S DNA is rapid, but the mechanism of its degradation is not known and its full function remains unclear (Clayton, 2003; Bogenhagen and Clayton, 1977). There is no confirmation if the existing 7S DNA fragments are being used for initiation (as primers) of the H-strand replication, and are being elongated, or a novel process of replication initiation occurs (Clayton, 2003; Clayton, 1996). However, as the nascent H-strands and the 7S DNA fragments are having the same 5' end it seems that each newly synthesized strand becomes either 7S DNA strand or a nascent strand. Doda *et al.*, in 1981, has proposed that the premature termination process of the nascent strand is a template-sequence-directed event,

at TAS. TAS is 15 bp long conserved sequence, which is a potential *cis*-acting sequence and is present in multiple copies, upstream from the termination site (Doda *et al.*, 1981). Kai *et al.*, in 1999, have used Ligation-Mediated PCR (LM-PCR) (Kang *et al.*, 1997) and site-specific primers, to distinguish the nascent H-strands leading to 7S DNA formation from the total nascent H-strands. They claim that the premature termination has regulatory role in mtDNA replication and some of the 7S DNA molecules are temporarily terminated and re-elongated for successful replication. In an experiment with proliferation stimulated cells, the termination of the nascent strands simply decreases and in this way the replication gets up-regulated (Kai *et al.*, 1999). In depletion experiments, directly after applying ddC, the nascent strand termination gets down-regulated, and this effect is strongest after ddC removal; these experiments suggest that the release of the elongation and the control of termination at the D-loop, are crucial for mtDNA copy number maintenance and recovery of depleted mtDNA (Brown and Clayton, 2002). It has been estimated that around 95% from the leading strands get terminated prematurely and the cells are capable of much greater replication capacity then demanded under normal circumstances (Bogenhagen and Clayton, 1978; Brown and Clayton, 2002).

1. 5. 2 Bidirectional replication model

After electron microscopy of mtDNA from rat hepatocytes and HeLa cells, which revealed mtDNA duplex replication intermediates (Koike and Wolstenholme, 1974; Crews *et al.*, 1979), a hypothesis raised for coupled leading and lagging strand replication, in opposition to the asynchronous model (Figure 8) (Holt *et al.*, 2000). In this mechanism the replication is symmetrical, with leading and lagging strand synthesis progressing from multiple bidirectional replication forks. The initiation zone (ori-Z) was proposed to be a broad zone covering several kilobases in solid tissues (Bowmaker *et al.*, 2003) with multiple origins of replication, and smaller zone in the non-coding region in cultured cells (Yasukawa *et al.*, 2005).

The later investigation proposed a bidirectional origin of replication close to the 5’ end of the non-coding region, a replication starting from that point would be terminated at the TAS region and would be effectively unidirectional for the most part (Yasukawa *et al.*, 2005). In this model the lagging strand is being the result of maturation of Okazaki fragments, that are joined to create the novel nascent strand. Ruhanen *et al.*, (2011) have suggested that Ribonuclease H1 (RNase H1) is responsible for the removal of RNA primers from the lagging strand and DNA ligase III is responsible for the ligation of the newly synthesized Okazaki fragments.

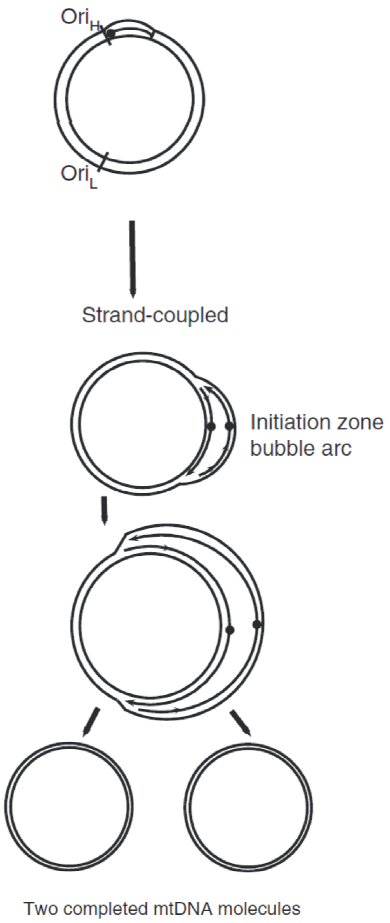

Figure 8 Bidirectional model of mtDNA replication (modified from Kasiviswanathan *et al.*, 2012).

In 2002, Yang *et al.* claimed that the strand-coupled mechanism is exclusively the replication mechanism existing in the mitochondria, and that the single stranded replication intermediates observed previously from Holt *et al.*, 2000, are an artifact of DNA extraction, as the strand-coupled mechanism includes mostly double-stranded replication intermediates but contains widespread regions of RNA-DNA hybrids which are formed by incorporation of ribonucleotides on the light strand, that afterwards are converted to DNA; exactly these ribonucleotide-rich regions can be easily degraded during mtDNA extraction and can result in single stranded replication intermediates. In the experiments performed by Yang *et al.*, (2002) by the usage of an RNase H they could show the formation of single stranded replication intermediates (Yang *et al.*, 2002). Brown *et al.*, (2005) have performed atomic force microscopy, and their findings pointed towards the orthodox strand-displacement model of replication, but interestingly, it showed the existence of alternative lagging strand replication origins, which is in consistance with the earlier investigations of Robberson *et al.*, (1972); Koike and Wolstenholme, (1974); and Pikó *et al.*, (1984). As the observed replication intermediates included also single stranded ones, which can only be products from

asymmetric replication, Holt *et al.*, (2000) suggested that both models of replication exist simultaneously in the cell and the switch between the mechanisms depends on the needs of the cell.

1. 5. 3 RITOLS

In 2006, Yasukawa *et al.* described a novel model of replication, the ribonucleotide incorporation throughout the lagging strand (RITOLS) model. In that model newly synthesized RNA can cover the parental H-strand prior to lagging L-strand synthesis. The RNA may build up the whole lagging strand before it is converted to DNA. The synthesis of the RNA was suggested to be a result of the activity of a primase or alternatively, it is laid by pre-existing processed transcripts (Figure 9, panel 1), in that way the RNA fragments are being hybridized to the parental strand with the advancing of the replication fork (‘bootlace' mechanism, Reyes *et al.*, 2013).

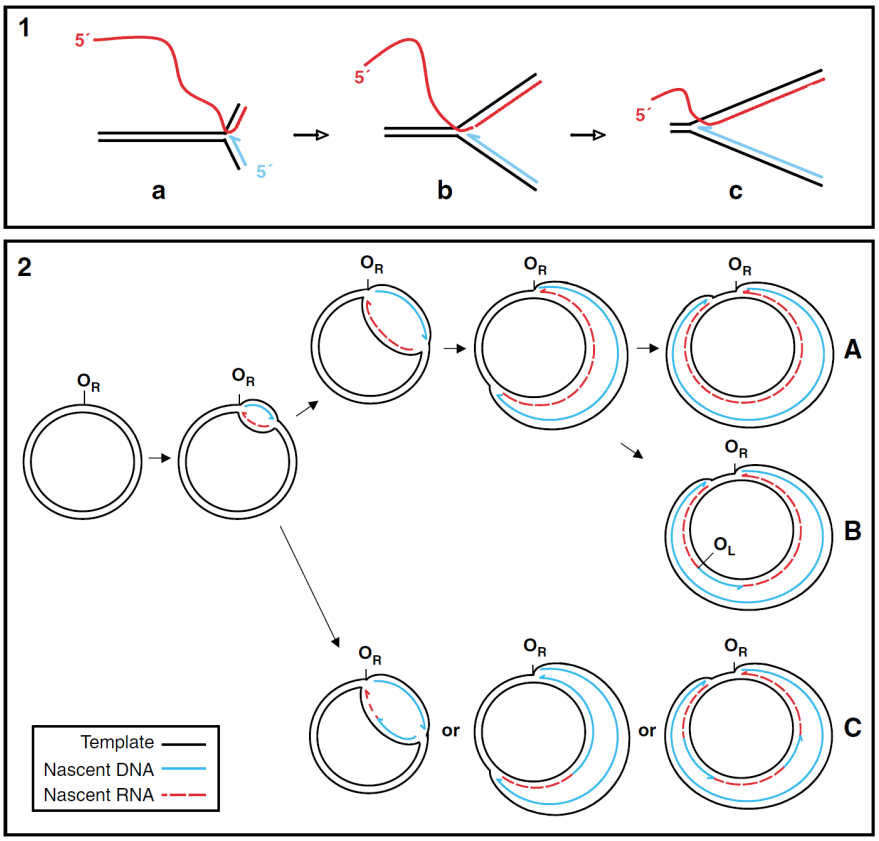

Figure 9 RITOLS model of mtDNA replication. Red line, RNA primers; blue line, newly synthesized mtDNA strand (adapted from Yasukawa *et al.*, 2006).

In 2008, Wanrooij *et al.* described the POLRMT that can act as a lagging strand primase. The enzyme was shown to be able to synthesize RNA primers with length from 25 to 75 nucleotides on a single strand template *in vitro.* These primers can be then used by POLG to initiate the lagging strand synthesis (Wanrooij *et al.*, 2008). The degradation of the RNA and its substitution with DNA happens in the maturation phase, where a putative RNase fragments it. They suggested that this function might be performed by RNase H1 mitochondrial isoforms. The slow degradation of RNA into fragments may release exactly the needed RNA primers for the lagging strand synthesis (Yasukawa *et al.*, 2006).

In the RITOLS model, replication is initiated in a unidirectional manner at the replication origin O_R. O_R is located either at O_H or at an alternative site present in the non-coding region, several hundred nucleotides away from O_H, around nucleotide position 16,197, close to the TAS region (Yasukawa *et al.*, 2006; Yasukawa *et al.*, 2005). In some molecules, as mentioned above, the RNA is laid all over the parental strand prior to its converting into DNA (Figure 9, panel 2A), in other molecules the maturation starts already when the incorporation of RNA has proceeded until the O_L (Figure 9, panel 2B) or at dispersed sites (Figure 9, panel 2C). Such a model can generate all replication intermediates described till now (Yasukawa *et al.*, 2006).

2D agarose gel electrophoresis (2D-IMAGE) of intact mitochondrial DNA, performed by Kolesar *et al.*, (2013), revealed broad range of double-stranded forms of the mtDNA, such as super coiled molecules (covalently closed circles, CCCs), nicked circles and multiple catenated species, as well as single-stranded DNA structures, which they suggest to be replication intermediates (Kolesar *et al.*, 2013). By ethidium bromide (EtBr) depletion the same group has observed accumulation of high molecular weight mtDNA (under strong depletion conditions), and after the release of the replication arrest, firstly covalently closed circles and head-to-tail circular dimer formations were detectable, and their intensity was diminishing after 6 hours of released replication, therefore, it is possible that different mtDNA templates are being used in different conditions, speaking of multiple mechanisms of replication dependent on the cell conditions (Kolesar *et al.*, 2013), which was also proposed by Holt *et al.*, in 2000.

1. 5. 4 Main participants in the mtDNA replication

All proteins involved in the mtDNA replication are nuclear encoded. The *POLG* gene encodes the catalytic subunit of the mitochondrial DNA polymerase gamma (POLG). For its function, POLG requires the full activity of its subunits – POLG A and POLG B (Ropp and Copeland, 1996). POLG A is the catalytic unit of the polymerase and POLG B is its processivity unit (Gray and Wong, 1992). For the successful replication of the mtDNA, POLG

needs a mitochondrial replicative DNA helicase called TWINKLE (Spelbrink *et al.*, 2001), the mitochondrial single-stranded DNA-binding protein (mtSSB) (Tiranti *et al.*, 1993), and the mitochondrial RNA polymerase (POLRMT) (Tiranti *et al.*, 1997) (Figure 10), that constitute the minimal replication machinery *in vitro*, defined by Korhonen *et al*., 2004.

The POLG holoenzyme contains single A and two B subunits and it is an asymmetric 245 KDa heterotrimer (Yakubovskaya *et al.*, 2006). POLG has 5'→3' polymerase activity and 3'→5' exonuclease proofreading activity. Both functions are fulfilled by subunit A. Subunit B has accelerating function for the processivity of the holoenzyme and increases the affinity of the A subunit for the mtDNA (Wanrooij and Falkenberg, 2010). POLG has as well 5' deoxyribose phosphate (dRP) lyase activity, which is important for its participation in the repair of oxidative base lesions (Graziewicz *et al.*, 2006). The POLG holoenzyme functions cooperatively with the mitochondrial helicase TWINKLE and the mitochondrial single strand binding proteins.

TWINKLE (T7 gp4-like protein with intramitochondrial nucleoid localization) was discovered in 2001 by Spelbrink *et al.* and it is the replicative helicase in mitochondria. It has double-strand DNA affinity (Farge *et al.*, 2008) and it unwinds it in a nucleotide triphosphate (NTP) dependent manner; it functions in 5'→3' direction. It has been speculated that TWINKLE participates in recombination; moreover, its helicase domain contains the same conserved organization as RecA involved in homologous recombination in bacteria (Wanrooij and Falkenberg, 2010).

The mtSSB has protective role over the single stranded mtDNA by stopping it from refolding and being degenerated by nucleases. The human mtSSB is similar to the one existing in *Escherichia coli* (Tiranti *et al.*, 1993). The single stranded mtDNA is wrapping around the mtSSB in electropositive channels (Yang *et al.*, 1997). It was proposed that TFAM and mtSSB can influence the D-loop turnover and that they play crucial role for the stabilization of the D-loop and the mitochondrial DNA overall (Takamatsu *et al.*, 2002). The mtSSB is enhancing the primer recognition and the processivity of POLG (Williams and Kaguni, 1995). Only in its presence POLG is able to synthesize longer then 16,000 bp products (Korhonen *et al.*, 2004; Wanrooij and Falkenberg, 2010).

POLRMT was discovered in a human cell line by Tiranti *et al*., in 1997. POLRMT initiates transcription with the help of TFAM and transcription factor B2. It is responsible for the RNA primer synthesis needed for replication initiation of both leading and lagging strand. It synthesizes primers with length of about 25 bp (Wanrooij and Falkenberg, 2010).

1. 5. 5 mtDNA replication machinery

All components of the replication fork are shown schematically on Figure 10. The TWINKLE helicase (shown in blue) slides over the mtDNA in 5'→3' direction and unwinds it. Right away the mtSSB protein (dark green) binds the single stranded mtDNA and supports the affinity of the POLG holoenzyme (red and gray) to process the synthesis of mtDNA. POLRMT (light green) is responsible for the RNA priming (yellow line) on the lagging strand, once the unwinding has reached the light strand origin of replication (O_L). The single stranded O_L adopts a stem-loop structure, which prevents the binding of mtSSB and thus the POLRMT can initiate primer synthesis from a poly-dT stretch in the O_L. After the primer synthesis has taken place POLG performs the lagging strand synthesis (red line) (Wanrooij and Falkenberg, 2010).

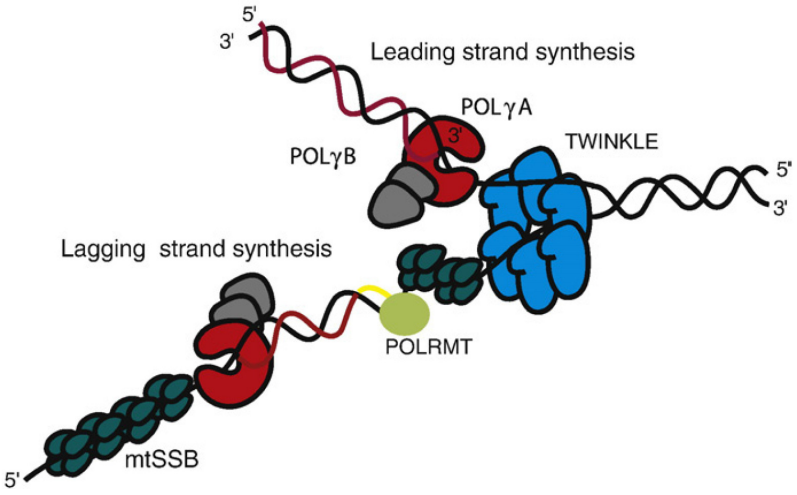

Figure 10 mtDNA replication scheme (adapted from Wanrooij and Falkenberg, 2010).

1. 6 mtDNA damage and repair

mtDNA mutations can arise form different factors such as DNA polymerase errors during the process of replication, exposure to environmental mutagens (Shokolenko *et al.*, 2009) or oxidative damage, with the lattermost, being the most well studied damage (Alexeyev *et al.*, 2013). Mitochondria are the main source of endogenous reactive oxygen species (ROS) produced by the partial reduction of oxygen during the process of oxidative phosphorylation. High production of ROS leads to oxidative stress, resulting from the incapability of the cellular antioxidant defense system to handle its excessive production (Ray *et al.*, 2012). The mtDNA, specifically, is highly exposed to ROS damage, because of its endogenous formation during mitochondrial respiration and close proximity of the mtDNA to the

respiratory chains (Wiesner *et al*., 2006). It is broadly assumed that the damages to the mtDNA caused by ROS are reason for the process of mtDNA mutations accumulation and mitochondrial damage, leading to respiratory chain dysfunctions and consequent further increase in ROS production. This 'vicious circle' might lead to the general damage of the whole cellular function, aging and cell death (Shokolenko *et al.*, 2009; Wiesner *et al*., 2006; Miquel, 1992).

ROS induces DNA strand breaks, via lesion formation in the DNA backbone, or causes oxidation of bases. Complex I is considered as main site for (ROS) formation, due to possible leakage of electrons and easy interaction with oxygen molecules. Between 0.2 and 1.5% of the electron transport in the mitochondrial respiratory chain is ending with the formation of superoxide anion. The formation of superoxide anion as side product of the respiratory chain function is a normal ongoing process in the mitochondria. The superoxide anion is being dismutated into hydrogen peroxide by Mn-superoxide dismutase, and later on the hydrogen peroxide is converted into water and oxygen, by enzymes as catalase and glutathione peroxidase (Kudin *et al.*, 2004; Chance *et al.*, 1979; Liu *et al.*, 2002). The hydrogen peroxide is relatively stable and can diffuse through the membranes and can spread in the entire cell. Through Fenton reactions (in the presence of redox-active metal ions such as Fe^{2+}) it can generate reactive hydroxyl radical that can cause effective damage, such as single-strand or double-strand DNA breaks (Alexeyev, 2009; 2013; Henle *et al.*, 1996; Kudin *et al.*, 2004). In support to the 'vicious circle' theory, higher amounts of hydrogen peroxide cause local elevation of hydrogen peroxide production in rat brain mitochondria (Kudin *et al.*, 2004). DNA pyrimidine damage leads to the formation of the low mutagenic thymine glycol, which causes damage due to inhibition of polymerase activity (Wang *et al.*, 1998; Hanes *et al.*, 2006; Alexeyev *et al.*, 2013). The purine damage results in the production of the highly mutagenic 8-dihydro-8-oxo-2'-deoxyguanosine (8-oxoG), responsible for the formation of G to T transversions (Alexeyev *et al.*, 2013; Hanes *et al.*, 2006; De Bont and van Larabeke, 2004; Wang *et al.*, 1998). Excessive amounts of ROS cause oxidative stress and predispose to development of different pathological conditions; therefore, the right balance of ROS production and degradation is very important. For example, reduced levels of glutathione were found in substantia nigra pars compacta of patients with Parkinson's disease (Sian *et al.*, 1994; Dringen *et al.*, 1999). The main reason for mtDNA mutation accumulation is the failure of the mtDNA repair machinery or the unsuccessful degradation of damaged mtDNA molecules (Shokolenko *et al.*, 2009).

1. 6. 1 Single strand mtDNA break and repair

A single strand break (SSB) occurs when only one of the two mtDNA strands is affected, by loss of single nucleotide and damage of the 5' end, the 3' end or both termini at the break site (Alexeyev *et al.*, 2013); in this case its complementary strand can be used as a template to remove the break. SSB can be converted in double-strand break (DSB) by an approaching replication fork or if SSBs are located close on opposing DNA strands. There are SSB nicks resulting from oxidative attack directly on the DNA sugar backbone, but also SSB (gaps) can occur indirectly as a result of base excision repair (BER) after oxidative damage (Friedberg *et al.*, 2006). It was proposed that in mitochondria the BER process is analogous to the nuclear BER. There are two different types of BER, a single nucleotide BER (SN-BER) and multinucleotide repair patch or long patch BER (LP-BER) (Liu *et al.*, 2008; Szczesny *et al.*, 2008). In case of LP-BER, POLG performs a strand displacement synthesis that results in the frequent formation of 5'-single-strand DNA (5'-ssDNA) flaps. In the nucleus the processing of this flap structures is being performed by flap structure specific endonuclease 1 (FEN1) and DNA replication helicase/nuclease 2 (DNA2) with endonuclease activity (Copeland and Longley, 2008). DNA2 cannot cleave overhangs at junction between ssDNA and dsDNA, thereafter, it would rather leave a 5' overhang that can be processed by FEN1 (Sykora *et al.*, 2012). Even though the function of DNA2 and FEN1 in the nucleus is very well studied, their existence and function in mitochondria is not clear.

Zheng *et al.*, (2008) have demonstrated that DNA2 in humans localizes to mitochondria and forms a complex with POLG and stimulates its activity, in opposite to other species. DNA2 has important role for the stability and maintenance of the mtDNA replication. Its association with POLG might be due to its function in RNA primer removal during the process of replication (Zheng *et al.*, 2008).

The functionality of FEN1 in mitochondria is still a matter of dispute, but its existence would lead to faster removal of the RNA primers during replication (Budd and Campbell, 1997; Zheng and Shen, 2011; Zheng *et al.*, 2008). In 2013 Kazak *et al.*, discribed a shortened form of FEN1, which is mitochondrially targeted and translated from internal start codon, a mitochondrial FEN1 isoform. They named it FENMIT and represented results showing that FENMIT has an R-loop substrate preference, observed frequently in the D-loop region where replication starts at GC-rich sequences promoting this R-loop formation (Aguilera and García-Muse, 2012; Kazak *et al.*, 2013). FENMIT has role in stabilizing these structures and is imported in mitochondria upon accumulation of RNA-DNA hybrids near the origin of replication (Kazak *et al.*, 2013). Most probably the truncated version of FEN1 participates in the process of mtDNA repair by using the lagging RNA strand as a template to fix or bypass lesions on the leading DNA strand, which might be possible only by reverse

transcriptase activity in the mitochondria. FENMIT might also play role in processing mitochondrial polycistronic transcripts as this process is occurring while the DNA is still hybridized with RNA (Kazak *et al.*, 2013; Carré and Atardi, 1978).

Another enzyme, EXOG, required for repairing of endogenous SSBs was shown to localize to the mitochondrial inner membrane space (IMS) and eventually plays similar role to FEN1 and DNA2 in LP-BER. EXOG has both exo and endonuclease activity and acts in 5'→3' direction (Cymerman *et al.*, 2008). Its depletion leads to persistent SSBs accumulation, which is initiation signal for apoptosis. The mtDNA amplification is decreased when EXOG is depleted. EXOG precipitates together with POLG (Tann *et al.*, 2011).

Ligase 3 (LIG3) re-establishes the continuity of the mtDNA strand in both BER pathways. It has 5'-P to 3'-OH ligation activity as all other ligases in eukaryotes and is ATP dependent (Zheng *et al.*, 2008; Stumpf and Copeland, 2011). LIG3 has putative zinc-finger motif (ZnF) which may help its attachment to DNA secondary structure elements, which can be met at sites of DNA damage (Martin and MacNeill, 2002).

1. 6. 2 Double strand DNA break and repair

Very hazardous is the situation in which both mtDNA strands are damaged and double-strand breaks (DSBs) are formed and no intact complementary strand is available, because they can cause genome rearrangements (Watson *et al.*, 2004). The DSBs can be result from ionizing radiation or the collapse of replication forks at a single strand break of the mtDNA. DSBs can occur also during replication, due to stalling of the POLG (in the coupled strand replication model). Prolonged formation of DSBs can lead to formation of multiple deletions and their accumulation, as well as to profound absence of full length mtDNA and mtDNA depletion (Song *et al.*, 2011). The accumulation of damaged mtDNA leads to cellular heteroplasmy of the mtDNA pool, and when it reaches a threshold for deleted mtDNA molecules (Moraes *et al.*, 1992; Mita *et al.*, 1990; Greaves *et al.*, 2012) and not enough functional mitochondria have remained the cell would fail maintaining the ATP production and the mitochondrial dysfunction might lead to cell death.

DSBs can be repaired by homologous recombination (Krishnan *et al.*, 2008) or nonhomologous end-joining (Graziewicz *et al.*, 2006). The process of mtDNA homologous recombination in mammals is a matter of dispute and appears to be an event, detectable in mtDNA depletion models (D'Aurelio *et al.*, 2004) and induction of multiple DSB (Bacman *et al.*, 2009). Great number of mtDNA recombination junctions and catenation were described in adult heart mitochondria (Kajander *et al.*, 2000); such formations seem to be missing in rodents and infant mitochondria (Pohjoismäki *et al.*, 2009; 2010; Alexeyev *et al.*, 2013).

Homologous recombination-dependent DNA repair was proposed to be involved in the formation of deletions with breakpoints flanked by direct repeats (Krishnan *et al.*, 2008).

1. 6. 3 mtDNA deletions

According to the mitochondrial theory of aging, point mutations and deletions accumulate with age (Khrapko *et al.*, 1999) and a single deletion can spread in the whole cell through its clonal expansion (Kowald *et al.*, 2014). The clonal expansion is supported either by random genetic drift (Elson *et al.*, 2001; Chinnery and Samuels, 1999) connected with random clonal expansion of mutations which occurred once in life, or because of the replicative advantage of the deleted molecule, as they are smaller in size (Diaz et *al.*, 2002; Wallace, 1992b; Lee *et al.*, 1998; Kowald *et al.*, 2014). Simulation studies from Kowald *et al.*, (2014) claimed that replication advantage due to smaller size is very unlikely to explain the clonal expansion of a single deleted mtDNA molecule, due to differences in the replication times and the half-life of the mtDNA. For example, a mutant which has lost 30% of its mtDNA would overtake the wild-type mtDNA in 150 years.

The formation of mtDNA deletions might result from failure in the function of mtDNA maintenance factors, maternal inheritance (generation in the mothers germ line) or stochastic formation. However, mtDNA deletetions are rarely inherited and are rather formed sporadicly (Fukui and Moraes, 2009). mtDNA deletions are being formed and accumulate naturally in the tissues during the process of aging (Wiesner *et al.*, 2006).

Many studies have shown that deletions often occur between direct repeats (DR) (up to 85% of the deletions (Bua *et al.*, 2006; Samuels *et al.*, 2004)) or stem-loop structures on the mtDNA (Lakshmanan *et al.*, 2012; Solano *et al.*, 2003) and appear mostly in the ‘major arc’ of the mtDNA (Kraytsberg *et al.*, 2006). About 60% of the deletions are surrounded by perfect homologous direct repeats, forming Class I deletions. In approximately 30% of the deletions the flanking sequences are imperfect, imperfect repeats, and these deletions are classified as Class II. When formed between DRs, most of the deletions retain their 5’ end repeat (45% of the deletions in neurons and 75% of the deletions in muscle) (Samuels *et al.*, 2004; Krishnan *et al.*, 2008). Class III deletions represent 10% of the deletions and have no repeats (Samuels *et al.*, 2004). Samuels *et al.*, (2004) stated that there is no specific association between repeats and breakpoints distribution. All three classes of deletions share great similarity in the distribution of the breakpoints, which is pointing to a general underling deletion formation mechanism.

Slip-replication (Shoffner *et al.*, 1989), recombination (Schon *et al.*, 1989; Mita *et al.*, 1990) and DSB repair (Krishnan *et al.*, 2008) are mechanisms associated with the deletion formation between DRs (Guo *et al.*, 2010). The slipped-strand model of deletion formation

(Figure 11) (Krishnan *et al.*, 2008) proposes that an upstream DR on the H-strand binds to downstream DR on the L-strand, during lagging strand replication (Figure 11a and b) and forms a light strand loop. A POLG error in the downstream repeat or single strand break in the loop (Figure 11c) leads to its degradation till double-strand region is reached (Figure 11d). Ligation of these free ends of the heavy strand, followed by continuation of the replication leads to the formation of one wild-type molecule and one deleted molecule (Figure 11d–f) (Eimon *et al.*, 1996; Schon *et al.*, 1989). The slipped-strand mechanism of deletion formation is strongly associated with the strand asynchronous model of replication and would result in large-scale deletion formation in the mtDNA major arc (Shoffner *et al.*, 1989; Krishnan *et al.*, 2008).

A study by Krishnan *et al.*, (2008), showed that only 12% of repeats larger then 10 bp and 21% of repeats with size of 5 to 9 bp are present in the minor arc, which would suggest that formation of deletions in the major arc is simply due to lower number of deletion formation sites present in the minor arc and the limiting effects of the two origins of replication (Samuels *et al.*, 2004).

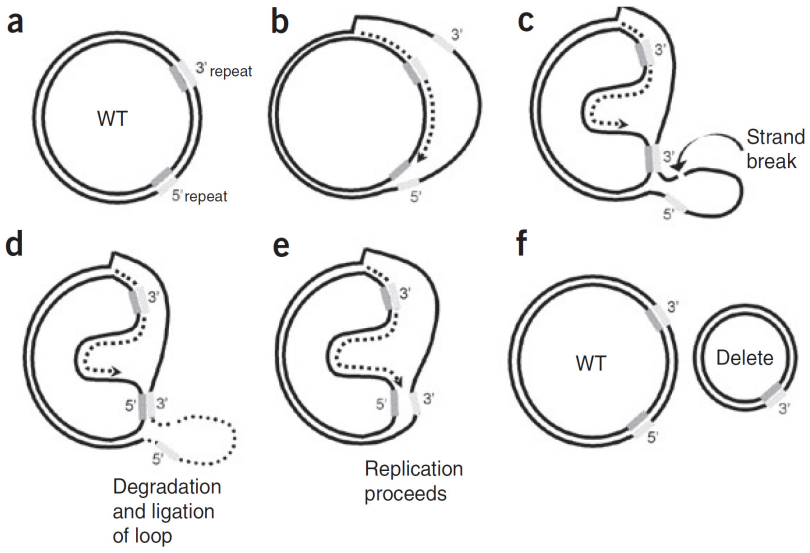

Figure 11 Slipped-strand mechanism of deletion formation (adapted from Krishnan *et al.*, 2008).

Therefore, the slipped-strand model of deletion formation cannot be defined as the major way in which large scale deletions are formed. Hence, Krishnan *et al.*, (2008) suggested that deletions can occur during DSB repair (Figure 12). After DSB formation, when under exonuclease activity at the DSB (Figure 12a–c) or due to mistakes in the POLG 3'→5' exonuclease repair activity, single strands are formed (Figure 12d) and they can anneal to other homologous single stranded mtDNA regions or the D-loop; further repair,

ligation and degradation of the left over single strand pieces (Figure 12e–f) leads to the formation of intact deleted mtDNA molecules.

Samuels *et al.*, (2004) addressed another issue of O_L being a limiting factor for the 5' deletion breakpoint. According to their studies and previous findings, deletions removing the O_L are detectable in low levels and are amplifiable by PCR in post-mitotic tissues (Baumer *et al.*, 1994; Moslemi *et al.*, 1997; Kajander *et al.*, 2000; Marzuki *et al.*, 1997), or in connection with mtDNA duplications (Manfredi *et al.*, 1997; Dunbar *et al.*, 1993; Miyabayashi *et al.*, 1991), and can influence the possibility of propagation of the deletion to high level, but does not influence the formation of the deletions themselves.

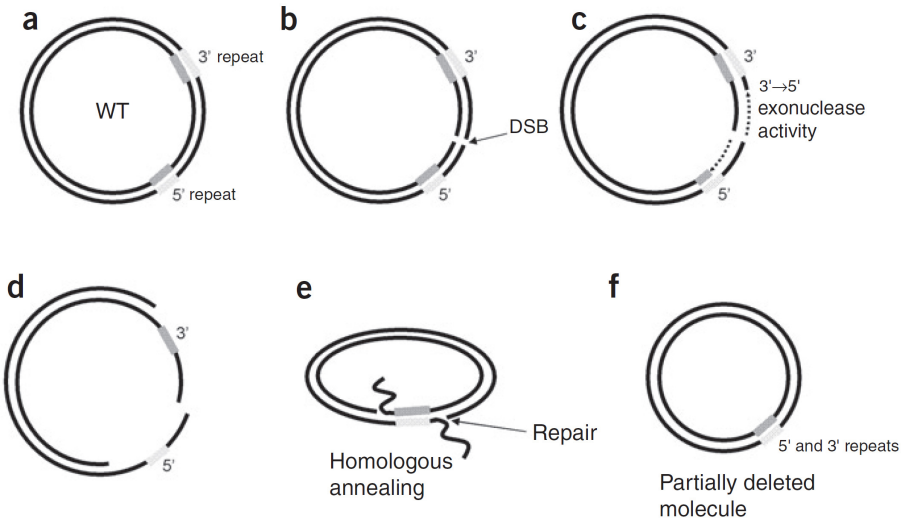

Figure 12 Mechanism of deletion formation during DSBs repair (adapted from Krishnan *et al.*, 2008).

The distribution of the deletional breakpoints is probably dependent of the mechanism by which the deletions are formed. The 3' end of the deletions often is in the region between 16,000 np and 16,100 np, (Samuels *et al.*, 2004) and the 5' breakpoints lay in the region between 7800 and 8600 np. No deletions exceeding np 16,268 have been described (Samuels *et al.*, 2004) and only four deletions at position above 16,085 are listed in the literature (Kajander *et al.*, 2000; Barrientos *et al.*, 1996; Samuels *et al.*, 2004). For example, hippocampal samples from temporal lobe epilepsy (TLE) patients with Ammon's horn sclerosis (AHS) contain 10-fold more deletions than a normal hippocampus and these deletions are containing a double-strand breakpoint hotspot at position 16,070, that is suggested as hot spot to the action of ROS (Zeviani *et al.*, 1989; Srivastava and Moraes, 2005; Imlay and Linn, 1988; Guo *et al.*, 2010). Another study suggests that at that position a replication fork arrest might occur and DSB formation can be accelerated (Wanrooij *et al.*, 2004), also due to the possible existence of a replication fork barrier (Bowmaker *et al.*, 2003).

Krishnan *et al.*, (2008) claims that this hotspot might be due to the single stranded nature of this region in the mtDNA and its participation in deletions formation through single strand homologous annealing in their model of deletion formation by DSBs repair (Figure 12). It seems that deletions carrying no or small repeats tend to cluster at that region (Samuels *et al.*, 2004). The most frequently detected deletion in human, the 'common deletion', is also formed between 13 bp long perfect DRs (Schon *et al.*, 1989). The common deletion removes 4977 bp from the mtDNA between np 8482 and np 13,459 (Holt *et al.*, 2007; Schon *et al.*, 1989) and it was shown that it accumulates with the age in post-mitotic tissues (Kukat and Trifunovic, 2009) and is indicative trait for elevated oxidative damage (Lee and Wei, 2007). Samuels *et al.*, (2004) suggested that the 13 bp long repeats, characteristic for the common deletion, are basic factor for the formation of most deletions and the exact breakpoint location is probably influenced by local sequence features. Guo *et al.*, (2010) have performed deletional spectra analysis and have stated that the deletion formation is dependent mostly on secondary structures, such as long regions of up to 50 nt length with partial homology, that bring together distant parts of the mtDNA and participate in the deletion formation (Shoffner *et al.*, 1989; Mita *et al.*, 1990; Guo *et al.*, 2010). The possibility of formation of deletions between these long regions is higher then only between simple perfect repeats (Guo *et al.*, 2010).

In difference to the homologous recombination end joining repair, the non-homologous end joining (NHEJ) repair of DSBs can be much more hazardous and it is the mechanism in which deletions absent of DRs are formed (Gredilla *et al.*, 2012). After DSB formation, POLG can remove single strand ends formed during the DSB and these intermediates can undergo NHEJ in a stochastic manner (Fukui and Moraes, 2009). Knock out mice absent of POLG proofreading activity also tend to form large scale deletions without DRs (Vermulst *et al.*, 2008; Fukui and Moraes, 2009). Some of these deletions have very small nucleotide homologies at the breakpoint position, which has been detected in aging and disease (Krishnan *et al.*, 2008). However, these types of deletions are rarely detectable in comparison to the deletions formed between DR (Krishnan *et al.*, 2008).

1. 7 Alterations of mtDNA in disease

The mtDNA molecules in a single cell coexist in heteroplasmic state with the mutated ones (Bua *et al.*, 2006). The accumulation of mutated mtDNA fraction by clonal expansion is leading to heteroplasmic drift reaching certain threshold at which a biochemical phenotype occurs (Rossignol *et al.*, 2003). At that stage the physiology of the cell might be severely impaired. As each cell reaches this threshold at a different time, these different heteroplasmic mtDNA levels in the cells lead to the mosaic pattern of the tissue, when

stained for mitochondrial enzymes activity (Lane *et al.*, 1996). Muscle containing dysfunctional mitochondria often displays mitochondrial proliferation, visualized by staining with modified Gomori trichrome. Muscle fibers representing such phenotype are ragged-red fibers (RRF). Depending on the distribution and proportions of wild-type and mutated mtDNA molecules in different tissues, the patholgical manifestation of the mitochondrial disease can have different organ and age onset (Debrosse and Parikh, 2012). Lactic acidosis, myopathy, neurodegeneration and peripheral neuropathy are some of the symptoms connected with mitochondrial disorders.

Defects of the respiratory chain subunits and mitochondrial disorders affect 1 in 5000 live births (Skladal *et al.*, 2003; Vafai and Mootha, 2012). More then 200 mitochondrial diseases are associated either with point mutations in mtDNA encoded respiratory chain proteins and tRNAs or single clonally expanded deletions (Chabi *et al.*, 2003). Leber's Hereditary Optic Neuropathy (LHON) and the Leigh Syndrome are examples of mitochondrial disorders based on point mutations in the mtDNA. Mutations m.11,778G>A in the ND4 gene (Wallace *et al.*, 1988), m.3460G>A in the ND1 gene (Huoponen *et al.*, 1991), m.14,484T>C in ND6 gene (Johns *et al.*, 1992) and m.14,495A>G also in the ND6 gene (Chinnery *et al.*, 2001) are the mutations found most frequently in LHON patients and all of them are affecting Complex I of the respiratory chain. Point mutations in the ATPase domains are associated with the Leigh Syndrome (m.8993T>G or m.8993T>C, mutations in the ATPase 6 gene; de Vries *et al*., 1993) or Subacute Necrotizing Encephalomyelopathy. Its milder form with lower heteroplasmy causes neuropathy, ataxia, and retinitis pigmentosa (NARP) (Debrosse and Parikh, 2012; Leigh, 1951; Rahman *et al.*, 1996). The mitochondrial tRNA genes frequently are found to carry point mutations in mitochondrial disease and are related to diseases such as MELAS and MERFF (myoclonic epilepsy with ragged red fibers) (Suzuki *et al.*, 2011). MELAS patients suffer from mitochondrial myopathy, encephalopathy, lactic acidosis and stroke-like episodes, which give name of the disease. For example, MELAS is associated with mutations located in the mtDNA encoding for the tRNA Leu (m.3243A>G) but other tRNA mutations also can manifest in a similar way. The epileptic seizures in these patients are based on metabolic strokes, which often lead to focal or generalized epilepsy (Vafai and Mootha, 2012; Debrosse and Parikh, 2012). MERFF patients with mutation in the tRNA Lys (m.8344A>G) develop ataxia, hearing loss and peripheral neuropathy; they may represent generalized seizures and myoclonic epilepsy (Debrosse and Parikh, 2012).

Mitochondrial single deletion syndromes are asscociated with the formation of a single deletion and its clonal expansion. They are usually characterized by large scale deletions from to 2 to 10 kb. In the different syndromes different tissues are affected, thereafter, the phenotype varies (Debrosse and Parikh, 2012). Such single mitochondrial deletion syndromes are the Pearson Syndrome (PS) (Williams *et al.*, 2012; Debrosse and

Parikh, 2012) and the Kearns-Sayre syndrome (KSS) (Debrosse and Parikh, 2012; Harvey and Barnett, 1992; Berenberg *et al.*, 1977). One of the most frequent mitochondrial disorders caused by single or multiple mtDNA deletions is CPEO or chronic progressive external ophthalmoplegia. Very often CPEO is accompanying other diseases such as MELAS and mitochondrial maintenance disorders. PS, KSS and CPEO symptoms and pathology often overlap in different patients (Debrosse and Parikh, 2012; Berenberg *et al.*, 1977).

Defects in the replication machinery and repair are broadly connected with the formation of multiple mtDNA deletions leading to 'multiple mtDNA deletion disorders', or mtDNA depletion represented with reduction of the copy number of mtDNA molecules and 'mtDNA depletion syndromes' (MDS). Both the clinical and genetical phenotypes of these two groups of syndromes often are overlapping in the patients; therefore, they are called collectively 'mtDNA maintenance disorders' (MMD). MMDs have broad pathological manifestation. Their phenotype may affect multiple organs in early childhood or they can be tissue specific pathologies appearing in later age.

MMDs are associated with mutations in nuclearly encoded genes all of them coding for proteins involved in mtDNA replication or repair, or involved in the mitochondrial salvage pathway of deoxyribonucloside-5'-triphosphates (Nishino *et al.*, 1999, Kaukonen *et al.*, 2000; Ostergaard *et al.*, 2007). One of the most frequent example for defects in the mitochondrial replication machinery are mutations in the *POLG* gene. The POLG patients are characterized with great diversity of phenotypes, that can be explained with the different kinetic mechanisms and unique enzymatic activities involved in each disease caused by different mutation in the same gene (Sohl *et al.*, 2013). Mutations in *POLG2*, encoding for the accessory subunit of the POLG holoenzyme (Yakubovskaya *et al.*, 2006) and a missense mutation in it, c.1352G>A (G451E) were found to be cosegregating with autosomal dominant form of progressive external ophtalmoplegia (adPEO) (Longley *et al.*, 2006) and a heterozygous 24 bp insertion in its exon 7 leads to missplicing, late-onset ptosis and myopathy (Walter *et al.*, 2010).

adPEO is mainly associated with mutations in the nuclear genes *POLG*, *TWINKLE* or adenine *nucleotide translocator 1* (*ANT1*). The patients represent multiple deletions and accumulation of point mutations, they show ragged red fibers and lowered respiratory capacity in muscle (Graziewicz *et al.*, 2006; Bohlega *et al.*, 1996; Copeland, 2008; Van Goethem *et al.*, 2001; Zeviani *et al.*, 1989; Spinazzola and Zeviani, 2005). More then 40 mutations in *C10Orf2* (*TWINKLE*) have been reported (Young *et al.*, 2011). Missense mutations in it cosegregate with adPEO, hepatocerebral syndrome with mtDNA depletion syndrome, and infantile-onset spinocerebellar ataxia (Longley *et al.*, 2010).

The Alpers-Huttenlocher syndrome is another MMD inherited in autosomal recessive way, characterized by depletion of the mtDNA and based on mutations in *POLG*, but in

opposite to the adult-onset adPEO, it has early childhood-manifestation (Huttenlocher *et al.*, 1976; Sandbank and Lerman, 1972; Naviaux *et al.*, 1999; Zsurka *et al.*, 2008).

Except the dysfunction of the replication machinery, dysfunction of the mitochondrial deoxynucleoside triphosphates metabolism also leads to mtDNA depletion and subsequent mitochondrial disease (Leanza *et al.*, 2008). Eight genes have been described in the literature in connection with impaired deoxynucleoside triphosphates metabolism, mitochondrial dysfunction and MDS; this group of genes includes, for example, the thymidine kinase 2 (TK2), leading to myopathic MDS (Götz *et al.*, 2008; Saada *et al.*, 2001) and the mitochondrial inner membrane protein MPV17 associated with hepatocerebral MDS (Götz *et al.*, 2008; Spinazzola *et al.*, 2006). The mitochondrial dNTP pools disbalance can be mutagenic, causing replication errors as A · T → G · C transitions. Low mismatch repair activities in mitochondria accelerate the replication errors (Song, *et al.*, 2005; Mathews, 2006).

Emerging evidence shows that MMDs are tightly connected also to the mitochondrial dynamics, and the processes of active fusion and fission of mitochondria are responsible not only for the mitochondrial morphology and number, but obviously are also involved in the mitochondrial mtDNA maintenance (Wang *et al.*, 2009). For example, mutations in *Mfn2*, involved in the process of fusion of the mitochondrial outer membrane, were found to cause autosomal dominant neuropathy, Charcot–Marie–Tooth Neuropathy Type 2A (CMT2A), that affects the long axons of motor and sensory neurons (Züchner *et al.*, 2004). Its phenotypes were associated with mtDNA instability, which was not observed in CMT2A patients until recently. Mutations in *OPA1*, responsible for the merging of the IMM during fusion, are associated with autosomal dominant optic atrophy 'plus' phenotypes such as ataxia, chronic progressive external ophtalmoplegia, mitochondrial myopathy etc., (Amati-Bonneau *et al.*, 2008). Rouzier *et al.*, (2011) reported a large family carrying mutation in *Mfn2*, representing autosomal dominant optic atrophy 'plus' phenotype, a phenotype usually linked to mutations in *OPA1*. Mitochondrial DNA deletions, respiratory chain deficiencies in fibroblasts from the patients, mitochondrial network fragmentation and MFN2 depletion classify MFN2 and mitochondrial fusion as responsible for mtDNA stability (Rouzier *et al.*, 2011). All these facts lead to the current assumption that impaired mitochondrial fusion leads to instability of the mitochondrial genome, insufficient mitochondrial content mixing and incapability for recovery after oxidative stress (Rouzier *et al.*, 2011; Chen and Chan, 2010).

Alterations in mitochondria, such as changes in their structure, decline in their respiratory function, mtDNA mutation accumulation and increasing oxidative stress, and subsequent oxidative damage are also signs of the ongoing process of aging. Multiple mitochondrial deletions are detectable in patients with idiopathic Parkinson's disease. They are wide spread in the substantia nigra pars compacta. In consensus with the development

of Parkinson's disease with advancing of the age, mitochondrial deletions are accumulating in the process of aging (Bender *et al.*, 2006; Kraytsberg *et al.*, 2006). The accumulated deletions in these neurons are triggering neuroprotective compensatory mechanisms in the mitochondria, leading to higher pathogenic threshold in the dopaminergic neurons (Perier *et al.*, 2013).

Swerdlow *et al.*, (2004) proposed the Alzheimer's disease "mitochondrial cascade hypothesis" for its late onset. Alzheimer's disease is characterized by dementia, extracellular amyloid protein aggregations, and intracytoplasmic tau protein aggregations. Mitochondrial dysfunction, such as impaired energy metabolism, electron transport chain enzyme dysfunction and ROS production appear to be an early sign of Alzheimer's disease (Chen and Yan *et al.*, 2010).

Campbell *et al.*, (2011) gave evidence that mitochondrial dysfunction is involved as well in multiple sclerosis and is part of the pathomechanism of the disease, plus the chronic inflammation in its progressive stages. In amyotrophic lateral sclerosis (ALS) mitochondrial transport in the axons was shown to be disrupted as well as the mitochondrial fission and fusion (Shi *et al.*, 2010). Morphological changes in mitochondria were found in both humans and animal models of ALS. Patients with secondary progressive multiple sclerosis (SPMS) represent respiratory chain deficiency of complexes II and IV in comparison to aged controls. This pathology is result of the formation of clonally expanding multiple mitochondrial deletions inducible by inflammation and their impaired repair. The deletions have breakpoints in the major arc as in other neurodegenerative diseases (Campbell *et al.*, 2011).

1. 8 Goals

The focus of this PhD thesis was to gain insight into the different pathological mechanisms that lead to mitochondrial dysfunction through an impairment in mtDNA maintenance. (i) I was investigating the novel mitochondrial exonuclease MGME1 that we have discovered in three families with mtDNA maintenance disorder. Mutation in MGME1 leads to decreased mtDNA copy number and generation of unusual large rearrangments. The exact function and the molecular consequences of MGME1 deficiency has been investigated in detail. (ii) Defect of other genes, not directly involved in mtDNA replication, can also have an effect on mtDNA maintenance. Mitofusin 2 is known to play a crucial role in fusion of mitochondria. Proper mitochondrial dynamics are required for adequate content mixing, i.e. complementation of impaired proteins, RNA and DNA molecules through their healthy counterparts. We aimed to show that dysfunction of mitofusin 2 can lead to insufficient mtDNA replication and the formation of deletions. (iii) Alterations of the mitochondrial genome have been demonstrated in epilepsy, especially in the hippocampus, the seizure focus of temporal lobe epilepsy (TLE) patients with AHS. So far, it is not clear whether mtDNA damage and hippocampal neurodegeneration is a cause or result of the epilepsy. By investigating the complex mixture of multiple deletions in brain samples of patients having different forms of TLE, we aimed to identify specific mechanisms relevant for chronification of epilepsy.

2. Materials and Methods

2. 1. Synthetic oligonucleotides

The following oligonucleotides used in different PCR reactions for the nuclear single copy gene *Kir4.1*, for the mitochondrial genome (mtDNA) and ligation-mediated PCR, were designed by using software 'Primer' and were purchased from Thermo Fisher Scientific GmbH (Ulm, Germany) and MWG Biotech AG (Ebersberg, Germany). They are listed in Tables 1, 2, 3 and 4. F, forward primer; R, reverse primer; TM, TaqMann probe; number in the name indicates the 5′ nucleotide of the primer.

Locus	Name	Lenght	Sequence
Kir4.1	KIR835F	19	5'-GCGCAAAAGCCTCCTCATT-3'
Kir4.1	KIR857TM	27	5'-FAM-TGCCAGGTGAACAGGAAAACTG CTTCAG-TAMRA-3'
Kir4.1	KIR903R	19	5'-CCTTCCTTGGTTTGGTGGG-3'

Table 1 Oligonucleotides for the nuclear gene *Kir4.1*.

Locus	Name	Lenght	Sequence
synthetic sequence	LMP25	25	5'-GCGGTGACCCGGGAGATCTGTATTC-3'
synthetic sequence	LMP11	11	5'-GAATACAGATC-3'

Table 2 Oligonucleotides used for linker synthesis.

Locus	Name	Lenght	Sequence
mtDNA	16,557TM	25	5'-FAM-AGACATCACGATGGATCACAGGTCT-TAMRA-3'
mtDNA	10F	30	5'- TCTATCACCCTATTAACCACTCACGGGAGC-3'
mtDNA	108F	22	5'-AGCACCCTATGTCGCAGTATCT-3'
mtDNA	174F	27	5'-CAATATTACAGGCGAACATACTTA CTA-3'
mtDNA	379F	25	5'-AGCCTAACCAGATTTCAAATTTTAT-3'
mtDNA	521F	21	5'-ACACCGCTGCTAACCCCATAC-3'
mtDNA	16,074F	23	5'-ATCAACAACCGCTATGTATTTCG-3'
mtDNA	16,099F	23	5'-CATTACTGCCAGCCACCATGA-3'
mtDNA	16,196F	23	5'-GCTTACAAGCAAGTACAGCAATC-3'
mtDNA	16,285F	25	5'-ACCTACCCACCCTTAACAGTACATA-3'
mtDNA	16,520F	24	5'-CATAAAGCCTAAATAGCCCACACG-3'
mtDNA	16,525F	21	5'-AGCCTAAATAGCCCACACGTT-3'
mtDNA	35R	24	5'-CCGTGAGTGGTTAATAGGGTGATA-3'
mtDNA	45R	22	5'-TGGAGAGCTCCCGTGAGTGGTT-3'
mtDNA	67R	21	5'-CCAGACGAAAATACCAAATGC-3'
mtDNA	136R	21	5'-CAAAGACAGATACTGCGACAT-3'
mtDNA	208R	26	5'-ACACACTTTAGTAAGTATGTTCGCCT-3'
mtDNA	288R	25	5'-TTTGTTATGATGTCTGTGTGGAAAG-3'
mtDNA	485R	25	5'-ATGAGATTAGTAGTATGGGAGTGGG-3'
mtDNA	16,075R	22	5'-ATGGGTGAGTCAATACTTGGGT-3'
mtDNA	16,115R	21	5'-GGTGGCTGGCAGTAATGTACG-3'
mtDNA	16,148R	25	5'-GGTCAAGTATTTATGGTACCGTACA-3'
mtDNA	16,185R	21	5'-GGTTTTGATGTGGATTGGGTT-3'
mtDNA	16,263R	18	5'-AGGGGTGGCTTTGGAGTT-3'
mtDNA	16,282R	21	5'-GTTGGTATCCTAGTGGGTGAG-3'
mtDNA	16,308R	24	5'-ATGTACTGTTAAGGGTGGGTAGGT-3'
mtDNA	16,413R	19	5'-ACGGAGGATGGTGGTCAAG-3'
mtDNA	16,496R	32	5'-CGGATACAGTTCACTTTAGCTACCCCC AAGTG-3'
mtDNA	16,503R	23	5'-CAGATGTCGGATACAGTTCACTT-3'

Table 3 mtDNA primers in the D-loop.

Locus	Name	Lenght	Sequence
mtDNA	1056F	22	5’-AGCTAAGACCCAAACTGGGATT-3’
mtDNA	2101F	22	5’CAAAGAGGAACAGCTCTTTGGA-3’
mtDNA	3137F	26	5’-GAGAAATAAGGCCTACTTCACAAAGC-3’
mtDNA	3150F	20	5’-TACTTCACAAAGCGCCTTCC-3’
mtDNA	3922F	25	5’-GAACTAGTCTCAGGCTTCAACATCG-3’
mtDNA	5462F	28	5’-CCTTACCACGCTACTCCTACCTATCTC C-3’
mtDNA	7027F	25	5’-CCCACTTCCACTATGTCCTATCAAT-3’
mtDNA	8282F	20	5’-CCCCTCTAGAGCCCACTGTA-3’
mtDNA	11,226F	20	5’-GCTCCCTTCCCCTACTCATC-3’
mtDNA	12,062F	21	5’-ACCCTCATGTTCATACACCTA-3’
mtDNA	14,588F	24	5’-CCCCCATAAATAGGAGAAGGCTTA-3’
mtDNA	15,081F	21	5’-CCTGAAACATCGGCATTATCC-3’
mtDNA	15,965F	25	5’-AAGTCTTTAACTCCAACCATTAGCAC-3’
mtDNA	15,974F	23	5’-ACTCCACCATTAGCACCCAAAGC-3’
mtDNA	638R	22	5’-GGTGATGTGAGCCCGTCTAAAC-3’
mtDNA	1144R	22	5’-AGTGTTCTGGCGAGCAGTTTTG-3’
mtDNA	2223R	22	5’-TAGTGGGTGTTGAGCTTGAACG-3’
mtDNA	3246R	22	5’-GGCTCTGCCATCTTAACAAACC-3’
mtDNA	4036R	26	5’-CTAGGAAGATTGTAGTGGTGAGGGTG-3’
mtDNA	4833R	24	5’-TGCCTTGGGTAACCTCTGGGACTC-3’
mtDNA	5985R	25	5’-CTCCAGCTCATGCGCCGAATAATAG-3’
mtDNA	12,135R	20	5’-GAGGAAAACCCGGTAATGAT-3’
mtDNA	13,684R	24	5’-GGGTGGGGTTATTTTCGTTAATGT-3’
mtDNA	14,695R	20	5’-GGTTGTAGTCCGTGCGAGAA-3’
mtDNA	15,180R	20	5’-ACTGTGGCCCCTCAGAATGA-3’
mtDNA	15,623R	20	5’-CAAGGACGCCTCCTAGTTTG-3’

Table 4 Primers in the mtDNA coding region.

2. 2 Enzymes, chemicals and solutions

All enzymes were provided with their commercial reaction buffers.

Enzyme	Company	Headquater
iTaq DNA polymerase	BIO-RAD	Hercules, California, U. S.
JumpStart AccuTaq LA polymerase	Sigma-Aldrich	St. Louis, USA
JumpStart *Taq* polymerase	Sigma-Aldrich	St. Louis, USA
LongAmp *Taq* DNA polymerase	New England Biolabs	Ipswich, United Kingdo
Ranger DNA polymerase	BIOLINE GmbH	Berlin-Brandenburg, Germany
TaKaRa LA Taq HS	TAKARA BIO INC	Ōtsu, Shiga, Japan
Mung Bean Nuclease	New England Biolabs	Ipswich, United Kingdo
T4 DNA ligase	New England Biolabs	Ipswich, United Kingdo
T4 DNA polymerase	New England Biolabs	Ipswich, United Kingdo
Proteinase K	QIAGEN N.V.	Venlo, Netherlands
Trypsin	PAA Laboratories GmbH	Pasching, Austria

Table 5 Enzymes.

Chemical	Company	Headquater
Acrylamide/Bis Solution, 40%, 37.5:1	BIO-RAD	Hercules, USA
Agarose	Sigma-Aldrich	St. Louis, USA
Ammonium persulfate	Carl Roth GmbH & Co. KG	Karlsruhe, Germany
Bromophenol blue	Sigma-Aldrich	St. Louis, USA
Bovine serum albumin	Sigma-Aldrich	St. Louis, USA
2'-3'-dideoxycytidine	Sigma-Aldrich	St. Louis, USA
Digitonin	Serva Electrophoresis GmbH	Heidelberg, Germany
dNTPs	Sigma-Aldrich	St. Louis, USA
DMSO	Merck	Darmstadt, Germany
DMEM	PAA Laboratories GmbH	Pasching, Austria
Double distilled water	Sigma-Aldrich	St. Louis, USA
EDTA	Sigma-Aldrich	St. Louis, USA
EGTA	Sigma-Aldrich	St. Louis, USA
Ethidium bromide	Sigma-Aldrich	St. Louis, USA
FBS	Invitrogen Corporation	Carlsbad, USA
Glycerol	Sigma-Aldrich	St. Louis, USA
HEPES	Sigma-Aldrich	St. Louis, USA
Hydrogen peroxide solution	Sigma-Aldrich	St. Louis, USA
Mannitol	Sigma-Aldrich	St. Louis, USA
$MgCl_2$	Sigma-Aldrich	St. Louis, USA
Nagarse	Sigma-Aldrich	St. Louis, USA
N,N,N′,N′-Tetramethylethylenediamine	Sigma-Aldrich	St. Louis, USA
PBS pH 7.4	Invitrogen Corporation	Carlsbad, USA
Penicillin Streptomycin	Invitrogen Corporation	Carlsbad, USA
ROX Reference Dye	Invitrogen Corporation	Carlsbad, USA
Sucrose	AppliChem GmbH	Darmstadt, Germany
SYBR Green I nucleic acid gel stain	Sigma-Aldrich	St. Louis, USA
TBE	Sigma-Aldrich	St. Louis, USA
Tris-EDTA buffer solution	Sigma-Aldrich	St. Louis, USA
Uridine	Sigma-Aldrich	St. Louis, USA
Xylene cyanol	Merck	Darmstadt, Germany
1 kb DNA Ladder	New England Biolabs	Ipswich, United Kingdo
2-Log DNA Ladder (0.1-10.0 kb)	New England Biolabs	Ipswich, United Kingdo
25 bp DNA Ladder	Invitrogen Corporation	Carlsbad, USA

Table 6 Chemicals.

Solution	Ingredients
Cell freezing media	90% [v/v] FBS, 10% [v/v] DMSO
Fibroblasts media	DMEM (4.5g/l glucose, GlutaMAX^{TM}, 1mM sodium pyruvate), 10%[v/v] FBS, uridine (0,005g/l), penicillin (100 000 U/l), Streptomycin (0.1g/l)
Loading Dye	1×TBE buffer, 30% [v/v] glycerol, 0.04% [w/v] bromphenol blue, 0.4% [w/v] xylene cyanol
MSE solution	225 mm mannitol, 75 mm sucrose, 1 mm EGTA, 5 mm HEPES, 1 mg/ml BSA, pH 7.4
MSE-nagarse solution	0.05% nagarse in MSE solution
MSE-digitonin solution	0.02% digitonin in MSE solution

Table 7 Solutions.

2. 3 Kits

Kit	Company	Headquater
iQ™ SYBR® Green Supermix	BIO-RAD	Hercules, USA
QIAamp DNA Mini Kit	QIAGEN N.V.	Venlo, Netherlands
QIAquick Gel Extraction Kit	QIAGEN N.V.	Venlo, Netherlands
QIAquick PCR Purification Kit	QIAGEN N.V.	Venlo, Netherlands
Quick Blunting™ Kit	New England Biolabs	Ipswich, United Kingdo

Table 8 Kits.

2. 4 Equipment and software

Electronic equipment	Model	Company	Headquater
Analytical balance	TE214S	Sartorius	Elk Grove, USA
Camera	3CCD Color Video Camera, Model DXC-9100P	Sony Corporation	Minato, Japan
Gel-electrophoresis chamber	Sub-Cell GT System	BIO-RAD	Hercules, USA
Haemocytometer	BLAUBRAND®, Neubauer, IVD	BRAND GMBH & Co K.G	Wertheim, Germany
Phase contrast microscope	Axiovert 40C	Carl Zeiss AG	Jena, Germany
PCR thermocycler	GeneAmp® PCR system 9700	Applied Biosystems	Carlsbad, USA
PCR thermocycler	MJ Research PTC-100	GMI, Inc.	Ramsey, USA
PCR thermocycler	MJ Research PTC-200	GMI, Inc.	Ramsey, USA
Quantitative real time PCR (qPCR) thermocycler	iCycler iQ™ cycler	BIO-RAD	Hercules, USA
Spectrophotometer	Cary 50 scan	Varian, Inc.	Palo Alto, USA
UV-illuminator	Geldoc™ XR	BIO-RAD	Hercules, USA

Table 9 Equipment.

Application	Software	Company	Headquater
Vector graphic editing	Corel Draw	Corel Corporation	Ottawa, Canada
Image processing and analysis	ImageJ	Wayne Rasband NIH	public domain
Image acquisition	Quantity One 1-D Analysis Software	BIO-RAD	Hercules, USA
Plotting and data imaging	Sigma Plot 2001	Sysat Software Inc.	San Jose, USA
Primer design	Primer		
qPCR	MyiQ™	BIO-RAD	Hercules, USA
qPCR	iQ5	BIO-RAD	Hercules, USA
Spectrophotometry	CaryWinUV	Varian, Inc.	Palo Alto, USA
Sequence analysis	scftk	Dr. Zsurka	in house

Table 10 Software.

2. 5 Patients and samples

All experiments with human samples were performed according to the guidelines of the University Ethical Comission. All patients or their care attendants gave written informed consent for the scientific use of their anonymized data and samples. The clinical information needed was provided by the Departments of Epileptology and Neurology, University Bonn.

All muscle samples were obtained after routine diagnostic skeletal muscle biopsy and all brain samples after therapeutical hippocampectomy of patients with drug resistant temporal lobe epilepsy. The samples were used either for direct DNA isolation and biochemical analysis, or were frozen in liquid nitrogen. When enough tissue material was available from the selected samples, they were used for mitochondrial purification and isolation of mitochondrial DNA enriched samples.

When possible, DNA was isolated as well from urine, blood samples and skin fibroblast from the patients and their relatives. Aliquotes cultured skin fibroblasts were frozen in liquid nitrogen.

All control samples used in this study were from age matched individuals without mitochondrial diseases.

2. 6 Cell culture

Skin fibroblasts from control patients, patients with mitochondria maintenance disorders and Charcot–Marie–Tooth neuropathy were grown in cell culture. The fibroblast samples were stored in liquid nitrogen (at -195°C) in cryo reaction tubes. They were taken into culture, after quick thawing at 37°C. The cells were grown into tissue culture flasks (with size of 25 cm², 75 cm² and 175 cm²) in high-glucose DMEM medium containing 10% FBS, 200 µM uridine and 1% penicillin-streptomycin. After the cells have attached to the flask the medium was exchanged with fresh one. The cells were grown in humid CO_2 incubator at 37°C and 5% CO_2.

2. 6. 1 Cell passaging

By 95% density of the cells in the flask they were split for further breeding. The old fibroblast media was discarded by aspiration and the cells were washed with 1× PBS. To detach the cells from the 175 cm² flask 5 ml (1 ml for 25 cm² and 3 ml for 75 cm² flsks) of 2.5 mg/ml trypsin solution was used for 5 minutes at 37°C. The trypsinization was controlled under microscope. After the cells were detached, the activity of the trypsin was blocked with the addition of fibroblast media, and the cells were alliquoted into new tissue culture flasks with fresh media.

2. 6. 2 Cell counting

Detached cells resuspended in 20 µl medium were counted on Neubauer haemocytometer under light microscope. The counted cells from three repeats of eight type A squares of the haemocytometer, with volume 1 mm^3 (or 1 µl = 0.001 ml) each, were averaged and the data was used to calculate the amount of cells with the formula:

Concentration of cells/ml = (total cells counted/ # of squares used)(10^4 ×dilution factor)

2. 6. 3 Freezing of cells

Trypsinized cells resuspended in desired amount of media were centrifuged for 5 minutes at 1000× *g*. The supernatant was discarded by aspiration and the cell pellet was resuspended in ice cold freezing media. The cells were alliquoted in cryo reaction tubes. At first they were stored at -20°C for an hour and subsequently at -80°C for 24 hours. Finally, the cells were transferred to liquid nitrogen.

2. 6. 4 Cell pelleting

Cells were trypsinized as for passaging (2. 3. 1) and were transferred into a Falcon tube, and PBS was filled in up to 50 ml final volume. At this step the cells were checked for vitality and counted. After spinning the cells for 5 minutes at 3000 rpm, the pellet was resuspended in 750 µl PBS and transferred to an Eppendorf tube to which PBS was added up to approximately 1500 µl. The tubes were centrifuged for 5 minutes at 3000 rpm and following 50 seconds at 10,000 rpm. The supernatant was discarded by pipeting and the pellet was frozen directly at -20°C or was directly used for DNA extraction, or enzymatic measurements (Siddiqui *et al*., 2012).

2. 7 Depletion and repopulation experiments

The mtDNA depletion experiments were performed over 32 days. 16 flasks (75 cm²) derived from a single passage were used for the experiments. Samples were collected on the first day before depletion and afterwards every second day. The depletion was achieved by adding
2', 3'-dideoxycytidine (ddC) with final concentration of 20 µM. The ddC was exchanged with fresh one every second day. The ddC treatment continued 12 days for mtDNA depletion, on the 14th day the ddC containing medium was discarded and the cells were left for mtDNA recovery in fresh fibroblasts medium, which afterwards was exchanged every second day. Cells were counted every time when a sample was collected (Brown and Clayton, 2002). The cell pellets were frozen directly at -20°C for further DNA extraction.

2. 8 Hydrogen peroxide treatment of fibroblasts

To examine the effect of oxidative stress, hydrogen peroxide treatment experiments were carried on control fibroblast cell line. The cells were 70% confluent at the start of the experiments. After washing of the cells with PBS, medium containing the desired concentration of H_2O_2 (stock solution contains 30 wt. % in water) – 250 µM, 500 µM and 750 µM, was added to the flasks. For each concentration of the H_2O_2 treatment there were three repeats, and a control flask, incubated only with medium. After 10 minutes incubation the medium was discarded and the cells were washed with PBS and trypsinized. The cells were pelleted as in 2. 3. 5 and the pellet was used for DNA isolation.

2. 9 Purification of mitochondria from human brain samples

The protocol used for mitochondria purification is adapted from Kudin *et al*., 2004. The solutions used in this protocol are MSE solution, MSE-nagarse solution and MSE-digitonin solution; they were all chilled before the experiment.

Fresh tissue sample was obtained after brain surgery of epileptic patients and the brain slice was immediately transferred into MSE solution. After mincing the brain with a sterile scalpel, ice-cold MSE-nagarse solution was added and the tissue was homogenized at 600 rpm by potter homogenizer. Nagarse is a protease having strong and unspecific proteolytic activity (Picard *et al*., 2011). As a next step 20 ml of ice-cold MSE solution was added to the homogenate and it was centrifuged for 4 minutes at 2000× *g* in order to remove the nuclei. The mitochondria rich supernatant was filtered through cheesecloth and centrifuged for 9 minutes at 12,000× *g*. The pellet was dissolved in 10 ml ice-cold MSE-digitonin solution in order to permeabilize the synaptosomes. The prepared solution was homogenized 8 to 10 times in glass-homogenizer, until having homogenous suspension. As a final step it was centrifuged at 12,000× g for 11 min and the pellet was dissolved in 300 µl of MSE buffer. The suspension contained purified mitochondria, confirmed by biorespiration measurement of respiratory control (RC) value, performed by Dr. Kudin in our lab.

The RC value is calculated as a ratio between state 3 of respiration of the mitochondria (triggered by addition of 250 µM ADP to the mitochondrial suspension) and resting state 4 of the mitochondria. The higher the RC value, the better the quality of the mitochondria in the suspension. Afterwards, the protein content was determined spectrophotometrically (about 20 mg protein/ml), by Loury method (Kudin *et al*., 2004). The samples were directly used for mitochondrial DNA isolation or were stored in liquid nitrogen. The mtDNA enrichment obtained from isolated mitochondria has been checked by qPCR and was found to be at least 10 fold higher as compared to the total DNA.

2. 10 Mitochondria purification from human muscle samples

The purification of mitochondria from muscle was performed by Dr. Kudin in our laboratory, applying the protocol described by Kudin *et al*., 2005.

2. 11 DNA isolation with QIAamp DNA Mini Kit

Column purification of DNA was performed as described in the manual of QIAamp DNA Mini Kit (QIAGEN N.V., Venlo, Netherlands). Each sample was eluted twice in 200 µl elution buffer provided with the kit and was stored without freezing at 4°C.

2. 12 DNA concentration quantitation

The concentration and purity of the isolated DNA were estimated by measurement of its optical density (OD) with a spectrophotometer. Double-stranded DNA shows ultraviolet light absorption maximum at wavelength λ = 260 nm, while the proteins absorption maximum is at wavelength
λ = 280 nm. The DNA concentration (C) in ng/µl is calculated by the formula:

$C = [–36.0(OD_{280nm}–OD_{320nm}) + 62.9(OD_{260nm}–OD_{320nm})] \times$ dilution factor

The total yield of the isolated DNA (µg) is calculated by multiplying the DNA concentration C by the purified sample volume (ml). The ratio OD_{260nm}/OD_{280nm} provides an estimate of the degree of purity of the DNA. The quality of the DNA was considered suitable when the ratio was between 1.8 and 2. The DNA purity can be estimated by correcting for impurities detected at λ = 320 nm, OD_{320nm} with the formula:

DNA purity = $(OD_{260nm}– OD_{320nm})/(OD_{280nm}–OD_{320nm})$

2. 13 Gel electrophoresis

All PCR products with expected size bigger then 500 bp were visualized by agarose gel (1%) electrophoresis.

PCR products smaller then 500 bp were electrophoretically separated by polyacrylamyde gel electrophoresis, PAGE. The PCR products from all primer pairs used in the qPCR were optimized and checked for purity and size on PAGE gels. Multiplex PCR products, with size smaller then 500 bp were loaded on 3% agarose gels.

Reagents	Volume (ml)
5× TBE	2
Acrylamide	2.5
10% APS	0.1
TEMED	0.01
dd water up to 10 ml	

Table 11 Mixture for PAGE gel.

2. 14 Long-Range PCR (LR-PCR)

LR-PCR was used for the amplification of large fragments of DNA, up to 27–30 kb. LR-PCR was performed with *TaKaRa LA Taq Hot Start (HS)* or JumpStart AccuTaq LA enzymes (Table 12). They contain LA Taq™ (LA, long and accurate) polymerase mixture constituted by a highly processive thermostable polymerase and second thermostable polymerase with 3'→5' exonuclease activity (proofreading activity), which leads to strong reduction of the misincorporation errors, and supports the production of longer PCR amplicons, with greater accuracy. The *TAKARA LA Taq HS* kit contains a monoclonal antibody specific for the LA Taq™, which binds to it and inhibits the polymerase activity until the temperature escalates. In this way mis-priming and formation of primer dimmers during temperature elevation is being avoided. The antibody is being denatured in the first step of DNA denaturation. The PCR program (Table 13) and PCR mixtures (Table 12) were optimized by modifying the original protocols provided by the producer (TAKARA BIO INC and Sigma Aldrich).

Reagent	**Volume (µl)**
10× TaKaRa reaction buffer	2.5
TaKaRa dNTPs (2.5 mM)	2.5
FW primer (25 pmol/µl)	0.2
RW primer (25 pmol/µl)	0.2
TaKaRa LA Taq (HS) / AccuTaq LA	0.125 / 0.25
DNA (2 ng/µl)	10
ddH2O	up to 25 µl

Table 12 *TaKaRa LA Taq (HS)* and JumpStart AccuTaq LA LR PCR mixture.

PCR program	
1. 95°C, 2:30 min	
2. 92°C, 0:20 min 3. 68°C, 14:00 min	10×
4. 92°C, 0:25 min 5. 68°C, 16:00 min	20×
6. 72°C, 10:00 min	
7. 15°C for ever	

Table 13 LR-PCR program.

5 µl of the PCR products with 5 µl loading buffer were mixed and loaded on 1% agarose gel, and 1 kb DNA ladder or 2-log ladder for band identification. After electrophoresis at 180V for 1h, of the gel picture was visualized and captured with 3CCD Video Camera with 4 megapixels resolution, with UV-illuminator Geldoc^{TM} XR with excitatory wavelength between 254 and 365 nm. Deleted molecules were detected as bands of decreased size.

2. 15 Single-molecule PCR (smPCR)

In order to avoid laborious cloning procedures and to capture and analyze single-molecules of DNA and map their deletions, I have established a modified version of the single-molecule PCR (smPCR) described by Kraytsberg *et al*., 2008 (Tables 14 and 15).

Reagent	Volume (µl)
10× TaKaRa reaction buffer	2.5
TaKaRa dNTPs (2.5 mM)	2.5
FW primer (50 pmol/µl)	0.1
RW primer (50 pmol/µl)	0.1
TaKaRa LA Taq (HS)	0.125
Diluted DNA*	1
ddH2O	up to 25 µl

*diluted 10×, 100×, 1000× etc. mtDNA

Table 14 *TaKaRa LA Taq (HS)* smPCR mixture.

PCR program	
1. 95°C, 2:30 min	
2. 92°C, 0:20 min	10×
3. 68°C, 14:00 min	
4. 92°C, 0:25 min	32×
5. 68°C, 16:00 min	
6. 72°C, 10:00 min	
7. 15°C for ever	

Table 15 Single-molecule PCR program.

The DNA used in the smPCR is diluted to such an extent that in a set of repeats of the same sample only part of the repeat reactions would give a product. Firstly, a pilot experiment was performed for each analyzed sample (Figure 13a). The pilot experiment includes serial dilutions of the DNA in five repeats for each dilution, to adjust the right mtDNA concentration in order to detect single mtDNA molecules. On Figure 13a, a pilot experiment depicts the effect of serial mtDNA dilution and the decrease in the number of molecules detected in every step. For this sample at 1000× dilution there are still multiple bands in a single lane, therefore the right mtDNA single molecule concentration should be checked at even higher dilution (10,000×). For each gel electrophoresis a line with PCR product from undiluted mtDNA from the same sample was used as a PCR positive control (marked with C on Figure 13a). After determination of the right mtDNA dilution, a smPCR with a larger set of repeats (15–20) was performed (Figure 13b).

After successful amplification of single-molecule amplicons, they were either cut out of the agarose gel (Figure 13, red rectangles), the DNA was purified with QIAquick Gel Extraction Kit and reamplified; or PCR product, 30 fold diluted in double distilled water, was used for the re-amplification. The primers used in the re-amplification PCR were located within the amplified region and by ‘walking’ from both ends in the amplified product with different primers we aimed flanking of each deletion as close as possible, to size not exceeding 1500 bp. The reamplified PCR products were purified with QIAquick PCR Purification Kit and the exact breakpoints were determined by sequencing.

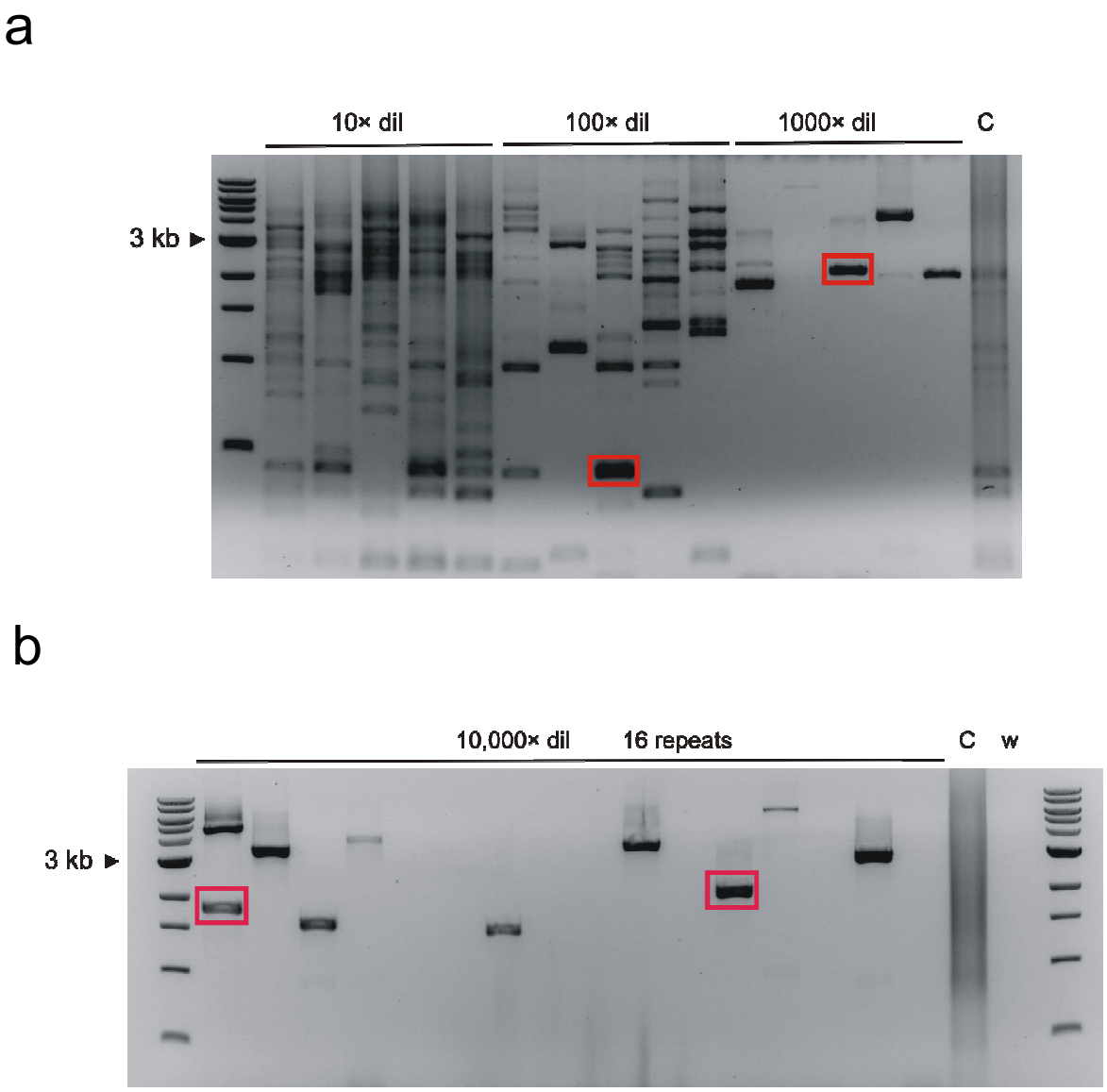

Figure 13 Single-molecule PCR. (**a**) smPCR pilot experiment for adjusting the right concentration of the mtDNA, for capturing single molecules, (**b**) smPCR in a big set of 16 repeats with optimized mtDNA concentration; C, undiluted sample; w, water control; red box, gel cut outs used for sequencing.

2. 15. 1 mtDNA deletions quantification by smPCR

In order to estimate the amount of deletions in a sample, two smPCRs with two different primer combinations were performed. The first PCR primer pair is amplifying either almost the whole mtDNA genome (10F/16,496R) or just the mtDNA major arc (3137F/45R), that is prone to deletion formation. The second primer pair amplifies a shorter region of the small arc (16,520F/4833R), which usually does not contain deletions and should be giving an estimate of the total amount of wild-type molecules. The ratio of deletions is calculated by

comparison of the number of positive PCR reactions and the degree of dilution of the total and deleted mtDNA molecules (Zsurka *et al*., 2008; Vielhaber *et al*., 2013; Kornblum *et al*., 2013). Both PCRs were performed with *TaKaRa LA Taq (HS).* The reaction mix and PCR program for total mtDNA estimation are the same as the ones used for the long product, but with 3 minutes elongation time (Table 14 and 15).

2. 16 Long extension PCR

Duplicated mtDNA molecules were detected by using a long extension PCR method modified from Williams *et al*., 2010. Primers 1057F and 1144R were used to amplify a short mtDNA fragment and additional extended elongation time enabled the polymerase to amplify fragments of several thousand base pairs in size. This kind of long molecules can be amplified along the short fragments, if more than one copies of the primer-binding region are present on some of the mtDNA molecules. The reaction mix and PCR program for long extension PCR are the same as the ones used for single-molecule PCR (2.12). All PCR products were analysed on agarose gel.

2. 17 mtDNA copy number determination

The mitochondrial DNA copy number was evaluated by quantitative Real-Time PCR (qPCR), a modified PCR method allowing the monitoring of targeted mtDNA amplification in *status nascendi*. For the detection of DNA products in qPCR either the fluorescent dye SYBR® Green I or sequence-specific DNA probes (oligonucleotides) labelled with a fluorescent reporter, such as TaqMan® Probe were used. In both cases the qPCR was performed with three different concentrations of the DNA sample – 5 ng/µl, 10 ng/µl or 20 ng/µl, with three repeats for each dilution. All primer pairs were optimized and checked by PAGE.

2. 17. 1 SYBR® Green I qPCR

The cyanine dye SYBR Green I binds preferentially to dsDNA and intercalates between the DNA strands and therefore stains the DNA in a not sequence specific way. The formed DNA/dye-complex absorbs blue light at λmax = 488 nm and emits green light at λmax = 522 nm. This increase in fluorescence intensity, which is measured at each PCR cycle, allows the DNA concentrations to be quantified. The primers used for total mtDNA determination were 3922F and 4036R. The primers used to detect the 7S DNA levels were 16,520F and 35R.

Reagent	Volume (µl)
iQ™ SYBR® Green Supermix	11.9
FW / RW primer mix (12.5 pmol/µl each)	0.6
DNA* (ng/µl)	12.5

* 1.6 ng/µl, 0.8 ng/µl or 0.4 ng/µl

Table 16 SYBR® Green qPCR mixture.

In order to verify the specificity of the product, a melting curve analysis was performed at the end of the qPCR. During it the temperature increases constantly from 55°C to 95°C, leading to melting of the DNA. At a specific temperature the dsDNA denatures and at that point the SYBR Green I is set free leading to decrease in the fluorescence. In case the PCR is specific only one high fluorescence peak should be observed. In table 17 this analytical phase corresponds to step 6.

PCR program	
1. 95°C, 7:00 min	
2. 95°C, 0:15 min 3. **°C, 1:00 min	45×
4. 95°C, 1:00 min	
5. 55°C, 1:00 min	
6. 55°C, 0:10 min + 0.5°C per cycle	80×
7. 15°C for ever	

** primer specific annealing temperature (in the range of 55°C to 70°C)

Table 17 SYBR Green qPCR program.

2. 17. 2 TaqMan® qPCR

Specific probes as TaqMan® assure higher specificity of the method, as they permit detection only after hybridization of the probe with its complementary DNA target (Holland *et al.*, 1991). The TaqMan probe has fluorescence reporter on one end and a quencher of fluorescence on the opposite end. The close proximity of the reporter to the quencher prevents the detection of fluorescence. The probe anneals to the complementary DNA strand and when the Taq Polymerase is synthesizing the new strand, it is fulfilling as well its 5'→3' exonuclease activity and it breaks down the probe and the unquenched emission of fluorescence gets free. Due to breakdown of the probe and release of its reporter in every cycle of the PCR, the increase of the targeted product can be detected.

Reagent	Volume (µl)
10× JumpStart reaction buffer containing 1.5% Triton X-100	2.5
$MgCl_2$	2.5
DMSO	0.38
dNTPs (25 mM)	0.2
50× ROX reference dye	0.13
FW primer (12.5 pmol/µl)	0.3
RW primer (12.5 pmol/µl)	0.3
TaqMann® Probe (12.5 pmol/µl)	0.2
JumpStart *Taq* polymerase	0.13
DNA* (ng/µl)	12
ddH_2O	up to 25 µl

*1.6 ng/µl, 0.8 ng/µl, 0.4 ng/µl

Table 18 TaqMann® qPCR mixture.

The PCR program used for Taqman qPCR is the same as for SYBR Green qPCR (Table 17).

2. 17. 3 Analysis of qPCR data

Data collected with qPCR were analyzed by SigmaPlot and were fitted with a sigmoidal regression curve, Chapman curve (Zhao and Fernald, 2005). The sigmoidal regression curve has four parameters – y_0 , a, b and c, determining its shape and the degree of exponential function. The parameters are provided by the software from the equation:

$$y = y_0+a(1-e^{-bx})^c$$

The Ct value is calculated at the inflection point of the fluorescence sigmoidal curve from the equation:

$$Ct = \ln(c)/b$$

As each sample was in triplicate the standard deviation was calculated. The Ct values for *Kir4.1* (reference gene), single nuclear gene, were used for calculation of the mtDNA copy number (Zsurka *et al*., 2008). Firstly, the cycle number difference was calculated by subtracting the Ct values of the mtDNA fragment (Ct_{mito}) of interest from the Ct values of the reference gene (Ct_{nuc}): $Ct_{nuc}–Ct_{mito}$. This value was used to calculate the mtDNA copy number

(CN). The relation between the diploid single nuclear gene and a mitochondrial sequence was calculated as follows:

$$CN = 2 \times 2^{Ctnuc - Ctmito}$$

The serial dilution (three different concentrations) of the measured Ct values of each DNA sample was plotted against their initial concentration in a semilogaritmic scale. The total amount of DNA is being duplicated in each PCR reaction cycle if the efficiency of the process was 100%. The negative correlation slope and the intercept should have a value of -1 and the slope *s* and the efficiency *E* are related to each other as following:

$$E = (1/s)(-100)$$

2. 18 Evaluation of mtDNA integrity

A qPCR-based method was used for detection of presence or absence of strand breaks between chosen primer positions, and evaluation of mtDNA integrity and quality. The method includes two PCRs performed on the same 96-well qPCR plate (assuring the same PCR conditions), for the same sample. Triplets of two different mtDNA dilutions, 20 ng and 10 ng DNA, were used. The first PCR amplifies a short product, flanked by primers 1057F and 1144R, with size of 88 bp and the second PCR amplifies a long 5379 bp PCR product, amplified by primers 11,226F and 35R. The method compares the amplification of the big mtDNA fragment to that of the small fragment of the mtDNA, with the later representing the overall amount of mtDNA. Any damage in the mtDNA would prevent the polymerase to amplify a full-length product. The further away the primers, the higher the chance that blocking damage occurs between them. Cycle number differences between the two PCRs (dependent on the short and the long product quality) were measured in the qPCR reactions and the data from the control untreated samples was used as reference. For all samples, first, the relative amplifiability difference was calculated by subtracting the Ct values for the long product from the wild-type mtDNA Ct values. Then the control sample amplifiability was taken as reference, to which the treated samples were compared in a ratio. In this case the control sample represents a value of 1, all treated samples containing less intact mtDNA should show a value smaller than 1. The calculations are performed as described previously.

Reagent	Volume (µl)
5× Ranger reaction buffer containing dNTPs	5
50× ROX reference dye	0.128
Ranger DNA polymerase	0.156
FW/ RW primer mix (12.5 pmol/µl)	0.6
500× diluted SYBR Green (in DMSO)	0.12
DNA (1.6 ng/µl or 0.8 ng/µl)	12
ddH_2O	7

Table 19 Ranger qPCR mixture.

The PCR program for mtDNA integrity determination is the same as described previously in Table 17, with elongation time of 14 min, at step 3.

2. 19 Ligation-Mediated PCR (LM-PCR)

I have established a modified version of the ligation-mediated PCR (LM-PCR) described originally by Kang *et al*. (1997), for detection of free DNA ends. In opposite to the original paper, blunt ends required for linker ligation were created by treating the DNA samples with Quick Blunting Kit (NEB) or Mung Bean nuclease for detection of free 5' or 3' ends, accordingly.

The Quick Blunting Kit contains T4 polymerase that is having 5' to 3' polymerase activity and 3' to 5' exonuclease activity. The kit contains T4 Polynucleotide Kinase for phosphorylation of the 5' end of the blunted molecules and its subsequent ligation.

The Mung Bean nuclease is a single-strand specific DNA endonuclease, which degrades all 3' and 5' single-stranded overhangs, leaving 5'-phosphorylated blunt ends.

After filling in or removing overhangs, the molecules represent blunt ends that are ready to be ligated. The ligation was done by using a T4-ligase and a linker. The linker 'adaptor' used in the LM-PCR has non-biological sequence and is prepared by the annealing of two complementary oligonucleotides, LMP25 and LMP11, with 25 bp and 11 bp length accordingly:

5'–GCGGTGACCCGGGAGATCTGTATTC–3'
3'–CTAGACATAAG–5'

The different length of the primers allows the formation of blunt end only on one side of the linker, which would prevent double sided ligation in the later steps (Kang *et al*., 1997).

Reagent	Final Concentration	PCR program	
LMP25	25 pmol/µl	1. 95°C x 3:00 min	185×
LMP11	25 pmol/µl	2. 95°C x 1:00 min	
TE Buffer		-0.5°C per cycle	

Table 20 Linker annealing mixture and conditions.

After ligation the reaction mix was used in blunt-end ligation-mediated PCR, to which I am going to refer to as LM-PCR, as in the original protocol by Kang *et al*., 1997; taking in account the introduced changes in the protocol. The LM-PCR reaction is using one primer complementary to the linker and a specific primer on the mtDNA for the 5' end detection. For detection of the 3' end the mtDNA primer should be a reverse one. The amplified products were purified and the free ends were determined by sequencing.

2. 19. 1 T4 polymerase blunting of mtDNA

Quick Blunting™ Kit was used to perform T4 polymerase blunting of mtDNA. The T4 DNA polymerase has both 3'→5' exonuclease activity, removing 3' overhangs and 5'→3' polymerase activity, filling 5' overhangs, in this way it creates blunt ends at the site of the original 5' end of one strand. The kit contains a T4 polynucleotide kinase which provides a phosphorylation of the 5' end, important for the following ligation of the linker 'adaptor'.

The Blunt Enzyme Mix is supplied from the company in: 100 mM KCl, 10 mM Tris-HCl (pH 7.4), 0.1 mM EDTA, 1 mM dithiothreitol, 0.1% Triton X-100 and 50% Glycerol. The 1X Blunting Buffer contains: 100 mM Tris-HCl, 50 mM NaCl, 10 mM MgCl2, 0.025% Triton X-100, and 5 mM dithiothreitol, with pH 7.5 at 25°C.

Mix	Volume (µl)	Incubation	Inactivation
DNA – 0.2 µg			
10× Blunting buffer	2.5		
1mM dNTPs	2.5	30 min at RT°C	10 min at 70°C
Blunt Enzyme Mix	1		
ddH_2O	up to 25 µl		

Table 21 Quick Blunting Kit treatment.

2. 19. 2 Mung Bean Nuclease blunting of mtDNA

The Mung Bean Nuclease removes single stranded ends in both orientations and leaves a phosphorylated 5' end. The Mung Bean Nuclease Reaction Buffer contains: 30 mM NaCl, 50 mM sodium acetate, 1 mM $ZnSO_4$, with pH 5 at 25°C.

Mix	Volume (µl)	Incubation	Inactivation
DNA – 0.2 µg (in water)	30	30 min at 30°C	Purification with QIAamp DNA Mini Kit
10× Mung Bean buffer	4		
Mung Bean Nuclease	0.2		
ddH_2O	up to 40 µl		

Table 22 Mung Bean Nuclease treatment.

2. 19. 3 S1 nuclease treatment of mtDNA

S1 nuclease degrades single stranded DNA and RNA and removes 3' and 5' overhangs, by leaving phosphorylated 5' end. It recognizes nicks and single nucleotide lesions on the nucleic acids and cuts them.

Mix	Volume (µl)	Incubation	Inactivation
DNA – 0.2 µg (in water)	30	30 min at 30°C	Heat deactivation at 70°C + 1 µl EDTA (optional); purification with QIAamp DNA Mini Kit
10× S1 reaction buffer	4		
S1 nuclease	0.2		
ddH_2O	up to 40 µl		

Table 23 S1 nuclease treatment.

2. 19. 4 Ligation of linker

The blunt-ended mtDNA samples were ligated with the linker 'adaptor' via T4 ligase in the following reaction:

Mix	Volume (µl)	Incubation	Inactivation
DNA – 0.2 µg blunted	50	O/N at RT°C	10 min at 65°C
Linker	5		
10× T4 ligase buffer	6.2		
T4 ligase	1		

Table 24 Linker ligation.

2. 19. 5 Amplification of linker ligated ends

The blunt-end LM-PCR was performed always with LMP25 primer and a mitochondrial primer with specific location and orientation.

Reagent	Volume (µl)
5x Ranger Reaction buffer containing dNTPs	5
LMP25 (25 pmol/µl)	0.3
FW/RW primer (25 pmol/µl)	0.3
Ligated DNA	1
Ranger DNA Polymerase	0.156
ddH_2O	up to 25µl

Table 25 LM-PCR mixture.

PCR program	
1. 95°C, 2:30 min	
2. 92°C, 0:20 min	10×
3. 63°C, 1:00 min	
4. 92°C, 0:25 min	25×
5. 68°C, 1:00 min	
6. 72°C, 1:00 min	
7. 15°C for ever	

Table 26 LM-PCR program.

2. 19. 6 Single-molecule LM-PCR

In order to determine the ends of the detected molecules, a single-molecule LM-PCR was performed, following the same principles as in smPCR, but with linker specific primer in combination with mitochondria specific primer.

Reagent	Volume (µl)
5× Ranger Reaction buffer containing dNTPs	5
LMP25 (50 pmol/µl)	0.6
FW/RW primer (50 pmol/µl)	0.6
Ligated DNA	1
Ranger DNA Polymerase	0.3
ddH_2O	up to 25 µl

Table 27 Single-molecule LM-PCR mixture.

PCR program	
1. 95°C, 2:30 min	
2. 92°C, 0:20 min	10×
3. 63°C, 1:00 min	
4. 92°C, 0:25 min	32×
5. 68°C, 1:00 min	
6. 72°C, 1:00 min	
7. 15°C for ever	

Table 28 Program for single-molecule LM-PCR.

The captured single molecules were cut out from the gel and were purified with QIAquick Gel Extraction Kit. Each purified PCR product was reamplified once with a LMP25 and a different mitochondrial primer within the fragment, to assure the amplification of mitochondrial, but not nuclear PCR product. And second, the product was checked by reamplification with double amount of LMP25 primer, to exclude short non-mitochondrial fragments ligated with LMP25 on both of their ends.

2. 20 Multiplex PCR

Multiplex PCR was used for the detection of two different deletions (the common deletion and a deletion of interest, simultaneously), on 3% agarose gel. The acquired data images were analyzed by ImageJ (Chapter 2. 21).

Reagent	Volume (µl)
10× TaKaRa reaction buffer	2.5
TaKaRa dNTPs (2.5mM)	2.5
FW primer (25 pmol/µl)	0.8
RW primer 1 (25 pmol/µl)	0.6
RW primer 2 (25 pmol/µl)	0.2
TaKaRa La Taq (HS)	0.125
DNA (2 ng/µl)	10
ddH_2O	up to 25 µl

Table 29 *TaKaRa LA Taq (HS)* multiplex PCR mixture.

PCR program	
1. 95°C, 2:30 min	
2. 94°C, 0:20 min	10×
3. 68°C, 3:00 min	
4. 94°C, 0:20 min	32×
5. 68°C, 3:00 min	
6. 72°C, 7:00 min	
7. 15°C for ever	

Table 30 PCR program for multiplex PCR.

2. 21 Sequencing PCR

The PCR used for re-amplification of smPCR products was performed with LongAmp *Taq* DNA polymerase.

Reagent	Volume (µl)
5× LongAmp reaction buffer	5
dNTPs (2.5 mM)	2.5
FW primer (25 pmol/µl)	0.2
RW primer (25 pmol/µl)	0.2
LongAmp Taq	0.25
DNA*	1
ddH_2O	up to 25µl

*1:30 diluted smPCR product or gel isolated smPCR product

Table 31 LongAmp PCR mixture.

PCR program	
1. 95°C, 2:30 min	
2. 94°C, 0:20 min	10×
3. 63°C, 2:50 min	
4. 92°C, 0:25 min	25×
5. 68°C, 3:00 min	
6. 72°C, 1:00 min	
7. 15°C for ever	

Table 32 PCR program for sequencing PCR.

2. 22 PCR purification

The PCR product column purification was performed according to the recomendation of the manufacturer (QIAquick PCR Purification Kit; QIAGEN N.V., Venlo, Netherlands). The PCR product purification after excision from agarose gel was performed as described in the manual of QIAquick Gel Extraction Kit (QIAGEN N.V., Venlo, Netherlands).

2. 23 Sequencing

After PCR purification, the DNA concentration of the amplicons was estimated with spectrophotometer and the samples were send for sequencing, performed by a commercial sequencing service at Eurofins MWG / Operon, Ebersberg, Germany. The sequencing primers mainly were identical with the PCR primers.

2. 24 ImageJ analysis

Semiquantitative analysis for deletions was performed by using Java-based image processing program ImageJ. The region of interest (ROI) on each LR-PCR picture was selected for every sample. The ROI included the wild-type (wt) band and the region under it, containing deleted molecules, the same ROI was used for all samples. By using the plotting option of ImageJ a two-dimensional graph of the intensities of pixels along the ROI was displayed. The X-axis represents distance along the ROI and the Y-axis is the pixel intensity. The peak amplitude corresponds to the intensity of the bands in the ROI. In this case, the wt band has the highest peak of intensity. A ratio between the wt band peak and the summed deletion peaks was calculated, and used for semiquantitative measurement of the deletions present in each sample. The background intensity was subtracted in the calculations. The same method was used for analysis of the images obtained by multiplex PCR, but in this case the intensity for the common deletion was compared to the intensity of the deletion of interest.

2. 24 Statistical analysis

Microsoft Office Excel was used for applying the unpaired, two-sided student's *t*-test in order to determine significant difference between pairs of data sets. It was used to calculate the probability of occurrence of a positive zero hypothesis, which is determined by the identity of two empirical determined mean values belonging to two sample populations. The level of significance was set to $p<0.05$ or smaller.

One-way analysis of variance (ANOVA) was used to analyse differences between the mean values of multiple (more then two) groups of data sets. ANOVA is based as well on the null hypothesis; in case of null hypothesis, all samples are random samples of the same population. Once a group of samples was identified as not random, a Dunnett's post-hoc test was applied to check which means differ. The ANOVA test and the Dunnett's post-hoc test were performed by Dr. Zsurka.

3. Results

3. 1 MGME1

Multiple mitochondrial deletions and mtDNA depletion syndromes (MDS) constitute a group of diseases known as mtDNA maintenance disorders (Blakely, 2012). The pathological changes and clinical manifestations in these diseases may affect single tissues or the function of the whole organism. They appear in different ages and have diverse impact on the patients (El-Hattab, 2013). The pathologic mechanisms in this group of diseases affect either the salvage pathway of deoxyribonucleoside 5'-triphosphates for mtDNA synthesis or the mtDNA replication. Mutations in *POLG*, *POLG2 and C10orf2* genes, all components of the replication machinery, were previously described to be involved in the disruption of the mtDNA replication and disease. Recently, *DNA2* (Ronchi *et al.*, 2013) and a truncated version of protein encoded from the nuclear *FEN1* gene (FENMIT) (Kazak *et al.*, 2013) have been added to the group of genes possibly involved in mitochondrial maintenance, by influencing its repair and replication. Nevertheless, many patients remain poorly diagnosed and problematic for treatment, as the exact molecular mechanisms and system damage are not clear (Kornblum *et al.*, 2013).

3. 1. 1 Patients with mtDNA maintenance disorders (MMDs)

Respiratory chain deficiency is the main biochemical trait in mitochondrial disorders. As the muscle is very rich of mitochondria, it is commonly used in the diagnostics for checking the mitochondrial function. Muscle containing dysfunctional mitochondria often displays accumulation of highly proliferating mitochondria or so called ragged-red fibers (RRF). I was working with samples from a Lebanese family having three children affected by MMD (P1976, P2061 and P3737) and unknown cause of the disease. The three patients showed respiratory chain insufficiency, confirmed by skeletal muscle histochemical staining and by biochemical measurements in fibroblasts (data not shown), performed by Dr. Schoeler. All affected children have similar symptoms since early childhood and have multisystemic mitochondrial disorder. The clinical symptoms include ptosis and mild PEO, mental retardation, respiratory distress and skeletal muscle waste. The family pedigree is shown on Figure 14a.

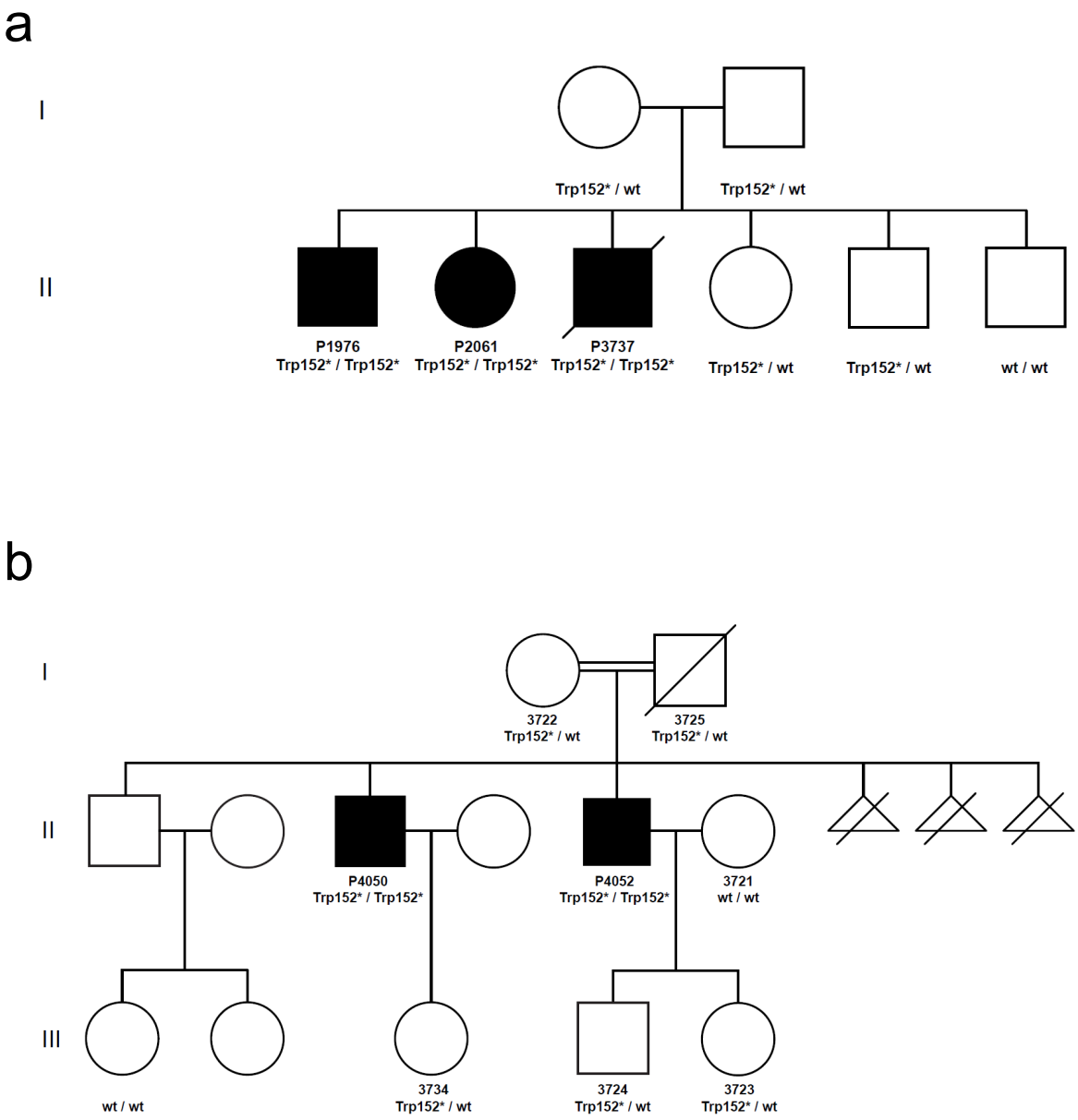

Figure 14 Pedigrees of MGME1 patients. (**a**) Lebanese Family (Family I) carrying *MGME1* mutation. This family carries c.456G>A (p.Trp152*) mutation in *MGME1* gene; (**b**) Pedigree of Italian Family (Family II) carrying *MGME1* mutation. This family carries c.456G>A (p.Trp152*) mutation in *MGME1* gene. Open symbols indicate healthy individuals; closed symbols indicate affected members of the family. Diagonal bar through the symbol denotes deceased individuals (Kornblum *et al.*, 2013).

Mutations in *POLG*, *POLG2 and C10orf2*, for the three patients, were excluded by Sanger sequencing, performed by Susanne Beyer, in our lab. As the patients did not carry any mutation in the well studied nuclear genes known to cause MMD, thereafter, in collaboration with the Institute of Human Genetics, in Munich, exome sequencing (Haack *et al.*, 2012) of P1976 sample, was performed.

The results from the exome sequencing of P1976, assuming the autosomal recessive inheritance of the disease and the possible mitochondrial targeting of the protein, pointed towards two genes, *SPTLC3* and *C20orf72*, as possible candidates. Both genes encode proteins targeted to mitochondria. Unlike *SPTLC3*, the *C20orf72* gene revealed c.456G>A (p.Trp152*) nonsense mutation in P1976. Following Sanger sequencing of the *C20orf72* gene, in the affected siblings' samples, confirmed the segregation of the mutation; all of them were carrying the c.456G>A (p.Trp152*) mutation in the gene. The healthy siblings were homozygous wild-type for the mutation and the parents were heterozygous carriers.

By targeted MitoExome sequencing (Calvo *et al*., 2012) performed by our collaborators, another affected Italian family (P4050, P4052) carrying the same mutation and clinical manifestation (Figure 14b) was discovered. The list of samples with mutations in the *C20orf72* gene was additionally extended with one sporadic patient from Germany (P931), which was added from our laboratory, by sequencing of the gene in a set of PEO samples, performed by Kerstin Hallman, MSc. Opposite to the other samples, this patient carried a different mutation, c.698A>G (p.Tyr233Cys) in the same gene.

Investigation over the affected protein's primary structure showed that it belongs to the PD-(D/E)XK nuclease super-family, whose members possess various nucleic acid cleavage activities. The c.456G>A (p.Trp152) mutation, discovered in the Lebanese and the Italian family, is placed before the PD-(D/E)XK motif, which would suggest non-functionality of the protein. The mutation discovered in the sporadic case from Germany affects a conservative amino acid residue.

We have decided to rename the enzyme and call it MGME1, standing for mitochondrial genome maintenance exonuclease 1.

3. 1. 2 *In vivo* consequences of *MGME1* mutations

To clarify the molecular consequences of mutation in the *MGME1* gene, all muscle samples from the patients were analyzed by LR-PCR (Figure 15 lower panel). A second sample from patient P4052, taken one year after the first biopsy, was included in the set. One *POLG* muscle sample, carrying the homozygous mutation p.Ala467Thr in the *POLG* gene was included in the study, as a sample rich of mtDNA deletions. LR-PCR was performed also with urine sediment and blood DNA samples from the Lebanese family. Two blood samples from the unaffected father and sister from this family were also included in the panel of samples (Figure 15 upper panel). The primers used for this experiment were primer pair 5462F/45R, amplifying a wild-type 11,153 bp product, covering the mtDNA major arc (Figure 15 upper panel), and primer pair 15,974F/15,623R, amplifying 16,219 bp product, which covers almost the entire mtDNA (16,569 bp) (Figure 15 lower panel).

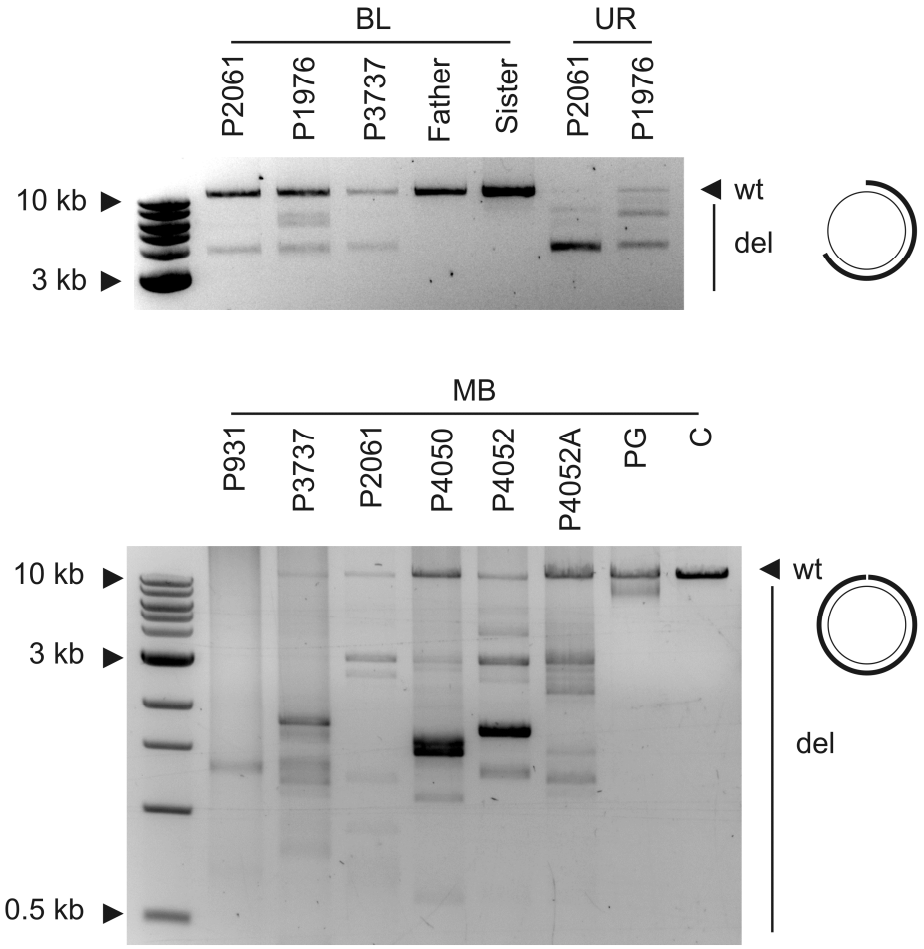

Figure 15 LR-PCR amplification of mtDNA from MGME1 patients. Upper panel, LR-PCR (primer pair 5462F/45R; 11,153 bp wt product) of blood (BL) and urine sediment (UR) samples from Family I. Blood samples from unaffected father and sister from the family were also included in the set. Lower panel, LR-PCR (primer pair 15,974F/15,623R; 16,219 bp wt product) of mtDNA isolated from muscle biopsy (MB) from all affected MGME1 patients included in this study. PG, POLG patient (carrying the homozygous mutation p.Ala467Thr in the *POLG* gene); C, control muscle (30 years old); wt, wild-type sized amplicon; del, deletion-specific PCR products. Thick line unclosed circle (close to the panels) indicates the PCR amplified region of the mtDNA (thin line closed circle). All samples from affected MGME1 patients contain apparent unusually large mtDNA rearrangments. The PG patient shows typical range of deletions. All unaffected members of the family and the controls show only wild-type molecules (Kornblum *et al*., 2013).

Both LR-PCRs detected an increased amount of rearrangements in different tissues from the MGME1 patients. In comparison to the POLG patient (PG) sample, in which most of the deletions were small and visible as high smear, close to the wild-type molecules, the MGME1 samples showed much shorter bands, representing specific pattern for the disease (Figure 15). In the MGME1 patients, the PCR products were small and were lacking most of the mtDNA.

The muscle from P931 carried very high amount of rearrangements, which is in correlation with the most advanced age of that patient at the time of biopsy, compared to the rest of the patients (Table 33).

The quantity of the rearranged mtDNA molecules was estimated by using a modified version of smPCR. In the smPCR the primers 10F and 16,496R were used to amplify a big mtDNA fragment, which amplifies almost the entire mtDNA. Simultaneously, a second smPCR for total mtDNA amount was performed, to amplify part of the minor arc of the mtDNA lying between primers 16,520F and 4833R. In both PCRs the DNA was diluted to such extent that a PCR product would be a result from the amplification of a single molecule. In successful case, half of the repeats would be positive. Most of the samples were screened for deletion amount also by using primer pair 3137F/45R (Table 33).

To calculate the rearrangements amount, the dilution used for getting single molecules was used to calculate the number of single molecules detected for both fragments at the same DNA concentration, and a ratio between the two was calculated. For example, if a sample shows 8 positive PCR bands out of 16 repeats for the wild-type mtDNA fragment at dilution 10^{-4}, at the starting concentration the sample shall contain 8×10,000 or 80,000 PCR products in 16 repeats. If the same sample, for the larger PCR product shows 7 rearrangements out of 16 repeats, at concentration 10^{-1}, the non diluted sample should contain 7×10 bands or 70 bands, and the ratio 70/80,000 would give a result of 0.000875 or 0.0875% deletions.

The quantification showed increased amount of rearrangements in the MGME1 patients, in the range from 0.4% to 1.5% (Table 33). The amount of rearrangements is comparable to the amount of deletions detected in the POLG patient. In MGME1 patients the rearrangements load was much higher when the quantification was performed with the primer pair amplifying almost the entire mtDNA. Thereafter, the observed MGME1 rearrangements are present all over the mtDNA. P931 had the highest amount of deletions, confirming the results from the LR-PCR pictures and this can be explained with the advanced age of the patient and the accumulation of deletions due to aging.

Amplified products from single rearranged mtDNA molecules were mapped and their breakpoints were determined by sequencing. Detected breakpoints are shown schematically on Figure 16a, and a list with the exact breakpoints can be found in Appendix I. As comparison,

I determined additionally deletion breakpoints in the POLG patient, Figure 16b (the exact breakpoints can be found in Appendix II). The POLG patient was having deletions affecting predominantly the major arc of the mtDNA and these rearrangements are visibly shorter then the ones observed in MGME1 patients.

Apart from the bigger size of the rearrangements in the MGME1 patients, many of the molecules did not contain their light strand promoter (LSP) or have lost their light or heavy strand replication origin (O_L or O_H) and were missing more then 2/3 of the mitochondrial genome.

Patients		Primer pairs	
Samples	**Age at biopsy**	**3137F/45R**	**10F/16496R**
MB 1976	10	n.d	$4.4 \times 10^{-4} \pm 1.9 \times 10^{-4}$
MB 3737	23	$5.0 \times 10^{-4} \pm 5.0 \times 10^{-5}$	$4.7 \times 10^{-3} \pm 2.0 \times 10^{-4}$
MB 2061	17	$7.5 \times 10^{-5} \pm 1.5 \times 10^{-5}$	$3.7 \times 10^{-4} \pm 3.5 \times 10^{-5}$
MB 931	57	$1.5 \times 10^{-3} \pm 7.9 \times 10^{-4}$	$1.5 \times 10^{-2} \pm 1.0 \times 10^{-3}$
MB 4050	31	$3.7 \times 10^{-4} \pm 1.9 \times 10^{-4}$	$2.6 \times 10^{-3} \pm 1.4 \times 10^{-3}$
MB 4052	36	$5.9 \times 10^{-4} \pm 4.2 \times 10^{-4}$	$3.7 \times 10^{-3} \pm 2.3 \times 10^{-3}$
MB 4052a	37	$1.4 \times 10^{-3} \pm 1.0 \times 10^{-4}$	$3.8 \times 10^{-3} \pm 1.2 \times 10^{-3}$
MB PG	19	n.d	$4.8 \times 10^{-4} \pm 0.9 \times 10^{-5}$
MB Control	30	$9.0 \times 10^{-7} \pm 0.0 \times 10^{-7}$	$4.2 \times 10^{-5} \pm 2.6 \times 10^{-5}$

Table 33 Amount of deletions in MGME1 muscle biopsy (MB) samples, control muscle and POLG muscle (PG). The quantification was performed by smPCR. All MGME1 patients showed higher amounts of mtDNA rearrangments, in comparison to the control MB. In MGME1 patients the amount of rearrnagments was approximately 10 fold higher when the deletions were estimated with the primer pair covering the entire mtDNA, which confirms the existence of apparent large deletions longer then the major arc.

Out of the 131 detected breakpoints in MGME1 patients, only one was having both breakpoints into the major arc, where most of the deletions are expected. The end positions of the detected rearrangements were laying between 13,000 and 16,000 bp position, as most described classical deletions, but their starting point was located in the minor arc, between the heavy strand origin of replication (O_H) and the heavy strand promoter (HSP), in the 12S ribosomal RNA gene; or downstream of the transcription termination factor mTERF1 binding site (Terzioglu *et al.*, 2013). As the O_L is important for the mtDNA maintenance and molecules that are not having it are supposed to be incapable of replicating (Wanrooij *et al.*, 2012). However, almost all affected individuals had specific breakpoint detected repeatedly, which would suggest their clonal propagation.

a

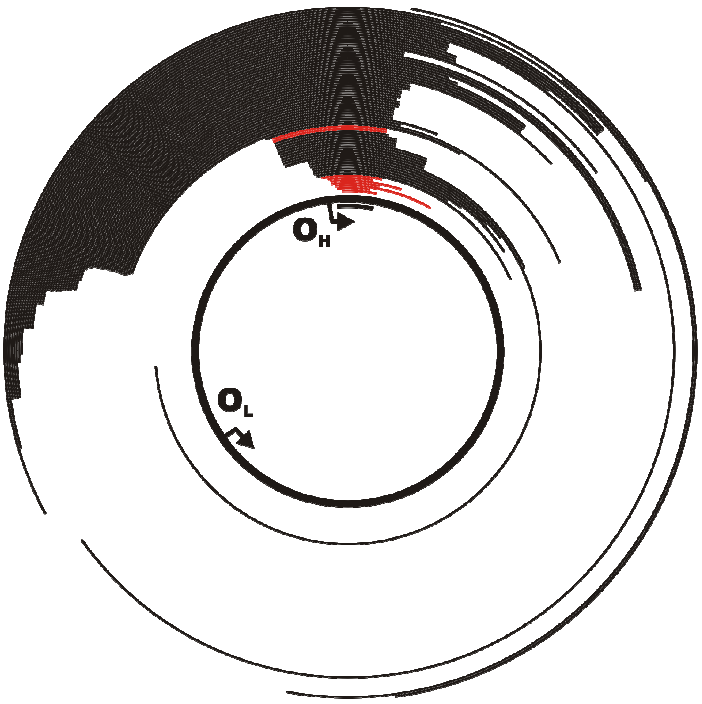

b

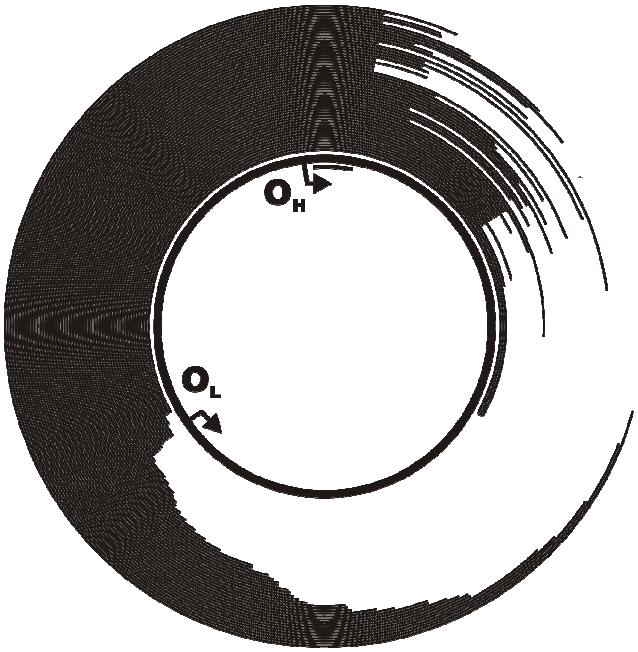

Figure 16 mtDNA rearrangements in MGME1 and POLG patients. Arcs represent retained parts of the mitochondrial genome. (**a**) mtDNA rearrangements in MGME1 patients. In red are marked deletions which are having at least one of the breakpoints between the light strand promoter (LSP) and termination-associated sequence (TAS); (**b**) mapped deletions in POLG patient. O_H, heavy strand replication origin; O_L, light strand replication origin.

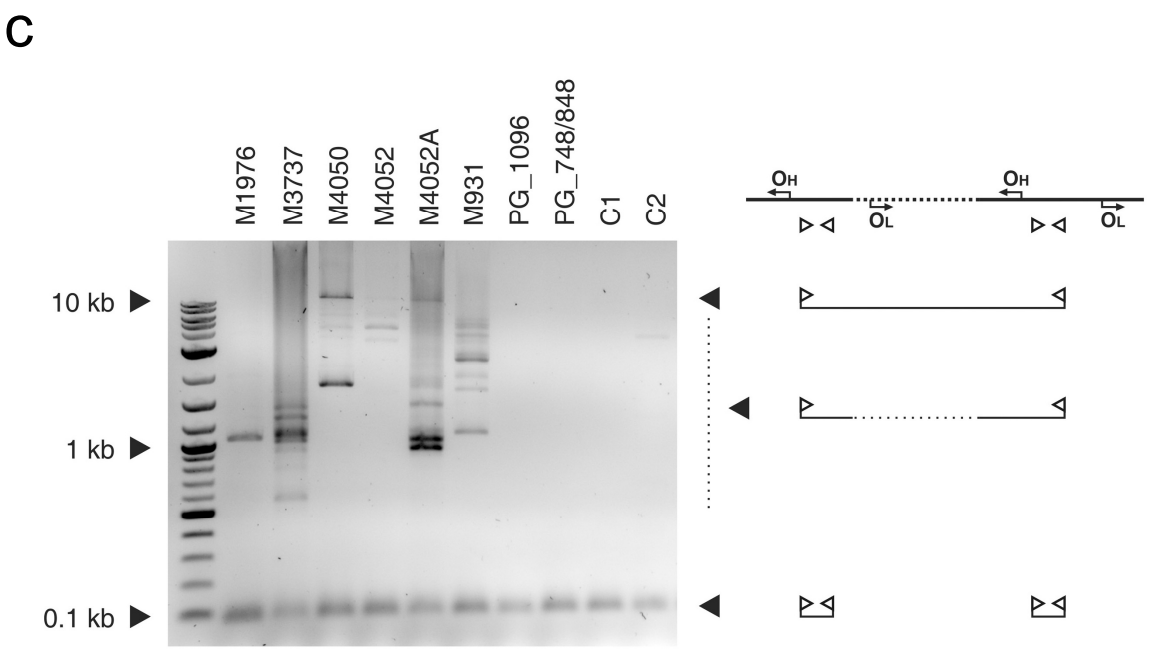

Figure 16 (**c**) Partially duplicated mtDNA molecules in skeletal muscle of MGME1 patients as detected by long extension PCR. Bands at the bottom represent the short PCR fragment. If a second copy of the corresponding region is present on the same molecule, longer PCR products are additionally observed. The upper bands, bigger then 10 kb, picture complete duplications and partial duplications are visible as lower bands under them. In healthy controls C1 and C2 and in samples with pathogenic *POLG* mutations (PG) no mtDNA rearrangements were detectable (Nichols *et al.*, *in preparation*).

As the detected rearrangments were missing important for their replication origins, alternatively, we assume that these breakpoints might be result from the detection of complex structures of partial duplications or concatamers. To address the issue whether breakpoints in the MGME1 patients could represent partial duplications instead of true deletions, long extension PCR was performed. This experiment showed that in addition to the expected short PCR product, with size of 88 bp, additional large products were also detectable in skeletal muscle samples of MGME1 patients (Figure 16c). Therefore, the short primer-binding region was present at least twice on the same mtDNA molecule, which is a hallmark of duplications and multiplications. In control skeletal muscle samples or in POLG samples rich of deletions no such products were detectable (Figure 16c).

Additionally, sequencing of the mtDNA of P931 revealed presence of insertions of small D-loop multimers in that patient (Table 34).

As patient P931 has different mutation than all the other MGME1 patients it was of interest to check if any of the other patients contains such multimers. Indeed, in P3737 such multimers appeared to be detectable. Such structures were previously described in humans (Wei *et al.*, 1996) and in POLG mouse model (Williams *et al.*, 2010), but the duplications described in that papers were much longer (150 to 880 bp), then the ones observed in the two MGME1 patients, between 13 and 200 base pairs.

Sample	FW primer	RW primer	Breakpoints (indicated by slash)
M3737	16,099F	136R	–16,122/16,070–16,125/16,267–16,553/29–
M3737	16,099F	136R	–16,245/16,083–16,132/16,348–
M931	3137F	45R	–3272/16,072–16,137/16,069–16,336/16,311–
M931	3137F	45R	–3272/16,072–16,137/16,069–16,336/16,311–
M931	3137F	45R	–3272/16,072–16,137/16,069–
M931	3137F	45R	–3272/16,072–16,137/16,069–
M931	3137F	45R	–3265/16,079–16,134/16,084–
M931	3137F	45R	–3610/16,077–16,151/16,074–
M931	10F	16,496R	–898/16,116–16,149/16,075–
M931	10F	16,496R	–898/16,080–16,117/16,082–
M931	10F	16,496R	–898/16,116–16,128/16,082–

Table 34 Small direct multimers in the D-loop of MGME1 patients. Highest number were detected in the sporadic case M931 that carries mutation c.698A>G (p.Tyr233Cys) in a conservative domain of the MGME1 and carries highest amount of mtDNA rearrangments in comparison to the other patients. With appropriate primers the repeats were detected also in M3737.

3. 1. 3 mtDNA depletion in MGME1 patients

Patients with MMD are characterized by mtDNA rearrangments accumulation or mtDNA depletion, or both simultaneously. As in MGME1 patients the amount of detected rearrangments present in muscle samples is insufficient to explain the mitochondrial dysfunction, it was essential to find out if the patients suffer from mtDNA depletion as well. To this end, the mtDNA copy number was determined by qPCR in the muscle samples. The copy number values were normalized to control value, obtained from eleven healthy control muscles of age of 18 to 33 years. All MGME1 patients showed depletion of the mtDNA in comparison to controls, with exception of P1976 (Figure 17a, grey bars). The observed normal copy numbers in that patient can be explained with the early age at which the sample was obtained (10 years old); at this age the patient also represented only mild clinical symptoms.

While performing the qPCRs for copy number determination I noticed difference in the copy numbers detected when using primers placed inside or outside of the D-loop region of the mtDNA (Figure 17). This phenomenon was detectable only in the MGME1 patients and was not visible to such extent in none of the control patients.

a

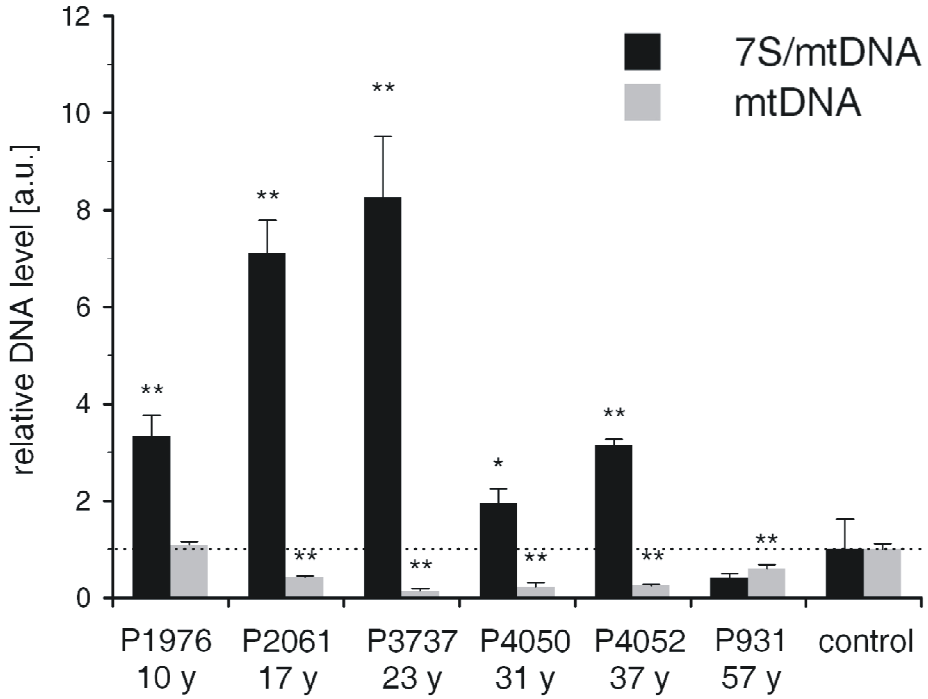

b

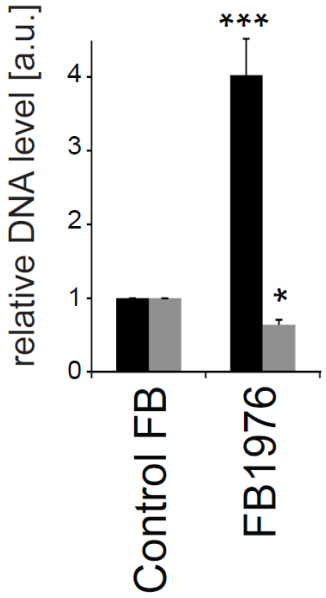

Figure 17 Relative mtDNA copy numbers in muscle and fibroblasts of MGME1 patients. (**a**) Relative mtDNA copy numbers in muscle, the data is result from three independent qPCR reactions and is normalized to a control value, which on the graph appears as 1. The control value was obtained from eleven control patient muscle samples in the age from 18 to 33. The control samples show 8146–11,416 mtDNA molecules per nucleus (Kornblum *et al*., 2013). (**b**) Relative mtDNA copy number in fibroblast sample from P1976 in comparison to control fibroblast cell line. The data is normalized to the control value, which on the graph appears as 1. Grey bars display the mtDNA relative copy number

outside the 7S DNA; black bars represent the relative copy number in the 7S DNA region; error bars are indicating the SD(+); * indicates the significance of the experiment; *p<0,05, ***p<0,001; two-tailed Student's *t* test (Kornblum *et al*., 2013).

7S DNA is a single stranded DNA belonging to the D-loop. It is proposed that the 7S DNA is a prematurely terminated product from mtDNA replication of the H-strand. The ratios of the 7S DNA to the total amount of mtDNA were different between the patients but varied between twofold and eightfold increase (Figure 17a black bars). A 1,5 fold increase is accepted as maximal theorethical accumulation of 7S DNA in healthy cells, if 100% of the mtDNA has 7S DNA. This finding suggests that MGME1 might participate in the turnover of 7S DNA.

In conclusion, the mtDNA in muscle from MGME1 patients is depleted and contains highly increased amounts of 7S DNA. If we assume that the 7S DNA accumulation is a result of prematurely terminated replication, its accumulation in these patients would suggest the direct involvement of MGME1 in mtDNA replication and its control of the 7S DNA turnover.

To find out if this 7S DNA accumulation is present also in other tissues than muscle, qPCRs were performed also with fibroblast sample from P1976 with the same primer pairs. The 7S DNA effect was clearly visible in the fibroblasts from P1976 in comparison to control (Figure 17b). The values are normalized to the control sample.

To confirm that blood is also a good source for detection of the 7S DNA effects, qPCRs were performed in the same conditions as in the previous experiments on blood samples from P2061 and P3737. The 7S DNA increase was also significant in both blood samples, which may be important for non invasive diagnostics. In consistence with the literature, the muscle contained the highest amount of total mtDNA, then the fibroblast and the mtDNA content was lowest in the blood.

In order to confirm that the copy number increase is detectable in the entire 7S DNA region, I optimized fourteen different primer pairs with SybrGreen qPCR, by which I could display the changes in the mtDNA copy numbers inside and outside the 7S DNA. As the 7S DNA increase was detectable in blood samples, the PCRs were performed with blood DNA from P1976, P2061 and P3737, as well as with one control blood sample (Figure 18).

All three samples showed similar pattern of high copy numbers in the entire 7S DNA region between np191 and 16,106, with strongest 7S DNA effect in P3737.

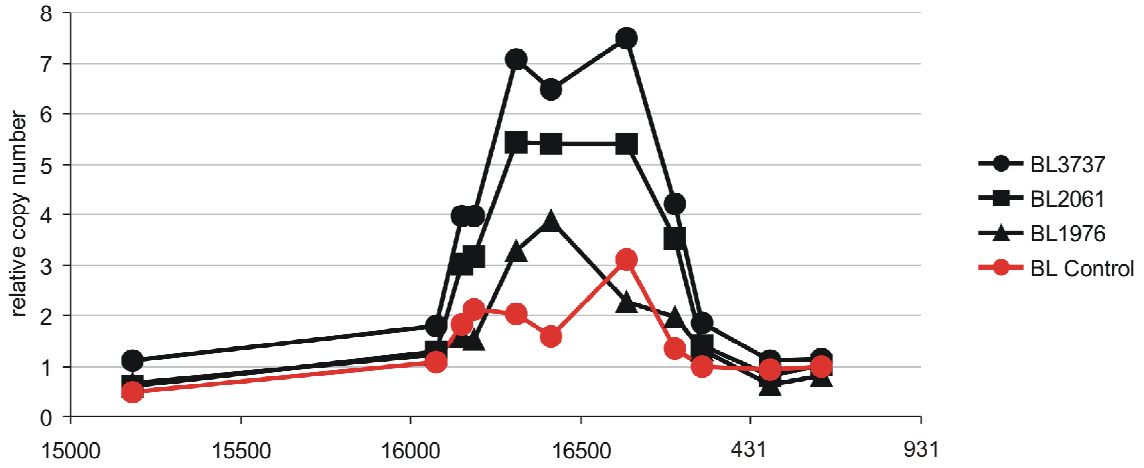

Figure 18 Relative mtDNA copy numbers, with eleven primer pairs outside and inside the 7S DNA region. Blood samples (BL) from three affected members from the Lebanese family, and a control sample were included in the experiment. The 7S DNA region starts from np 191 to np 16,106. The values are normalized to the BL control. All samples from affected members of the Lebanese family show elevated levels of 7S DNA in comparison to the control BL sample.

3. 1. 4 Overexpression of wild-type *MGME1*

Our collaborators in Munich have transfected fibroblast from P1976 with lentiviral wild-type *MGME1* expression construct, in order to examine whether rescue experiment would compensate the lack of MGME1. I used isolated DNA from that cell line to detect the 7S DNA levels and the total mtDNA amount. A possible compensatory effect would confirm the causative role of the MGME1.

Two weeks expression of the wild-type *MGME1* had decreased significantly the 7S DNA amount in the fibroblast from P1976 (Figure 19). Overxpression of MGME1 led to decrease in the overall amount of the mtDNA in the transfected cells, in comparison to controls and the non-transduced P1976 fibroblasts. Simillar effect on the 7S DNA and the overall amount of mtDNA was visible as well in the control cell line, after transduction with the wild-type construct (Figure 19a). This experiment is in line with the suggested exonuclease activity of the enzyme and its direct effect on the 7S DNA turnover.

To check the total mtDNA and 7S DNA decrease in the complemented cells, in comparison to the non-transduced P1976 fibroblasts, I have detected by qPCR the variation in the copy number inside and outside the 7S DNA with eleven primer pairs, as already shown for the blood samples of the MGME1 patients. The decrease in the 7S DNA was clearly visible and getting stronger with the increase of the lentivirus titer applied (Figure 19b).

a

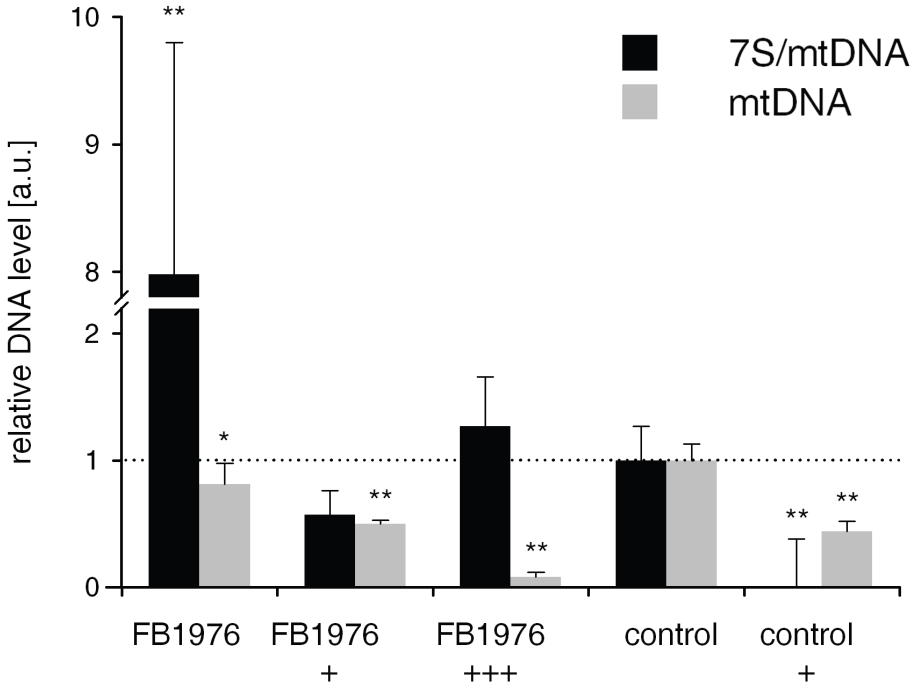

b

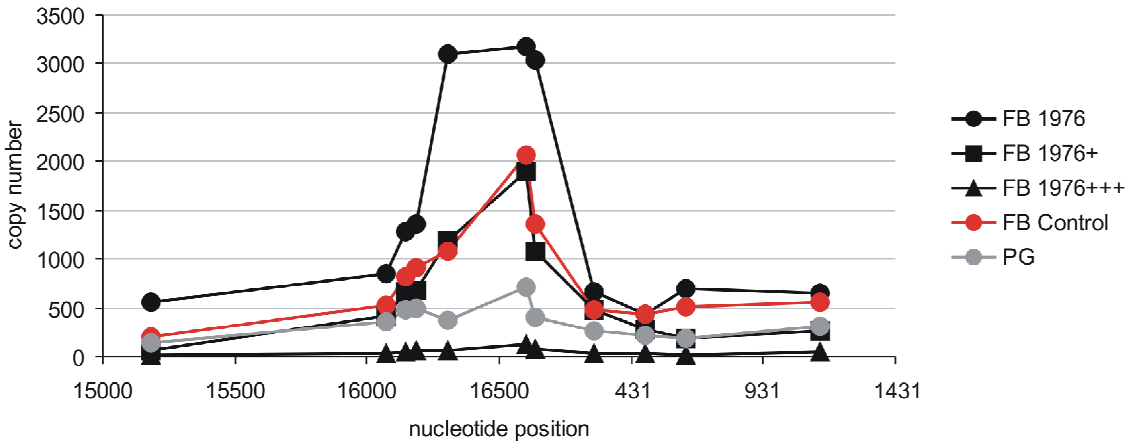

Figure 19 mtDNA copy number in fibroblasts from P1976, transduced with a viral construct overexpressing MGME1, compared to control and POLG patients. (**a**) mtDNA copy number in fibroblast sample from P1976 (FB1976) with and without overexpression of wild-type MGME1, in comparison to control fibroblast cell line. Grey bars represent the mtDNA relative copy number outside the 7S DNA; black bars represent the relative copy number within the 7S DNA region; error bars are indicating the SD (+); * indicates significance difference, *p<0,05, **p<0,01; two-tailed Student's *t* test (Kornblum *et al*., 2013). (**b**) Copy number representations with eleven primer pairs outside and inside the 7S DNA region in fibroblast samples from one control (FB Control), P1976 (FB 1976) with and without transduction with wild-type *MGME1* and one POLG patient (PG). The 7S DNA region spans from np 191 to np 16,106. +, fibroblast transduced with low titer of lentivirus; +++, fibroblast transduced with high titer of lentivirus.

The depletion of the mtDNA due to the overexpression of the wild-type gene is also visible on Figure 19b. The cells treated with higher titer of the lentivirus are almost loosing their 7S DNA, the experiment was confirmed as well by Southern blot by our collaborators in Cambridge.

3. 1. 5 mtDNA depletion and repopulation of MGME1 fibroblasts

To investigate the influence of mutated MGME1 on mtDNA replication, mtDNA ddC depletion and repopulation experiments were performed in fibroblast cell cultures from patient P1976 (Kornblum *et al.*, 2013), the Italian patient P4052 and controls (Figure 20). ddC acts as competitive inhibitor of POLG and as a terminator of nascent strand elongation (Stewart *et al.*, 2011). 12 days treatment of control and patient fibroblasts with the nucleotide equivalent ddC, led to mtDNA depleteion with mtDNA falling to less then 10% of the untreated steady state level. The results from the ddC treatment experiment revealed severely impaired mtDNA repopulation in MGME1 mutated cells. Only 8% of control mtDNA copy number in P1976 was reached after 16 days of repopulation without ddC. This demonstrates perturbed mtDNA replication, akin to the one observed in POLG patients (Wanrooij *et al.*, 2007). In P4052 after withdrawal of ddC, the copy numbers reached 55% of the control copy numbers, but still could not recover completely. Both patients showed inability to recover their mtDNA levels after mtDNA depletion.

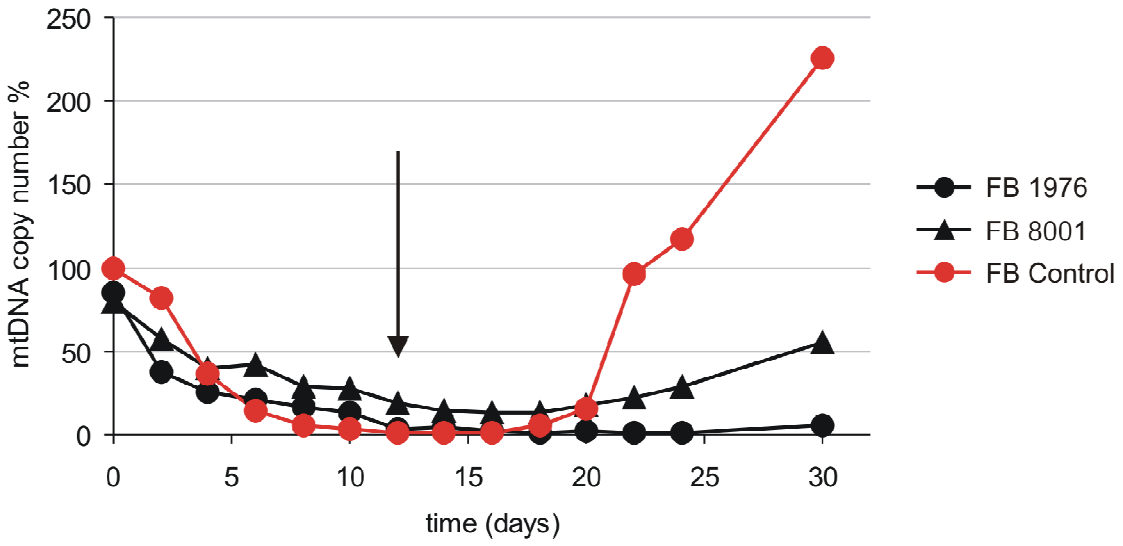

Figure 20 Changes in mtDNA copy numbers during induced mtDNA depletion and repopulation of fibroblasts from P1976, P4052 and a control. Arrow indicates the withdrawal of ddC. The mtDNA copy numbers were determined by qPCR. The data point for mtDNA copy numbers in the control is considered as 100% and the rest of the data points are normalized to it. The qPCR was performed by using the mitochondrial primers 3922F and 4036R.

3. 1. 6 Detection of 7S DNA ends in MGME1 patients

Our collaborators in Cambridge performed series of experiments confirming the function of MGME1 and its exonuclease activity (Kornblum *et al*., 2013). MGME1 showed 5' end exonuclease activity, it prefers single stranded DNA substrates, and can process flap structures, that may also contain RNA on their 5' end. Its 3' end processing activity is weak. As it is dysfunctional in MGME1 patients, and the patients show high amount of 7S DNA, it was interesting to check for free ends of the 7S DNA, and determine them in MGME1 patients, and preferentially the 5' end.

In order to detect single stranded free ends, without the need of radioactive labeling, I established a modified version of the ligation-mediated PCR (LM-PCR) described originally by Kang *et al.* in 1997. The method is simple enough to be used for screening of large numbers of samples and can successfully detect free 5' ends and 3' ends (Figure 21).

In order to visualize the 5' end of the 7S DNA, first, the DNA sample was treated with Quick Blunting Kit (NEB), containing T4 polymerase, having 5' to 3' polymerase activity and 3' to 5' exonuclease activity. The 5' end in this reaction does not lose any nucleotides. The kit contains dNTPs and T4 Polynucleotide Kinase for phosphorylation of the 5' end of the blunted molecules and its subsequent ligation.

Although, the 3' processing activity of MGME1 is weak, *in vitro*, I have checked for alterations also of the 3'-end of the 7S DNA. To this end the mtDNA was treated with Mung Bean nuclease (Figure 21), which is a single-strand specific DNA endonuclease, which degrades all 3' and 5' single stranded overhangs and leaving 5'-phosphorylated blunt ends.

After filling in or cutting out the overhangs, the molecules should have blunt ends suitable for ligation to the blunt-end linker. The linker serves as adaptor; it has a non-biological sequence consisting of two complementary primers LMP25 and LMP11, which form a blunt end only on one side of the adaptor. As the primers used for the linker synthesis are not phosphorylated but contain only a hydroxyl group at both ends, only one of the two strands will be ligated. Through the asymmetry of the linker, it will be ligated only unidirectionally to a free double-stranded blunt end, by the available 5' phosphate on the 7S DNA and the 3' hydroxyl group on the primer. The LM-PCR reaction is performed with the LMP25 primer used for the synthesis of the linker and a specific primer on the mtDNA for the 5'-end detection. For detection of the 3' end of the 7S DNA the mtDNA primer should be a reverse one.

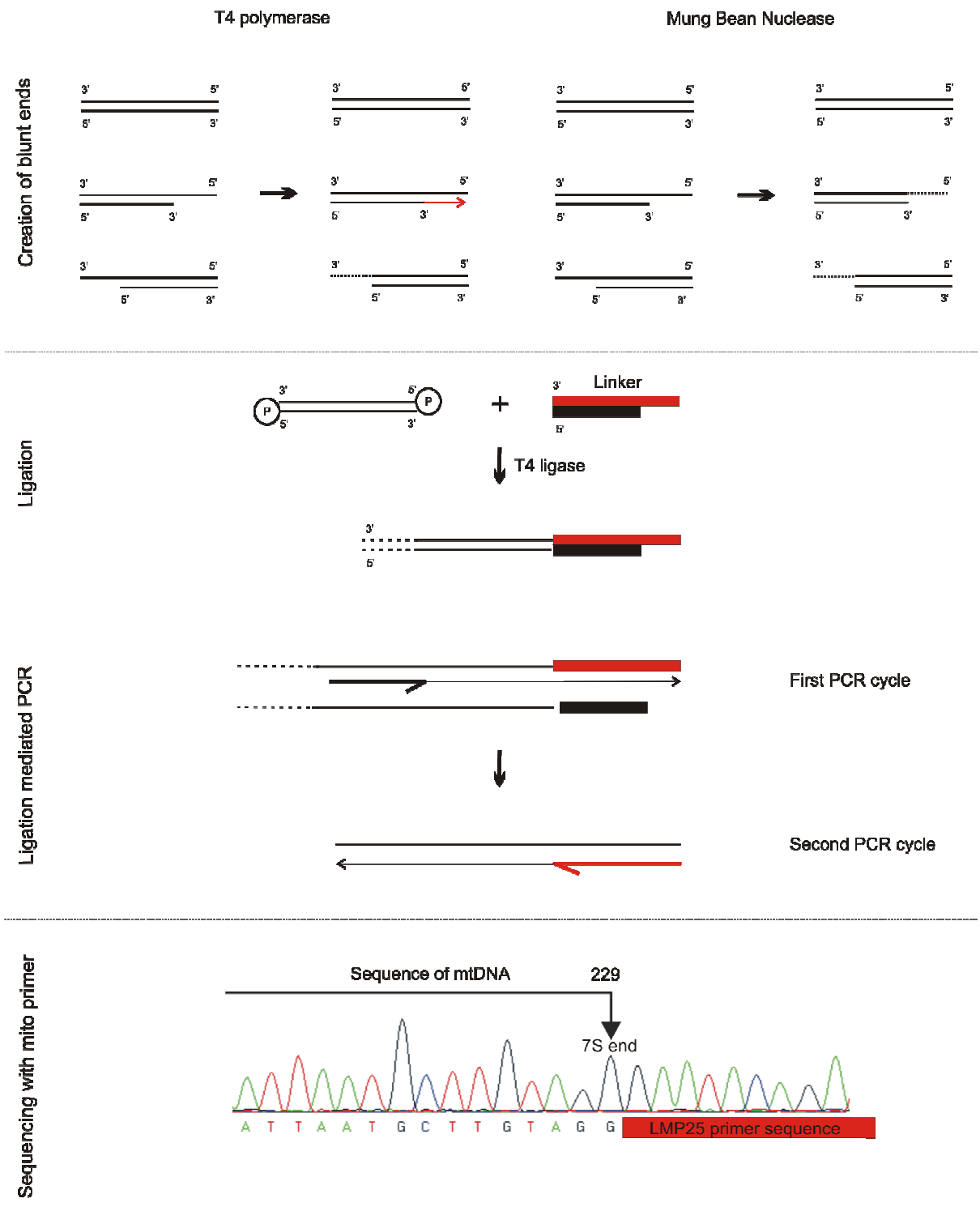

Figure 21 Schematic representation of LM-PCR for detection of free mtDNA ends.

At first, to test the specificity of the technique I performed LM-PCR with LMP25 primer annealing to the linker and five different forward primers annealing to the 7S DNA. There were prominent PCR products with the expected size, amplifying the 5' end of the 7S DNA (Figure 22a). On the gel picture one can notice that the products in the fibroblasts sample from P1976 are slightly longer then the ones in the control. To be sure that there were no PCR artifacts due to the ligation and the nuclease treatment of the DNA, I performed ligation incubations without adding linker or T4 ligase, and in both cases the PCRs did not amplify a product (Figure 22b). Additionally, I performed ligation of the DNA from P1976 and a control with only one primer (LMP25) (data not shown). There was no detectable PCR product, which confirmed that the observed reactions are amplifying mitochondrial blunt end molecules.

In MGME1 patients, for detection of the 5' 7S DNA end with nucleotide position 191 (Clayton, 1996), a linker primer LMP25 and mitochondrial primer 10F ware used, in LM-PCR (Figure 23 upper panel). If the 5' end of the 7S DNA is at np 191, the LM-PCR would give a product of 181 bp, which is indeed the observed PCR product in the fibroblast controls 1 and 2 (Figure 23). In both MGME1 patients the LM-PCR resulted in slightly longer products.

For detection of the 3' 7S DNA end at position 16,104–16,106 (Clayton, 1996) a linker primer LMP25 and mito primer 16,413R ware used in LM-PCR (Figure 23 middle panel). If the 3' end of the 7S DNA is at np 16,106, the LM-PCR would give a product of 307 bp, which was the observed PCR product in both MGME1 patients and controls. No changes in the 3' 7S DNA end were observed in MGME1 patients in comparison to controls. To confirm my results, I have treated the mtDNA from P1976 with S1 nuclease. It has single strand nuclease activity and also leaves phosphorylated 5' ends, but opposite to Mung Bean nuclease it cuts the DNA in single-stranded regions caused by a nick, gap, mismatch or loop. The results from the LM-PCR were the same as those with Mung Bean treatment and it was confirmed as well by sequencing (Figure 23 lower panel).

a

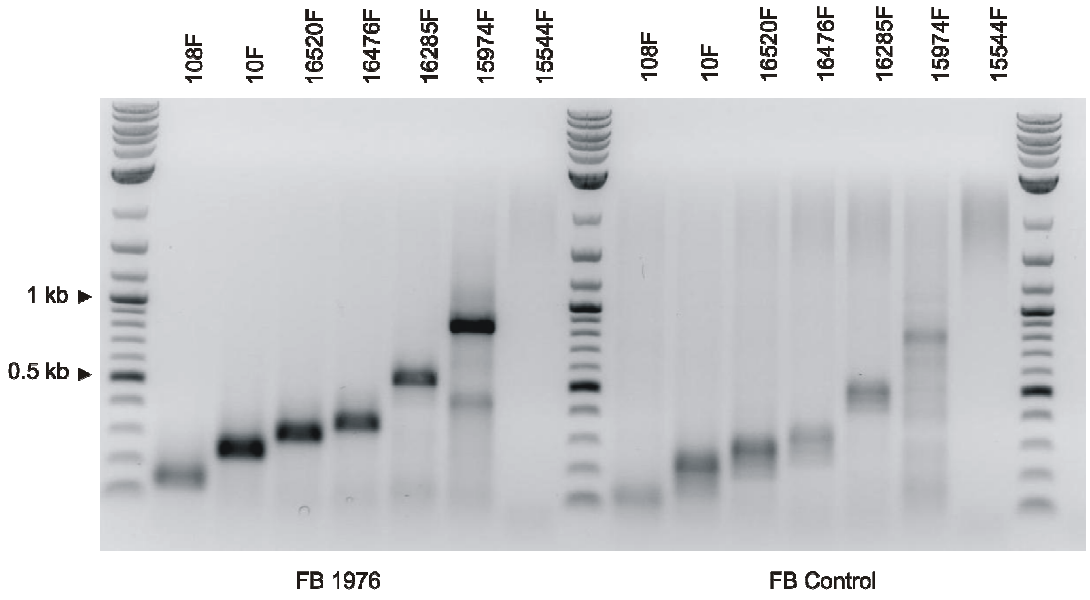

b

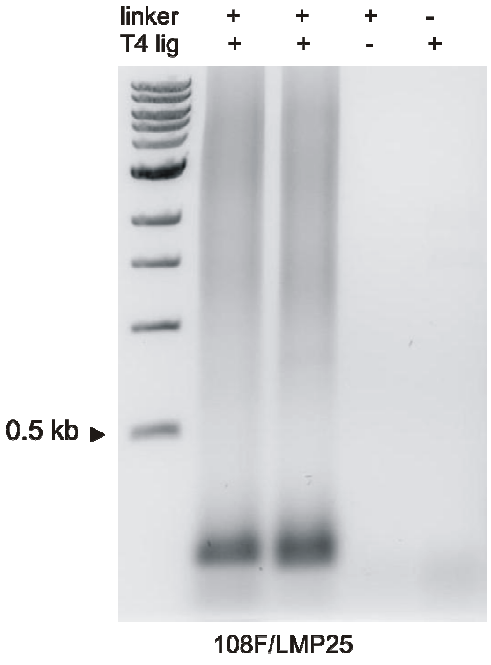

Figure 22 LM-PCR visualization of the 5' end of the 7S DNA. (**a**) Determination of 5' 7S DNA end with linker primer LMP25 and seven different forward primers in fibroblasts from P1976 (FB 1976) and a control (FB Control). (**b**) LM-PCR with mtDNA from human muscle mitochondria, and primers LMP25T7/108F, when either the linker or the T4-ligase is missing the reaction does not amplify a product.

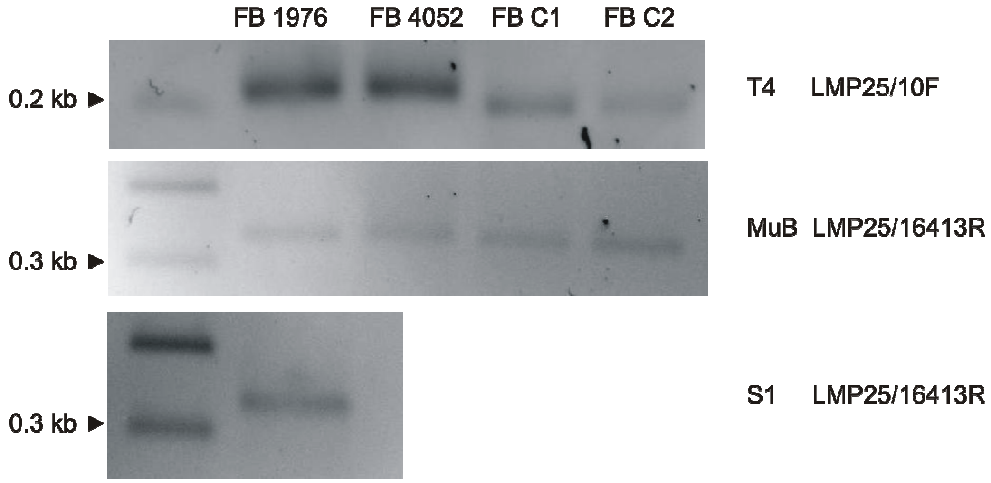

Figure 23 LM-PCR after T4-polymerase (T4), Mung Bean nuclease (MuB) and S1 treatment of fibroblasts from patients with MGME1 mutation and controls. The 5' 7S DNA end in the MGME1 patients (FB 1976 and FB 4052) is slightly longer then the one detected in controls (C1 and C2). The 3' 7S DNA end seems unaltered in both controls and MGME1 patients.

To detect the exact ends of the 7S DNA, I have performed a smPCR with the ligated mtDNA. For the 5' end, I have used the T4 polymerase treated DNA and for the 3'end the Mung Bean nuclease treated DNA. By Sanger sequencing, the sequence of the linker can be easily recognized from the mtDNA fragment and the exact nucleotide position of the 7S DNA end can be detected. To assure the amplification of mitochondrial DNA and also to exclude the sequencing of short non-mitochondrial ligated on their both ends fragments, each detected single molecule was re-amplified with the linker primer and another mitochondrial primer inside the amplified molecule. In this way I screened the fibroblasts sample from P1976 and one control fibroblasts cell line. The result revealed various 5' ends, which were longer in the MGME1 patient in comparison to the known size of the 7S DNA (Figure 24).

a

Sample	5' end (QBK)	3' end (MuB)
P1976	170; 183; 186; 191; 194; 197; 200; 204; 205; 206; 207; 215 229; 238; 298; 301	16,106
FB Control	151; 191	16,104

b

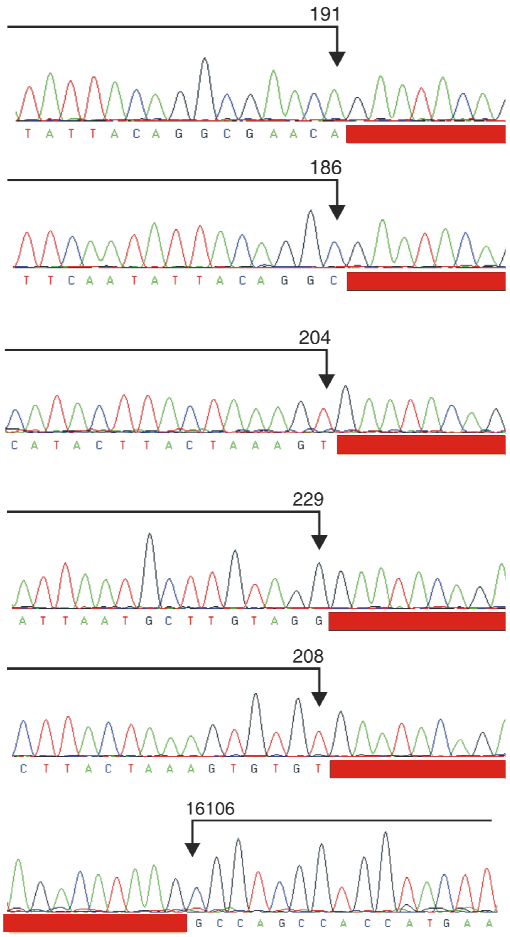

Figure 24 7S DNA ends mapped by single-molecule LM-PCR. (**a**) Free 7S DNA ends detected in fibroblast from P1976 and fibroblasts control cell line (FB Control). The 5' ends were detected after Quick blunting kit (QBK) treatment of the mtDNA, LM-PCR and sequencing. The 3' ends were detected after Mung Bean (MuB) nuclease treatment, LM-PCR and sequencing. In red are marked the 7S DNA ends known from the literature. (**b**) Example of six detected by smLM-PCR ends in fibroblasts from P1976. The linker is marked in red and the arrows indicate the free 5' and 3' end point.

The results in the control fibroblasts are in consistence with previous findings. The 5' end of the 7S DNA is at np 191 (Clayton, 1996) and the 3' end is at np 16,104. Several 5' ends have been described and they are all extending up to 191 np, for example, in controls

one of these ends was detected, at position 151. In opposite to controls, in the MGME1 patient P1976 there were many and various 5' ends of the 7S DNA, which were with ends predominantly above np 191. A scheme of some of the mapped free ends is shown in Figure 24b.

According to Clayton the 3' end of the 7S DNA is at positions 16,104 to 16,106. The 3' end of the 7S DNA seems to be unaltered in patients with MGME1 mutation. The 3' 7S DNA end in P4052 was also checked with Mung Bean treatment and represented the same end point of 16,104–16,106.

3. 1. 6. 1 Light strand origin of replication and free ends

As the ligation-mediated method is detecting free DNA ends, it should be able to detect any kind of double-stranded free ends and not exclusively only the 7S DNA ends. Therefore, I performed screening for free ends over the entire mitochondrial genome of P1976 fibroblasts sample and one control sample. I used thirteen different reverse mtDNA primers and the linker primer LMP25. In P1976 the LM-PCR with primer 5985R has amplified a free end, which is localized at the origin of replication of the light strand (O_L) and was not detectable in the controls. As O_L is covering a region from np 5721 till 5798, by using reverse primer at position 5985, a free end at O_L shall give a product with size between 212–289 bp (between the LMP25 and 5985R) (Figure 25).

The free O_L end was confirmed by sequencing of smLM-PCR products, the exact np position of the free end is 5771–5772, within O_L. The same free end was detectable as well in the Italian patient P4052. Therefore, it appears that loss of *MGME1* causes accumulation of free double-stranded ends around the light strand replication origin or accumulation of patient specific linear fragments. The data was confirmed also by Southern blot (experiment provided by our collaborators in Cambridge).

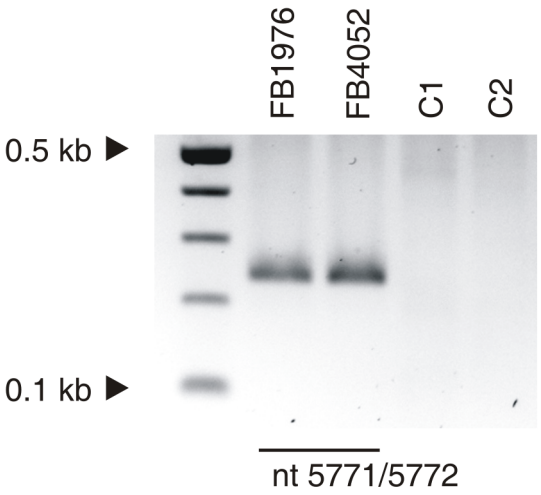

Figure 25 LM-PCR showing free end at the O_L of MGME1 patients. LMP25 and 5985R primer amplify a short product signifying free end around the origin of replication of the light strand (O_L). The product has size of 213–214 bp. Equal amounts of DNA were used for the reaction. The exact breakpoints were determined by single-molecule LM-PCR (Nicholls *et al.*, *in preparation*).

3. 2 Mitofusin 2 and Charcot–Marie–Tooth neuropathy

One of the most common neuropathies, affecting the peripheral nerves and associated with mitochondrial dysfunction, is Charcot–Marie–Tooth neuropathy (CMT). CMT type 2A (CMT2A) is an autosomal dominant disease, found to be associated with mutations in the nuclear gene encoding for mitofusin 2 (MFN2). MFN2 is targeted to mitochondria and belongs to the family of dynamin GTPases and plays crucial role in the process of outer mitochondrial membrane tethering during fusion of mitochondria (Koshiba, 2004). In this part of my doctoral work I investigated the functional effects of different *MFN2* mutations on mtDNA stability and maintenance, in skeletal muscle and fibroblasts samples from four different patients.

3. 2. 1 Patients

Four patients were diagnosed for CMT2A by direct sequencing of the *MFN2* gene. The sequencing was performed by Susanne Beyer in our lab, and in the lab of Dr. Vielhaber in Magdeburg. Each of the four patients (Patient 1 to Patient 4) carried different mutation in the *MFN2* gene, all affecting different protein domains (Figure 26). Patient 1 harbored a heterozygous single nucleotide substitution in exon 11 of the *MFN2* gene – c.1126A>G. The mutation affects highly conserved amino acid of the protein, in undescribed till now domain. As the patient was adopted at newborn age no investigation could be performed in the

parents. Patient 2 carried a heterozygous mutation in exon 18 of the gene – c.2120G>C, also affecting a conservative region of the *MFN2* gene in the HR2 domain. The parents of the patient did not show the mutation; therefore, it is a result of *de novo* mutational event. Patients 3 revealed a heterozygous in-frame deletion c.677_688del12 in exon 2 of the *MFN2* gene, encoding for the GTPase domain of the protein. Other affected relatives in the family carried the same heterozygous mutation. Patient 4 carried a heterozygous mutation in exon 4 – c.221A>G, at the P-loop nucleoside triphosphate hydrolase domain, not detectable in the mother and the brother of the patient. The mutations in P3 and P4 have not been described until now. The mutation in P2, has been recently published (Sitarz *et al.*, 2012).

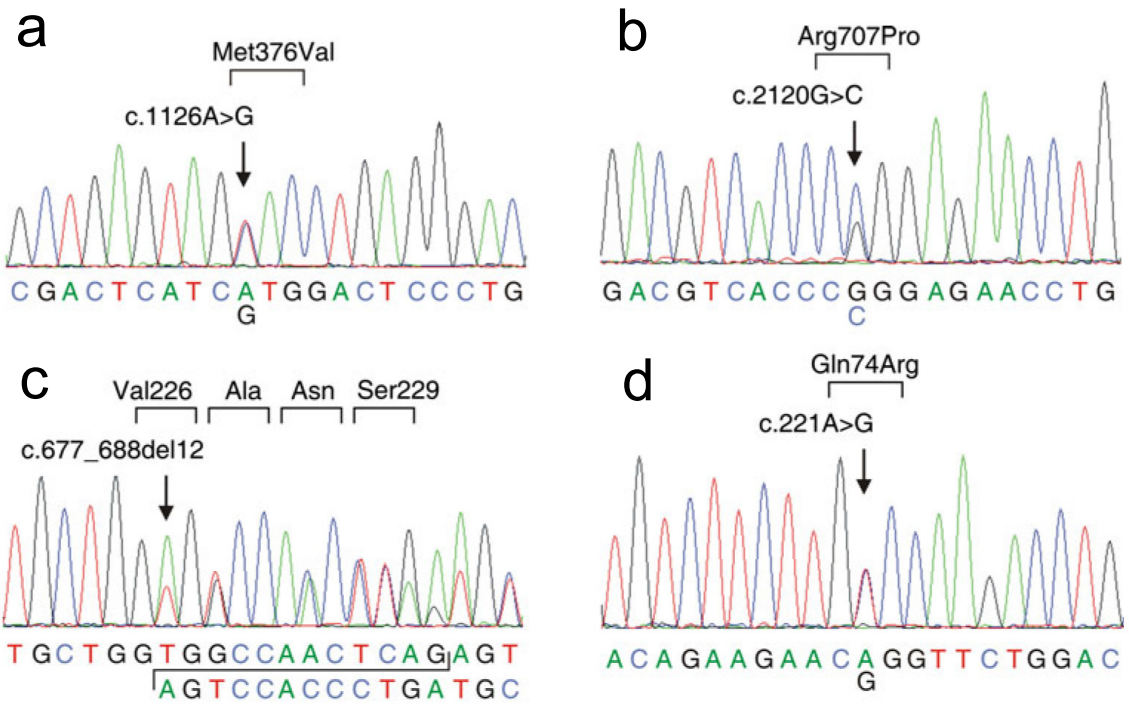

Figure 26 Partial sequences representing *MFN2* mutations in four patients with CMT2A. Patient 1 (**a**) (reverse sequence), Patient 2 (**b**), Patient 3 (**c**) and Patient 4 (**d**) (reverse sequence); arrow is indicating the mutation in each sequence (Vielhaber *et al.*, 2013).

Skeletal muscle biopsies from Patient 1 and Patient 3 were investigated for COX activity. Due to strong fatty muscle degeneration, the skeletal muscle of Patient 2 was unsuitable for histological examination, and no muscle sample was available from P4. The histological investigation from Patient 1 and Patient 3, performed by our collaborators (Vielhaber *et al.*, 2013), revealed mild changes and although no COX-negative fibers were visible, the mitochondria had an abnormal distribution in the fibers.

As a disease control patient, a sample from Charcot–Marie–Tooth type 1A (CMT1A) neuropathy patient was used. In this case the cause of the disease is a mutation in the gene

PMP22 causing subsequent demyelination of neurons, thereafter any changes in skeletal muscle in this form of the disease are consequences of neurogenic atrophy. As CMT2A is caused by a primary mitochondrial dysfunction, all alterations of mitochondrial function are expected to be specific, apart from signs of neurogenic atrophy. The appearance of the mitochondria in the CMT2A patients under electron microscopy (performed by our collaborators, Vielhaber *et al.*, 2013) was very different than the one in the disease control patient. The mitochondria appeared swollen, with smaller sizes and visible paucity. The results from the histological analysis suggested respiratory disturbances due to the changes in the mitochondria. Biochemical analysis in the fibroblasts and muscle from the patients performed by Dr. Schoeler showed only increased sensitivity of the respiration to COX inhibitor azide (data not shown). The MFN2 mutations appeared to have only mild effect on the respiration rate in the samples (data not shown). To elucidate the question how disturbed fusion of the mitochondria can affect the phenotype in these patients, I have performed genetic investigations of their mtDNA.

3. 2. 2 Copy number determination

The copy number of the mtDNA was measured by qPCR and the samples showed reduced copy number of the mtDNA in comparison to the healthy and the diseased controls (Table 35).

Sample	Skeletal muscle	Fibroblasts
Controls	16,045±8817 n=15	1297±188 n=8
CMT1A disease control	9116±891	942±87
CMT2A Patient 1	6211±571*	411±19**
CMT2A Patient 2	654 ±44*	889±73**
CMT2A Patient 3	11,440±632	798±64**
CMT2A Patient 4	no data	633±103**

Table 35 mtDNA copy numbers determined in four CMT2A patients, one diseased control patient with CMT1A and controls. The copy numbers were measured in fibroblasts and muscle DNA samples. The values were normalized to the values for the single nuclear gene *Kir4.1*. Standard deviation was calculated from three separate experiments. *p<0.05; **p<0.001; Student's *t*-test; n, number of samples.

The absolute copy numbers in tissue samples from all CMT2A patients showed a significant, almost twofold decrease, in comparison to both controls. Only Patient 3 had an insignificant decrease in the copy number. The highly reduced values in muscle sample from

Patient 2 can be explained with the fatty muscle substitution in that sample. As mtDNA depletion is often caused by mutations in the *POLG* gene, all patients were checked for mutation in it and all were negative (experiment performed by Susanne Bayer). As mtDNA depletion was not observed in the CMT1A disease control patient, the depletion was not result of neurogenic degradation, and this reveals new insight into the pathological effect of MFN2 mutations and might point to a potential causative role of mtDNA depletion in CMT2A neuropathy. To confirm that, a fibroblasts mtDNA depletion experiment with ethidium bromide, a strong mtDNA replication inhibitor, was performed by Dr. Schoeler and the data showed linear correlation between the reduction of mtDNA copy number and lower respiration (Vielhaber *et al.*, 2013). Altered mitochondrial dynamics lead to disturbed mtDNA maintenance.

3. 2. 3 mtDNA deletions in CMT2A neuropathy

To investigate the deletion load in MFN2 patients, I performed a common LR-PCR with primers 7027F and 45R. All samples showed accumulation of multiple deletions (Figure 27a). Deletion quantification was performed in skeletal muscle and fibroblasts from the patients by using smPCR. All samples showed accumulation of deletions (Figure 27b and c). Particularly, the skeletal muscle from Patient 3 had significantly increased amounts of deletions in comparison to controls. This patient showed previously less pronounced depletion in comparison to the other patients with CMT2A. Patient 3 is also the only one who has a deletion in the *MFN2* gene, affecting the GTPase domain of the protein; which might be relevant to the slightly different mtDNA status in comparison to the other patients. From this result it was evident that MFN2 mutations not only influence the copy number, but also cause accumulation of mtDNA deletions.

The deletion quantification showed approximately 8-fold more deletions in CMT2A skeletal muscle and 15-fold more deletions in CMT2A fibroblasts (Figure 27b) in comparison to age matched controls. The total level of deletions between 0.0006 and 0.0012 %, was only about 0.001 % of total mtDNA (Figure 27b), and therefore, the deletions were unlikely to explain the marked decrease of *in vivo* COX activity.

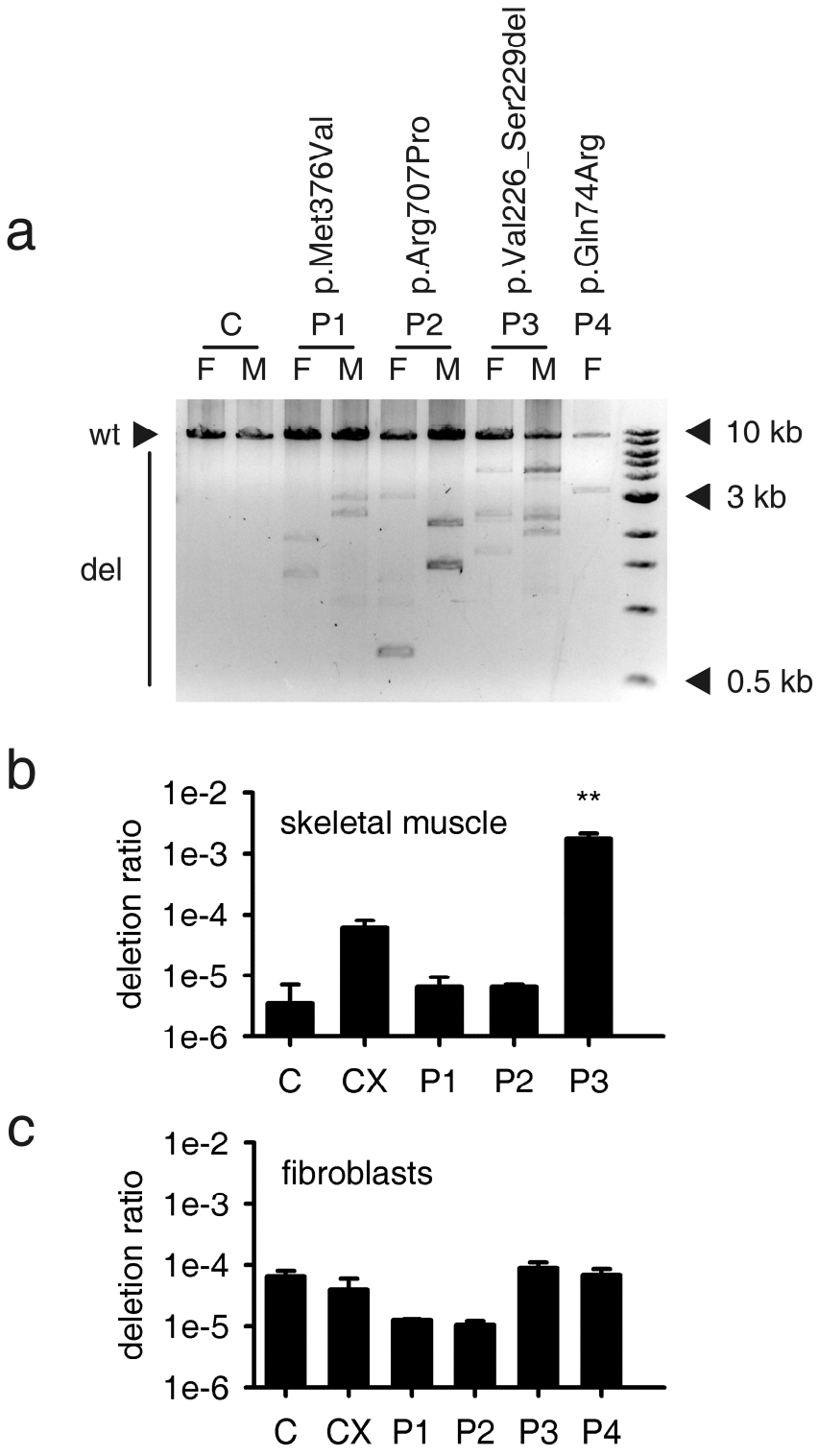

Figure 27 Deletions in CMT2A patients. (**a**) LR-PCR with CMT2A fibroblast (F) and muscle (M) samples from Patients 1 to 4 (P1–P4) and a control sample. Wt, wild-type amplicon; del, deletion specific PCR products. Deletion quantification in CMT2A muscle (**b**) and fibroblast (**c**) samples (P1–P4), as well as in one diseased control patient with CMT1A (CX) and a control patient (C). Error bars show the SEM from two independent experiments; the significance level was *p<0.05 or **p<0.005 (Vielhaber *et al.*, 2013).

a

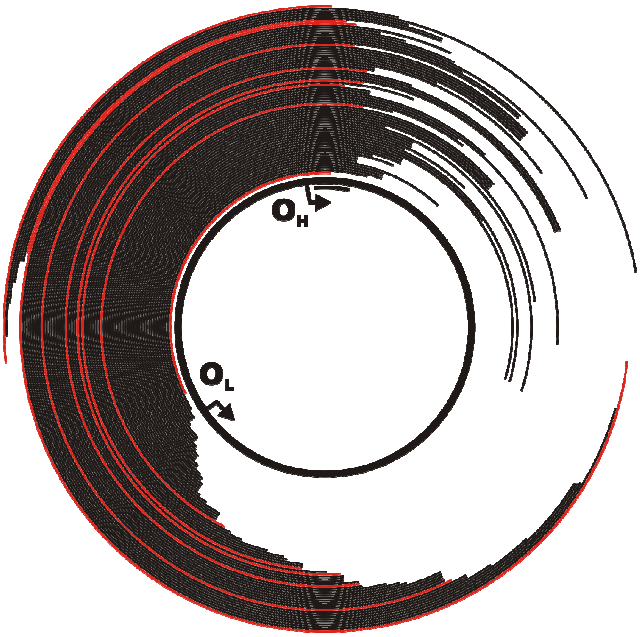

b

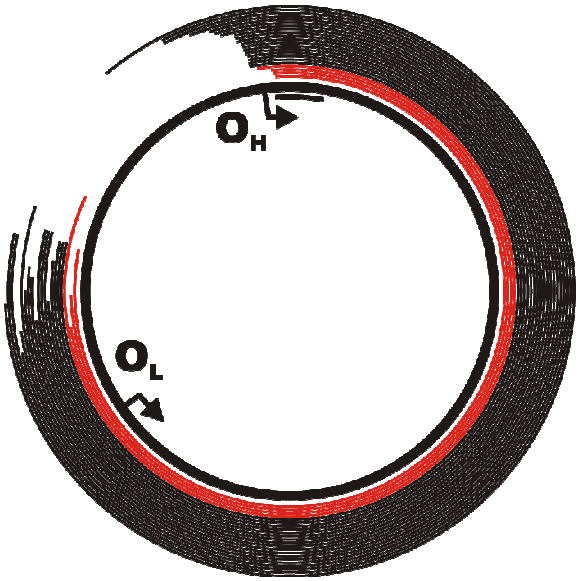

Figure 28 Mapped mtDNA deletion breakpoints in CMT2A patients. On the figure are shown retained mtDNA regions. (**a**) Mapped deletions in the major arc of CMT2A. The graph shows the amplified deleted molecules, missing parts of their major arc. In red are shown deletions which are missing their O_L or are spanning the TAS region of the mtDNA. (**b**) The graph represents the amplified deleted molecules missing parts of their minor arc. In red are shown deletions missing their LSP or O_H.

All single molecules amplified during the quantification were sequenced and their deletion breakpoints were determined (Appendix III). Surprisingly, there were deletion species lacking the heavy strand origin of replication (O_H), the light strand promoter (LSP), or their 3' breakpoint was spanning over the TAS region (Figure 28). These molecules probably cannot replicate and are unlikely to propagate by clonal expansion. They are most probably resulting from ongoing mtDNA mutagenesis. This is supporting also the finding that most of the mapped deletions were detectable only once and most likely are not clonally proliferating. After performing smPCR and detecting the deletions' breakpoints, it appeared that all samples contain deletions also in the small arc of the mtDNA (Figure 28b).

These non-conventional deletions in the mtDNA minor arc as well as deletions removing regions crutial for mtDNA replication might be related to elevated oxidative damage and double-strand breakage. To check if such deletions are detectable in samples exposed to high oxidative stress, I performed hydrogen peroxide (H_2O_2) treatment of healthy human fibroblast (Spitz, 2010). In order to detect the proportion of damaged mtDNA molecules correlating to the increase of oxidative stress caused by the treatment of the cells with H_2O_2, I established a qPCR method, for mtDNA integrity estimation (Figure 29). The method combines two PCRs, the first PCR amplifies a short product, flanked by primers 1057F and 1144R. The lenght of this PCR product is 88 bp and the probability of detecting a breakpoint in such small amplicon would be very low, therefore, the detected Ct value would show the total amount of mtDNA molecules. The second PCR amplifies a long 5379 bp PCR product, amplified by primers 11,226F and 35R. The difference between the two PCR Ct values would delineate the intactness of the mtDNA, by comparison of the short and the long PCR product amplifiability, which depends on the mtDNA quality. Cycle number differences between the two PCRs were measured in the qPCR reactions and the data from the control untreated samples were used as reference. For all samples, first, the Ct values for the long product were subtracted from the wild-type mtDNA Ct values. Then the control sample Ct difference was taken as reference, to which the treated samples were compared in a ratio. In this case the control sample represents a value of 1, all treated samples containing less intact mtDNA should give a value smaller than 1 (Figure 29).

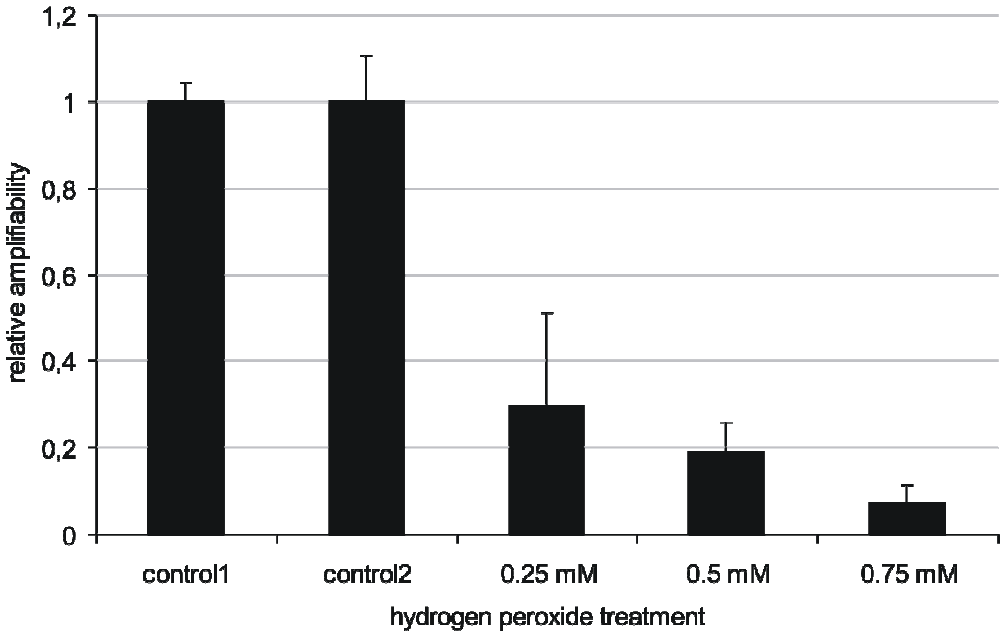

Figure 29 mtDNA damage upon oxidative stress by H_2O_2. The mtDNA damage is increasing in correlation with increase in the oxidative stress, by treatment with different concentrations of H_2O_2. The error bars indicate SEM (+) from three independent experiments.

Multiple deletions in the hydrogen peroxide treated samples were detected by smPCR. Breakpoints mapping unveiled that indeed deletions in the minor arc were detectable in H_2O_2 treated fibroblasts and some of them were removing the replication origin for the heavy strand at position 191 (Table 36). In the H_2O_2 treated fibroblasts, I detected as well deletions spanning the classical 3' deletion breakpoint at 16,000–16,100 np and entering into the 7S DNA (Table 36).

Deletions in H_2O_2 -treated fibroblasts

Minor arc deletions	Major arc deletions
129–4306	
980–4646	7486–16,247
674–4147	6248–16,046
24–2760	8104–16,319
129–3922	6297–16,192
333–4216	

Table 36 mtDNA deletions mapped by smPCR in H_2O_2 treated human fibroblasts. The deletions marked in red in the minor arc are removing the origin of H-strand replication. The deletions in red in the major arc are spanning the 16,070–16,090 region of the mtDNA, and are non-conventional deletions.

These non-conventional deletions detected in MFN2 patients and in H_2O_2-treated fibroblasts, cannot replicate and expand clonally due to the missing replication origins and

are most probably created *de novo*. In conclusion, higher oxidative stress might contribute to the elevated deletion formation in MFN2 patients.

3. 3 mtDNA deletions in Ammon's horn sclerosis

ROS production and oxidative stress are implicated as well in the pathology of TLE and mitochondrial dysfunction is suggested to play an important pathogenic role in the seizure generation and epilepsy. To characterize the dysfunction of mitochondria in temporal lobe epilepsy (TLE), I explored the mtDNA from 18 hippocampal brain samples, from patients with Ammon's horn sclerosis (AHS). AHS is characterized with extensive loss of neurons in the CA1 and CA3 regions of the hippocampus, and less damage in the AD and the PH regions (Margerison and Corsellis, 1966). As a control group, I selected 5 TLE brain samples, with no hippocampal sclerosis, and close brain lesion or tumor to the temporal lobe as primary cause of the epilepsy (lesion control group). It is known that deletions in the mtDNA accumulate with age (Linnane *et al.*, 1989; Bua *et al.*, 2006); therefore, in this study the age of the patients was limited between 20 and 40 years, and the detection of high levels of deletions due to advanced age was excluded. All samples were obtained from surgery of the hippocampus in pharmacologically intractable form of the disease. mtDNA from four different regions of the hippocampus – CA1, CA3, AD and PH were checked for deletions by LR-PCR. The primers used to perform the LR-PCR amplify large part of the major arc of the mtDNA, which is known to be highly prone to deletion formation in different pathological conditions (Shoffner, 1989). I used primer pair 5462F/16,115R, which amplifies a wild-type product with size 10,654 bp. Mutated molecules containing deletions appear as bands or smear under the wild-type sized molecules (Figure 30). All samples were semiquantitatively analyzed for deletions content by using ImageJ processing and analysis of the gel pictures. A ratio between the wild-type band peak and the summed deletion peaks was calculated, and used for semiquantitative measurement of the deletions present in each sample. The background intensity was subtracted in the calculations.

From the LR-PCR reactions of all the 18 AHS patients it was visible that the patients with hippocampal sclerosis show higher overall amount of deletions in the hippocampus in comparison to the lesion control patients (Figure 30a).

a

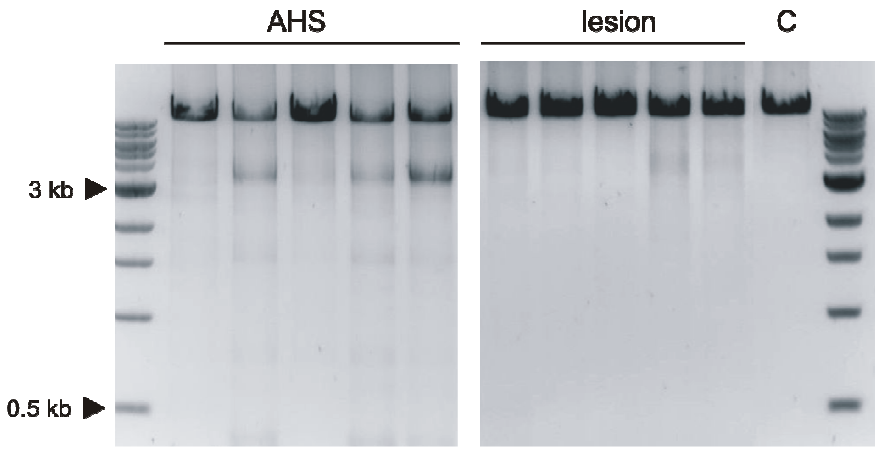

b

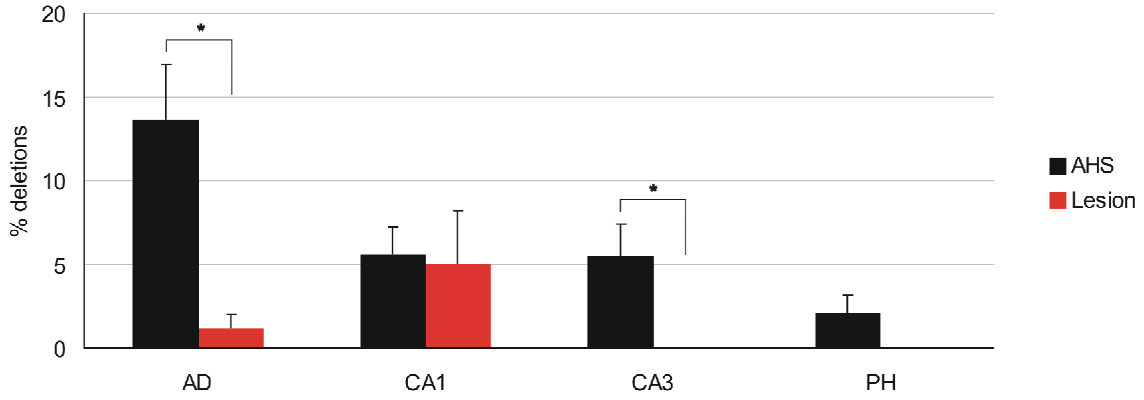

Figure 30 LR-PCR and semiquantitative analysis of mtDNA deletions content in TLE patients. (**a**) LR-PCR with mtDNA from CA3 hippocampal region from five AHS and five lesion samples, with primer pair 5462F/16,115R; left panel, AHS patients; right panel, lesion patients; C, blood control negative for deletions. The group of AHS samples shows higher amount of deletions in comparison to the lesion group of samples. (**b**) mtDNA deletion percentage in four different regions of the hippocampus of AHS and lesion patients with TLE. Primers used in the LR-PCR: 5462F/16,115R; AD, area dentate; CA1, cornu Ammonis 1; CA3, cornu Ammonis 3; PH, parahippocampus. Error bars indicate SEM (+). Standard student's *t*-test was used to indicate significant difference; * indicates $p< 0.005$. There is a significantly higher amount of deletions present in AD and CA3 regions of AHS patients in comparison to lesion patients.

The group of AHS patients showed accumulation in the CA3 region of the hippocampus, whereas the lesion controls had no detectable deletion. Furthermore, in comparison to the lesion TLE patients almost twelve fold higher amount of deletions was detected in the AD region of the AHS patients ($p<0.005$, a standard student's *t*-test was

used to test the significance of the difference) (Figure 30b). In the CA1 region both groups showed almost equal amounts of deletions. In the PH region the amount of deletions was very low in the AHS group and not detectable in the lesion TLE patients. This finding demonstrates that in difference to lesion TLE patients, significant amount of mtDNA deletions are accumulating in AD and CA3 regions of the hippocampus in AHS patients.

Both groups of patients suffer from TLE, but only the AHS group shows specific accumulation of higher amount of deletions in the most affected by the disease region CA3, this fact points to the causative function of the mtDNA deletions in TLE with AHS.

I compared the mtDNA deletion accumulation in four different hippocampal regions in 11 AHS samples in the age of 20–30 years and a control group of 3 lesion samples in the same age (Figure 31).

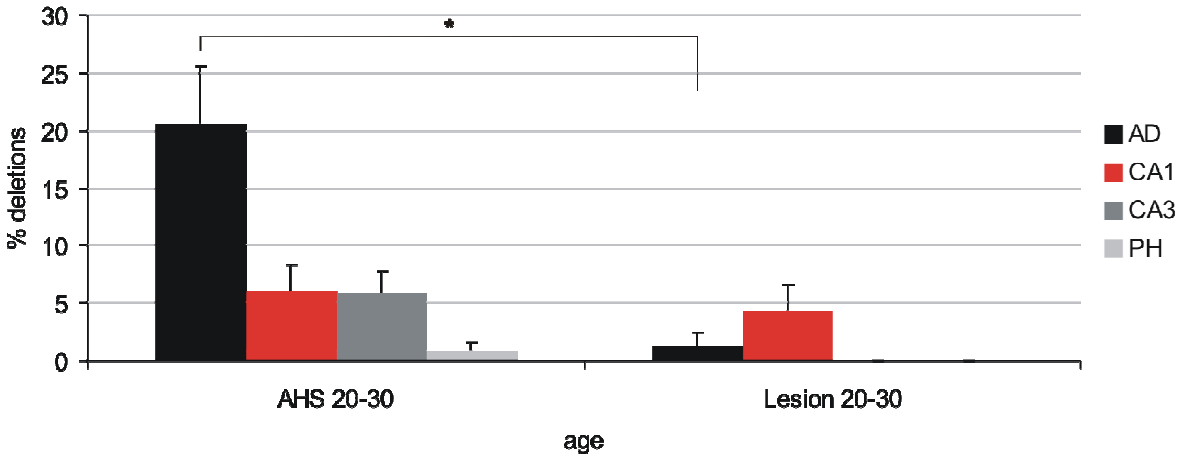

Figure 31 mtDNA deletion amounts in AHS and lesion patients, dependent on age. Primers used in the PCR, 5462F/16,115R; AD, area dentate; CA1, cornu Ammonis 1; CA3, cornu Ammonis 3; PH, parahippocampus. Error bars indicate SEM (+). Standard student's *t*-test was used to indicate significant difference; * indicates $p < 0.005$ between the two marked groups. There is high amount of deletions in the AD region of AHS patients, detectable in early age. There are significantly more deletions in AD region of AHS patients in comparison to lesion patients in the same age group (20–30).

Comparison between AHS and lesion patients at the age between 20 and 30 years, showed significant difference ($p < 0.005$) with 21% of deletions in AD region of AHS patients vs. 1.3 % deletions in lesion patients (Figure 31). This result demonstrates that specifically in AD regions of AHS patients high amount of deletions can be detected in very early stage of life.

3. 3. 1 Breakpoint 'hotspot' for TLE patients with AHS

In AHS patients, classical deletions of the mtDNA tend to have their 3' end breakpoint at nucleotide position 16,070–16,090 (Zeviani, 1989; Guo, 2010). These deletions are suggested to result from the attack of reactive oxygen species, due to impaired function of the mitochondrial respiratory chain (Baron, 2007; Imlay, 1988). To check if these deletions are the main fraction of deletions in AHS patients I performed screening for deletion content of the same set of patients with primer pair 5462F/15,623R, in the AD region. The location of the reverse primer is excluding the 16,070–16,090 region covered with the previously used primer 16,115R.

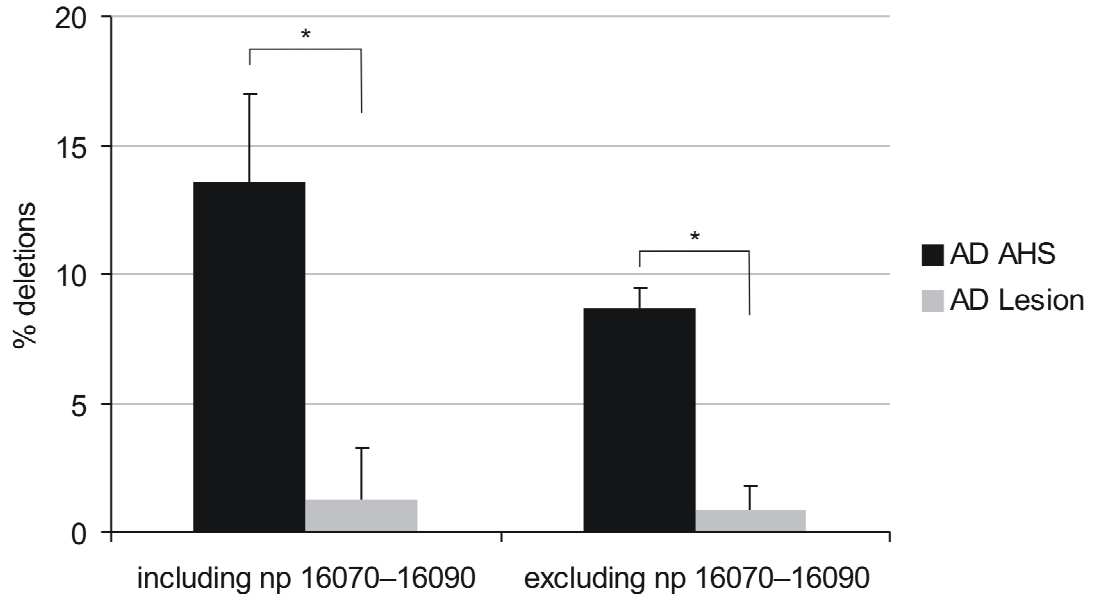

Figure 32 Comparison of relative deletion percentage in AD region, in AHS patients, with two different primer pairs. 5462/16,115, including the 16,070–16,090 region and 5462/15,623 excluding it. Error bars indicate SEM (+). Standard student's *t*-test was used to indicate significant difference; * indicates $p < 0.005$ between the two marked groups.

The change in the primer pair influenced the amount of detectable deletions in the AD region of AHS patients (Figure 32). In AHS patients, a great amount of the deletions seem to be deletions with 3' breakpoints in the 16,070–16,090 region. Change of the primer in lesion patients had no effect on the deletion / wild-type ratio. Overall, these results suggest a different pathological mechanism leading to deletions in AHS patients in comparison to lesion patients.

Previous single-molecule PCRs of AHS samples, performed in our lab have frequently detected one specific species of large scale deletion with np 8649–16,084 deleting a 7436 bp (7.4 kb) long part of the mtDNA, flanked by two 12 nt of long perfect direct

repeats. This deletion, with 3' breakpoint in the 16,070–16,090 region, has been described in different diseases such as cancer, endocrine disorders, and chronic disorders (Nicolino, 1997; Yamamoto, 1992) and its detection can be relevant indicator for underlying processes specific for AHS. Therefore, I checked its distribution among 66 AHS samples and 22 lesion TLE samples. All mtDNA samples were isolated from the CA3 region of the hippocampus. As a reference I amplified the ubiquitous 'common deletion' – 4977 bp, found to be surrounded by 13 nt direct repeats, and have compared its intensity with the intensity of the 7.4 kb deletion by ImageJ evaluation. The common deletion is frequently used as a biological marker for aging and has been used since long time as an indicator of ongoing mutagenesis of the mtDNA (Shoffner *et al.*, 1989; Berneburg *et al.*, 1999).

I detected the 7.4 kb deletion by using primers 8282F and 16,115R that flank the deletional breakpoints, when the deletion is present the amplified product has size of 398 bp. The 'common deletion' has breakpoints at 8482 and 13,459 bp position and is 4977 bp long. For its detection I have used primers: 8282F and 13,684R, when the deletion is present the PCR product has size of 426 bp. I set up a multiplex PCR, which can detect both deletions simultaneously (Figure 33). It is a PCR containing all three primers 8282F:13,684R:16,115R in ratio 4:3:1, optimized to increase the specificity of the PCR, assuring the detection of the common deletion even at lower levels. The PCR products of both deletions appear as two close bands, from which the upper band is the common deletion and the lower band is the specific deletion. After acquiring the images they were evaluated with ImageJ and ratio between the intensities of the two deletions was calculated. When the intensity ratio between the specific and the common deletion was higher then zero the sample was considered positive for the 7.4 kb deletion.

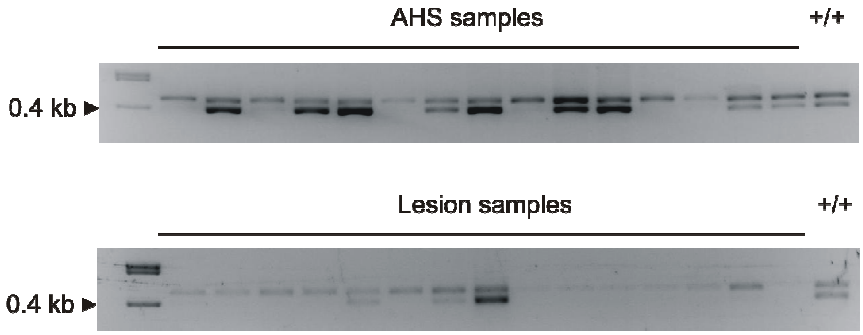

Figure 33 Multiplex PCR of AHS and lesion TLE samples. The upper panel includes 15 AHS samples and the lower panel 15 lesion samples, from the hippocampal CA3 region. Reaction products were loaded on 3% agarose gel. The upper 426 bp band represents the common deletion, 4977 bp; the lower 398 bp band represents the 7436 bp deletion (7.4 kb deletion); (++) positive control for both deletions.

In the experiment I included double positive brain sample, that reproducibly showed the same pattern. The positive sample was checked by sequencing of DNA extracted from excised from the gel product.

The analysis of the CA3 region of all 66 AHS samples and 22 lesion samples revealed that 63% of the AHS samples contained both the common deletion and the 7.4 kb deletion, in comparison to 9% of the lesion samples. This result confirms that deletion 8649–16,084 is more often detectable in AHS samples and is more specific for TLE with hippocampal sclerosis then lesion based TLE. 86% of the lesion samples contained only the common deletion, which confirms it as one of the most often described deletions in degenerative tissues. There was no sample containing only the specific deletion, neither in the AHS nor in the lesion group of patients.

After confirming the 7.4 kb deletion as one prominent deletion species from the 16,070–16,090 cluster, typical for CA3 region of AHS samples, it was interesting to find out if it is characteristic for other hippocampal regions of the AHS patients. I performed a screening of another 121 AHS samples, from which 25 samples from CA3, 46 samples from PH, 30 samples from CA1 and 20 samples from AD region. In the lesion group I checked 31 new samples, from which 7 samples from CA3, 12 samples from PH, 9 samples from CA1 and 3 samples from AD region. The result showed very high frequency of the 7.4 kb deletion in AHS samples in comparison to lesion samples. The deletion is characteristic for all brain regions in AHS samples with lowest frequency in the PH region, which is comparable to the lesion group of patients. Above 70% of the samples from CA1, AD and CA3 region were positive for the deletion. This result confirms the importance of 7.4 kb deletion and raises the question for its frequency and plausible function in seizure development or degeneration of the hippocampus in AHS patients.

AHS brain sample sequenced by Next Generation Sequencing in our group demonstrated plenty of classical deleted molecules carrying 5’ breakpoint at position 5786 and 3’ breakpoint at position 16,078, also layng in the hotspot region of 16,070–16,090 np. To check its segregation in other AHS samples I optimized a multiplex PCR for its detection, by using primers 5462F and 16,503R. I checked for the frequency of that deletion in 24 AHS and 16 lesion brain samples. 62.5% of the AHS samples were positive in comparison to 12.5% in the lesion samples. This result again points at the specificity of clonally expanding deletions in AHS brain. The absence of these types of deletions in lesion patients confirms the theory that clonally expanding deletions are having pathologic role in TLE with AHS and these deletions described above might be as well hotspots for deletion formation in TLE patients with AHS.

4. Discussion

4. 1 Exonucleases in mtDNA replication, repair and recombination

The processes of replication, repair and recombination rely, among others, on the activity of nucleases. Very little is known about the nucleases localized to mitochondria that act on the mtDNA. In humans, helicase/nuclease DNA2 was suggested to localize both to the nucleus and the mitochondria (Duxin *et al*., 2009) and recently, another endonuclease FENMIT, a mitochondria localized truncated isoform of FEN1 was described in humans (Kazak *et al*., 2013). FENMIT binds preferentially to flap structures containing 5' RNA flap and is recruited to RNA-DNA hybrids in conditions of inhibited replication. FEN1 is a 5'-flap endonuclease and 5'→3' exonuclease known to function together with DNA2 in the nucleus (Budd and Campbell, 1977). Similar to the function of DNA2 and FEN1 in the nucleus, it was suggested that in mitochondria they participate in the processing of flap structures and forked substrates in mtDNA repair through LP-BER and in mtDNA replication. Nevertheless, the knock down neither of FEN1 nor DNA2 disturbs the process of mtDNA replication (Ruhanen *et al*., 2011). Apart from FEN1 and DNA2, which have double localization, a third unique 5′-exo/endonuclease EXOG was also found to function in mtDNA repair. The involvement in mtDNA replication of FEN1, DNA2 and EXOG is not clear. Altogether, the knowledge over the mitochondrial nucleases is very poor and probably many nucleases are yet to be discovered. For example, the turnover of the mitochondrial 7S DNA molecule is very fast, but the enzyme involved in its degradation is unknown. Recently, we identified a novel 5'-exonuclease, MGME1 that might be involved directly in the processing of the 7S DNA molecule and its degradation.

MGME1 was shown to localize to mitochondria *via* immunohistochemical subcellular localization, by GFP-tagging and cell fractionation, performed by our collaborators in Cambridge (Kornblum *et al*., 2013). They performed detailed investigation of the enzymatic properties of MGME1, which revealed that it cleaves ssDNA, but not ssRNA or RNA-DNA hybrids. It has strong preference for ssDNA over dsDNA, and processes more efficiently 5' DNA ends then 3' ends (Kornblum *et al*., 2013). Such single stranded DNA is the 7S DNA, that can be substrate of MGME1.

There are several theories over the formation of the 7S DNA and its function. It was suggested that the 7S DNA participates in the priming of the heavy strand replication of the mtDNA and if it is true, its level has to be kept high in order to respond fast to the needs of the cell; or it is a result of replication stalling at the TAS region (Doda *et al*., 1981). On the other hand, in the strand-displacement model of replication, the formation of the 7S DNA fragment is being suggested to be the last step of the H-strand replication and formed by its

termination at the TAS region (Berk and Clayton, 1974) Another theory claims that 7S DNA is needed for maintaining the dNTPs pools, as with the increase of the dNTPs the 7S DNA levels as well elevate, but the mtDNA copy number does not change. Thus, the 7S DNA levels are changing in the different phases of the cell cycle in response to the needs of the cell (Antes *et al*., 2010). However, its generation, function and turnover are a matter of dispute.

Samples from MGME1 patients appeared to contain a huge amount of 7S DNA (Figure 17 black bars, Figure 18), far exceeding the broadly accepted 1.1 fold 7S DNA accumulation detected in healthy individuals. If 100% of the mtDNA molecules contain 7S DNA, the maximal theoretical accumulation of 7S DNA should not exceed 1.5 folds. In muscle from the MGME1 patients, the ratios of 7S DNA to the total amount of mtDNA were two to eight folds higher then in age matched controls, in five of the six investigated patients (Figure 17a). High 7S DNA level was detectable as well in the fibroblasts from the patients and was missing in the control fibroblasts cell line (Figure 17b). Blood samples and cells with MGME1 function down-regulated by siRNA (experiment provided by our collaborators in Cambridge) showed as well 7S DNA accumulation (Kornblum *et al*., 2013). In blood samples the elevated amount of 7S DNA was confirmed by qPCRs with different primers spanning the whole 7S DNA region (Figure 18). The accumulation of 7S DNA in MGME1 deficient samples, would suggest that MGME1 participates in the turnover of the 7S DNA. In support to that hypothesis, 7S DNA had elongated half life under mtDNA replication inhibition (performed by our collaborators in Cambridge) with fibroblasts from MGME1 patients. However, one should mention that strong MGME1 overexpression leads not only to 7S DNA degradation but also to overall mtDNA depletion, in MGME1 patients and in controls (Figure 19).

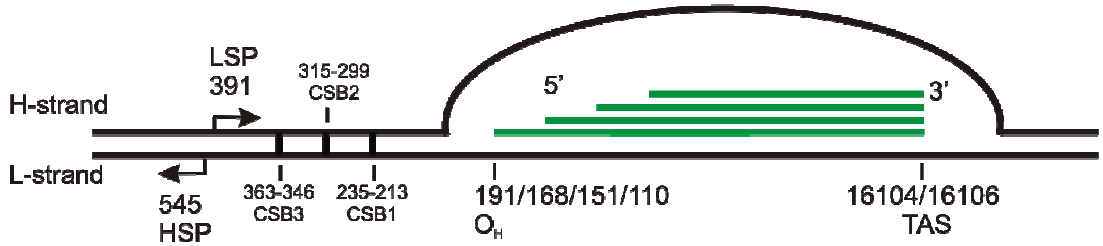

Figure 34 Structure of the D-loop containing the 7S DNA. In green is shown the 7S DNA; L, light; H, heavy; LSP, light strand promoter; HSP, heavy strand promoter; CSB, conserved sequence block; O_H, heavy strand origin of replication; TAS, termination associated sequence (modified according to Zhang and Pommier *et al*., 2008 and from our paper in preparation Nicholls *et al*.).

It has been shown that there are several types of 7S DNA (Figure 34), which differ in length, with 191 as the longest 5' end reported in the literature, defining as well the H-strand origin of replication (Clayton, 1996; Bogenhagen and Clayton, 1977). This fact might be related to the theory of 7S DNA playing priming role in H-strand replication.

Additionally to 191, np 168, 151 and 110 are the only identified 5' end positions listed in the literature until now (Crews *et al.*, 1979; Kang *et al.*, 1997; Pham *et al*., 2006). According to the literature the 3' end of the 7S DNA is at position 16,104–16,106, and it contains the termination associated sequence TAS (16,157–16,172). No variations were registered until now at the 3' end of the 7S DNA molecule (Clayton, 1996; Doda *et al.*, 1981).

As MGME1 is involved in the turnover of 7S DNA and it is a 5'-exonuclease processing single stranded DNA, a question raised if MGME1 performs processing of the 5' end of the 7S DNA molecule, and if so, how does this end look like in MGME1 deficiency. One has to remember that MGME1 activity on 7S DNA is possible only if the 7S DNA molecules are not completely annealed to the template DNA and a free 5' end is available (based on the *in vitro* data). The exact state of annealing of the 7S DNA was not studied until now. The formation of such 5' flap end close to the 191 np can be result of replication termination of the heavy strand of the mtDNA, which when fully replicated would displace the 7S DNA and create the 5' end flap. The formation of 5' 7S DNA flap end might as well occur due to the formation of secondary structures in the D-loop. It was suggested that the sequence of the D-loop at its 5' end allows the formation of a cloverleaf-like structure, which when folding would incorporate the CSB1 sequence and all major 5' 7S DNA ends. If this cloverleaf-like structure forms in the template L-strand subsequent to D-loop synthesis, the 7S DNA will not be able to anneal and will retain 5' free end, in the form a large flap (Brown *et al*., 1986).

By establishing a single-molecule blunt-end ligation-mediated PCR technique (Figure 21), using T4 polymerase blunting for detection of the 5' end of the 7S DNA and Mung Bean nuclease blunting for the 3' end, I confirmed the expected nucleotide positions, 191 (and shorter) and 16,104 for both ends of the 7S DNA in controls. In opposite to controls, MGME1 fibroblasts from P1976 had varying 5' 7S DNA ends, often exceeding position 191, and an unchanged 3' end (Figure 24). Most molecules detected in the MGME1 patients revealed longer 5' end of the 7S DNA. This result is in consensus with the impaired 5'-exonuclease activity of MGME1 in the patients. Thus, we conclude that the mutation in the MGME1 gene led to accumulation of 7S DNA molecules inefficiently processed at their 5' end. One possibility is that the longer 7S DNA molecules can be a result from aberrant RNA-DNA transitions. The longest detected 5' 7S DNA end is at position 301, which is close to the beginning of the CSB2 (299–315) (Figure 34), and the site of transcription termination and primer formation of the mtDNA (Pham *et al*., 2006). However, as shown by our collaborators

in Cambridge, treatment with RNase did not change the detectable 7S DNA ends; therefore, the RNA-DNA transitions are not affected in MGME1-null cells. In this case in the next step after the RNA-DNA transitions at the CSBs, the 5' DNA end of the 7S DNA precursor molecules has to be processed additionally by MGME1 to the known positions of the 7S DNA (191 and shorter) (Nicholls *et al*., paper in preparation). These findings are very important, as previously, it was not clear that the 5' end of the 7S DNA has to be processed, apart from removing the RNA primers. However, in MGME1 patients, this process is disrupted, which would explain the accumulation of longer 7S DNA molecules in these patients. In agreement with this, longer 7S DNA molecules were found to have greater stability and longest half-lives in mouse models for D-loop synthesis kinetics determination (Bogenhagen and Clayton, 1978), which might explain the accumulation of 7S DNA in MGME1 patients, eventually based on its slower degradation.

LM-PCR is a very powerful technique to detect free DNA ends; therefore, I checked the entire mtDNA genome for such free ends in controls and MGME1 fibroblasts. Surprisingly, in addition to the 7S DNA ends one other free end species was visible in the MGME1 patients and sequencing revealed a free end of a patient-specific linear mtDNA fragment at position 5771 and 5772. This position is located within the light strand origin of replication. Another free dsDNA end was as well detected at the O_H, by native DNA ligation (data not shown). Such free ends were not present in controls (Figure 25). A linear product with these ends would have size of around 11-kb and would include the entire mtDNA major arc. The formation of such 11-kb molecule between the two origins of replication was described in the POLG-deficient 'mutator mouse'. It was suggested that such fragments are being formed by spontaneous nicking of single stranded DNA at arrested replication forks near O_H and O_L (Bailey *et al.*, 2009). S1 treatment, as well, can generate these fragments, as the junctions near the origins of replication are very prone to nicking (Bailey *et al*., 2009). A chromosome breakage of a theta replication intermediate with ends at both replication origins might generate also such linear fragments. This is the first time that such DNA linear molecules are described in human mitochondrial pathology. As MGME1 acts preferentially on ssDNA *in vitro*, its putative role in the degradation of this blunt-end double-stranded mtDNA fragment is less probable; therefore, these molecules might be indeed product of replication stalling or a product of replication pausing at the origins of replication, providing a checkpoint of the replication process. Indeed, the restart of a stalled replication is known to be bound to the function of 5'→3' exonucleases, therefore, MGME1 might support the replication fork to pass the replication checkpoint; in such scenario, MGME1 absence would lead to lasting stuck replication and eventually to chromosomal breakage.

In this study, I showed that dysfunction of MGME1 protein leads also to the accumulation of mtDNA rearrangements, detectable with long-range PCRs in muscle

biopsies, blood and urine samples from all the affected patients (Figure 15). The rearrangements in the MMD patients were very big and atypical for other mitochondrial diseases, for example in comparison to the deletions observed in a POLG patient, which might be important for the easier diagnostics of MMD patients' carring MGME1 mutation (Figure 15). The amount of mtDNA rearrangements in MGME1 patients was in the range from 0.4% to 1.5% (Table 33). The amount of rearrangements detected in the MGME1 patients was higher in comparison to age matched controls and comparable to the amount of deletions detected in a POLG patient harboring a p.Ala467Thr mutation in the *POLG* gene. P931 showed the highest amount of rearrangements, which can be explained with the advanced age (57 years) at the time of biopsy in comparison to the other patients (10–37 years).

As the amount of deletions in POLG and rearrangements in MGME1 patients was similar, but the pattern of MGME1 rearrangements was very distinct, it was important to characterize and compare the breakpoints spectra in both pathological conditions. POLG patients showed mostly deletions affecting the mtDNA major arc between the two replication origins (Figure 16). MGME1 patients were missing the classical major arc deletions and the starting positions of the detected breakpoints were clustered in the minor arc around the $tRNA^{Phe}$ gene, in the 12S ribosomal RNA gene and near to the $tRNA^{LeuUUR}$ gene. In difference to the POLG patients MGME1 patients harbored multiple rearrangements erasing 2/3 of the mtDNA molecule, including the light strand origin of replication (Figure 16). The absence of light strand origin of replication makes these molecules unable to propagate. However, many of them were detectable repeatedly in the individual patients. One possible explanation could be, if the detected breakpoints are not actual deletions, but complex structures, such as partial duplications. Detailed analysis revealed that the detected breakpoints indeed originated mainly from partial duplications (Figure 16c). This finding can explain the clonality of these rearranged molecules missing apperantly their light strand origin of replication. In support to that finding, sequencing of the mtDNA of P931 and P3737 revealed presence of insertions of small D-loop multimers in these two patients (Table 34) and they can be result from the detection of more perplexing structures of the mtDNA. Such multimers were observed in the 'mutator mouse' (Williams *et al*., 2010) and it was suggested that they might indicate the ineffective replication termination, which needs the exonuclease activity of POLG (Brown *et al.*, 2005; Williams *et al*., 2010). In this case, our results would point out to the additional involvement of MGME1 in replication termination.

The 11-kb fragment might play role in the generation of these non-standard rearrangements, as free ends are widely accepted as precursors for deletion formation. Such precursors can be formed after double-strand break (DSB) at replication stalling sites. The repair of these DSBs is based on the mechanism of homologous recombination. However,

breakpoints close to the O_L were missing, therefore, the linear fragment detected with LM-PCR does not participate in recombination, or the mechanism of homologous recombination is not functioning properly, which actually can explain the missing major arc deletions, in MGME1 patients. These assumptions would suggest, that MGME1 is needed for the process of homologous recombination.

Three-dimensional modeling of the MGME1 active site and alignment comparison performed by our collaborators, showed high homology of MGME1 with the RecB catalytic residues of the RecBCD enzyme of E. Coli (Kornblum *et al*., 2013). Homology modeling of MGME1 active site based on the crystal structure of RecB in E. coli revealed very similar structure of the key catalytic residues of MGME1 (Kornblum *et al*., 2013). RecB is involved in end-processing in the process of recombination, which might be the case as well for MGME1. The homology of MGME1 to RecB is another confirmation of its function as an exonuclease that might be involved in recombination, and would turn MGME1 into the first described mitochondrial exonuclease directly involved in the processes of replication and recombination. The non-standard breakpoints detected in the MGME1 patients might occur by alternative forms of single-strand generation, in the absence of MGME1, in order homologous recombination to take place. The clustering of two of the breakpoints hotspots close to the D-loop might be explained by the higher probability for that region to be in a single-stranded state. And the third hotspot at $tRNA^{LeuUUR}$ is a mitochondrial transcription termination factor (mTERF1) binding site, which might lead as well to the formation of single-stranded regions, required during homologous recombination.

Analysis of the breakpoints detected in the MGME1 patients showed equal amount of both type of rearrangements, with and without direct repeats (with minimal length of 5 nt) (Appendix I), similarly to the analyzed deletions in the POLG patient (Appendix II), which does not point to a specific mechanism of the breakpoints formation in POLG and in MGME1 patients.

Besides mtDNA rearrangements, mtDNA depletion is common feature for MMD patients, it was interesting to find out weather this is the case in MGME1 patients. Substantial depletion was observed in all affected patients (Figure 17 grey bars), except in muscle from P1976, which might be in connection with the fact that the muscle biopsy was taken at the age of 10 and at that time the patient was mildly symptomatic. The fact that the MGME1 patients carry multiple mtDNA rearrangements and represent mtDNA depletion suggests that the primary cause of the disease in MGME1 patients is mtDNA maintenance perturbation and points to the importance of MGME1 in mtDNA maintenance.

In mtDNA depletion and repopulation experiments in fibroblast cell lines from patients P1976 and P4052 and a control fibroblasts cell line, we used 2'-3'-dideoxycytidine (ddC) that competes with the natural substrate deoxycytidine for DNA incorporation (Waqar *et al*., 1984)

and causes replication termination due to missing 3'-oxygen of the ddC (Mitsuya *et al*., 1987). Polymerase alpha, which is the main nuclear active polymerase, has low affinity to ddC which insures the low cytotoxicity of the method, whereas polymerase gamma in the mitochondria can use it as a substrate. In this way, only the replication in mitochondria is being specifically affected (Lee *et al*., 2009). 12 days treatment of control and patient fibroblasts with ddC, followed by 16 days of repopulation without ddC, led to recovery of only 5% of control mtDNA copy numbers in P1976 and 55% in P4052 (Figure 20). These results revealed severely impaired mtDNA repopulation in MGME1 mutated cells.

Figure 35 depicts our hypothesis over the function of MGME1 in mtDNA maintenance.

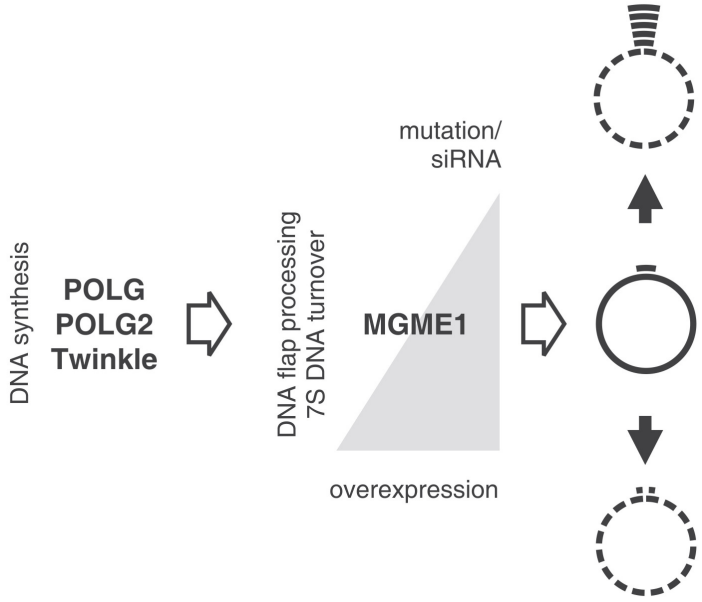

Figure 35 Proposed function of MGME1 in mtDNA maintenance (adapted from Kornblum *et al*., 2013). Replication intermediates are accumulating due to mutation in MGME1 or siRNA, which leads to mtDNA depletion and 7S DNA accumulation (right black arrow up). Overexpression of MGME1 leads to 7S DNA degradation and overall mtDNA depletion (right black arrow down).

Shortly after our publication, Szczesny *et al.* (2013) have described the same nuclease, and they have called it Ddk1 based on its predicted catalytic residues. They have shown that Ddk1 is metal-dependent nuclease, targeted to mitochondria, involved in the regulation of 7S DNA turnover, with single DNA strand affinity, and requiring free ends to fulfill its function. In contrast to our findings, the authors claimed that Ddk1 had a putative 3'→5' exonuclease function, which was not supported by later findings. In consensus with our findings, Ddk1 binds to the free end of a substrate and moves along it until hydrolysable site is reached, in this way it differs from all other DNAases described until now. This ability

of the enzyme to slide over RNA, might suggest involvement of Ddk1 in other mtDNA transactions (Szczesny *et al.*, 2013).

In conclusion, we have discovered a novel gene encoding for the protein MGME1, a 5'-exonuclease located to mitochondria. Its loss of function leads to the formation and accumulation of unusually large partial duplications. mtDNA depletion and accumulation of replication intermediates, such as the 7S DNA. It is the first dedicated mitochondrial exonuclease proven to be directly involved with the process of mtDNA replication. MGME1 is able to process DNA flap structures, as well as flap structures containing RNA at their 5' end. Nucleases described until now that function in mitochondria FEN1, DNA2 and ExoG have functions more focused on repair of the mtDNA, but their involvement in replication was not reported, and MGME1 seems a good candidate for flap processing of intermediates during mtDNA replication, for example of displaced DNA containing Okazaki fragments during lagging strand synthesis or in LP-BER (Kornblum *et al*., 2013).

Figure 36 sums up our knowledge for mtDNA replication; and in Figure 37 are summarized all findings over the dysfunction of MGME1 and its hypothetical involvement in replication and repair, as well as description of the possible 5' flap ends formations, which are substrates for its function.

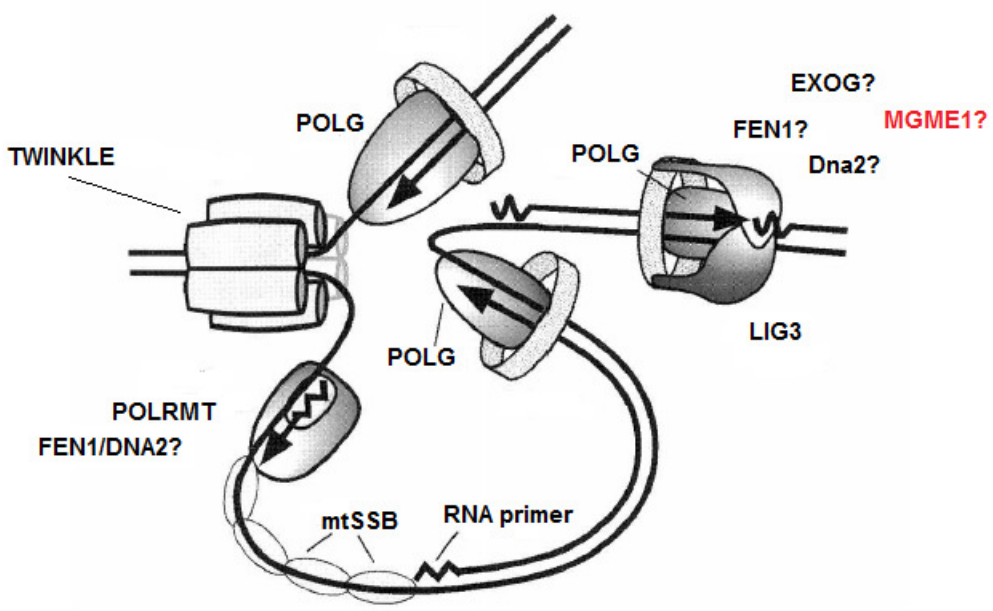

Figure 36 Replication fork at the mtDNA (adapted from nuclear replisome by Burgers and Seo, 2006).

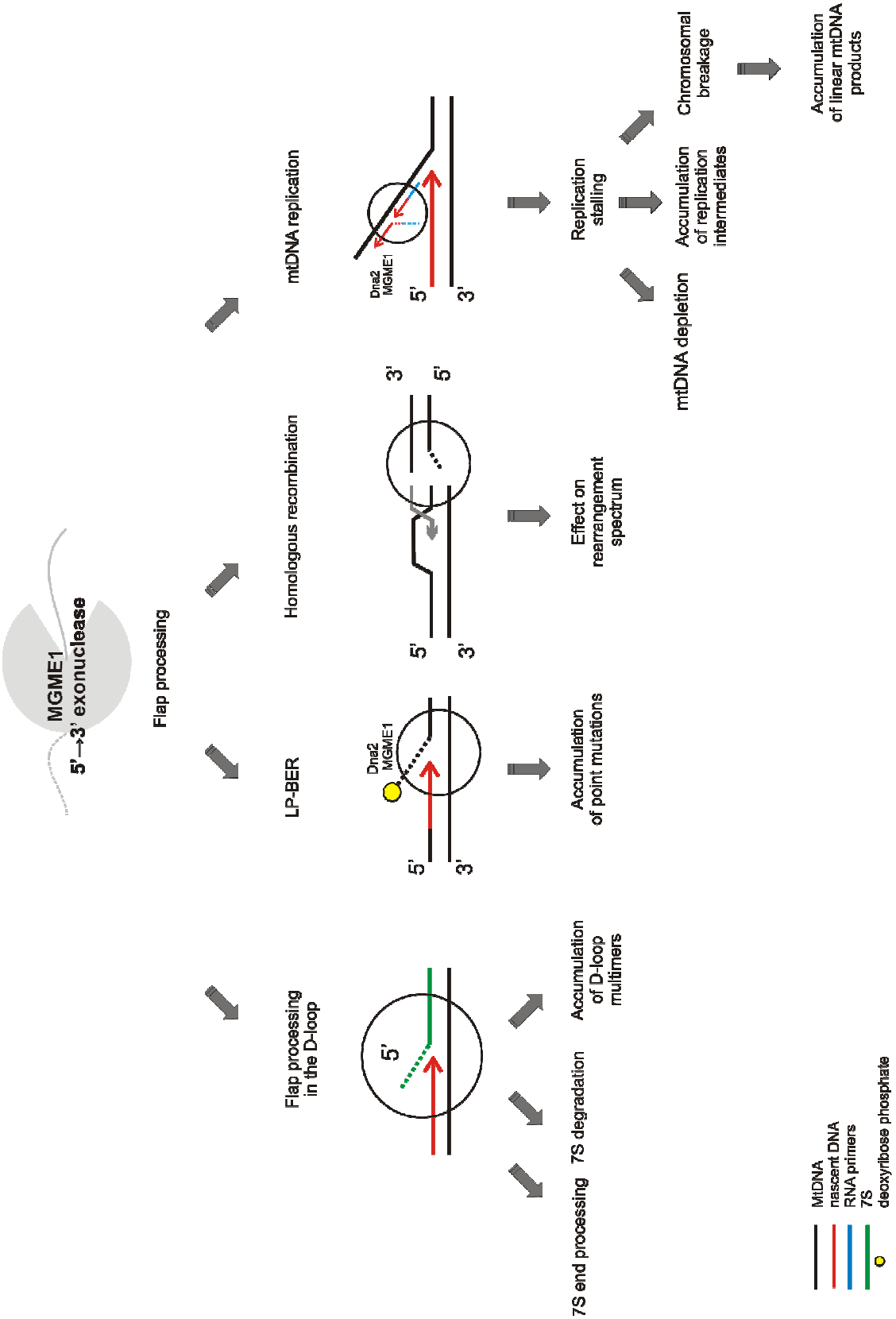

Figure 37 Proposed involvement of MGME1 in different processes of mtDNA maintenance, mtDNA replication and repair, and consequences from its dysfunction.

4. 2 Mitochondria dynamics and mtDNA maintenance

Impairment of mitochondrial dynamics due to mutations in nuclear genes encoding for proteins participating in the processes of fusion and fission, is leading to different mitochondrial disorders with unclear molecular pathologic mechanisms. Such disease is Charcot–Marie–Tooth neuropathy type 2A (CMT2A). CMT2A is an autosomal dominant axonal form of peripheral neuropathy caused by mutations in the *mitofusin 2* gene (*MFN2*), which encodes a mitochondrial outer membrane GTPase protein that promotes mitochondrial fusion (Züchner, 2004).

Neurodegeneration appears to be common phenotype in mice with targeted mutation in *MFN2* and cells lacking mitochondrial fusion show severe defect in their respiratory capacity (Chen, 2005). MFN-null mice for either of the mitofusins die during the embryonic development due to placenta defects, and show fragmented mitochondria in fibroblast (Chen *et al.*, 2003). MFN2 deletion mutant missing two transmembrane spans blocks mitochondrial fusion and represents phenotype as a dominant-negative mutant. Its overexpression leads to loss of membrane potential, which suggests function of MFN2 in maintaining it (Honda *et al.*, 2005). Knock out of MFN2 increases the distance between mitochondria and ER. In MEF and HEK cells, depolarization of the inner mitochondrial membrane, through protein junction transduces a signal to the outer membrane which is being bridged by MFN2 to the STIM1 protein (dynamic calcium signal transducer) and leads to activation of the CRAC channels (calcium release activated channels) responsible for the replenish of calcium into the ER. Disrupted connection between ER and mitochondria is found to be relevant in heart failure and heart myocites damage (Dorn and Maack, 2013). Dysfunction of the mitofusins (MFN1 and MFN2) leads to disruption of the mitochondrial network and the process of mitochondrial fusion.

An interesting hypothesis claims that by fusion and fission the process of effective complementation between the mutated mtDNA molecules, proteins and RNA allows the cell to tolerate higher levels of pathogenic mtDNA (Chen, 2010). In support to that studies showed that the process of mitochondrial fusion seems to be up-regulated in the presence of oxidated gluthation in the cells, which is a main oxidative stress indicator, and most probably the mitochondrial fusion is coupled as well to cellular stress response (Shutt *et al*., 2012). All these studies show the importance of mitochondrial dynamics for their proper function, but until now, it remains unclear how the mitochondrial fusion dynamics affects the mitochondrial function.

Big part of my PhD work was devoted to characterization of the mitochondrial phenotype in CMT2A patients carrying mutations in *Mfn2* in order to shed a light on the pathomechanism leading to disease. Our study included four CMT2A patients caring four

different mutations localized in different domains of the *MFN2* gene, two of which were not described before (Figure 26). We investigated the mutation effect on mitochondrial function in skeletal muscle and cultured fibroblasts. As CMT2A is caused by a primary mitochondrial dysfunction, all alterations of mitochondrial function would be expected to be specific for CMT2A, when different to signs of neurogenic atrophy. Therefore, a disease control patient sample from Charcot–Marie–Tooth type 1A (CMT1A) was included in the study, as all changes in the muscle and mitochondria in this patient are consequences of neurogenic atrophy, the potential mitochondrial alterations would be secondary.

In mice, the complete loss of function of both mitofusins led to severe respiratory deficiency in brain and muscle, while knocking out of only one of the mitofusins resulted in no specific phenotype (Chen *et al.*, 2005; 2007; 2010). All of the patients in our study carry a missense mutation on only one allele of *MFN2*, which would suggest that humans are much more sensitive to mild impairment in the mitochondrial dynamics or dominant negative effect of the mutations. Until now, oxidative phosphorylation impairment has been investigated only in fibroblasts from CMT2A and the results were very contradicting. Although one study on patients caring a mutation in the GTPase domain did not show any respiratory dysfunction (Amiott *et al.*, 2008), a complex IV deficiency was detected in fibroblasts from patients with an unusual for MFN2 mutation phenotype (Rouzier *et al*., 2012).

In our study, skeletal muscle histology analysis of two of the patients revealed abnormal mitochondrial distribution within the type 2A skeletal muscle fibers. Cytochrome *c* oxidase staining showed paucity of intermyofibrillar mitochondria that was confirmed by electron microscopy (from our collaborators in Magdeburg). The mitochondria were having reduced size and number, with abnormal slightly swollen appearance (Vielhaber *et al*., 2013). The cristae in the mitochondria were resembling reduced folding and empty appearance. The affected mitochondrial distribution and morphology is in consensus with previous studies in mice lacking both mitofusins (Chen *et al*., 2010).

Our data provided direct evidence for the functional impairment of oxidative phosphorylation in skeletal muscle and fibroblasts of CMT2A patients harboring different mutations in the *MFN2* gene. Mitochondrial respiration measurements and enzymatic activity determination in muscle and fibroblasts from all four patients revealed slightly reduced maximal respiration rate and increased respiration sensitivity to azide treatment, with consequent decrease of cytochrome *c* activity in the mitochondria (all the data was provided by Dr. Schöler). The only patient without respiratory chain function impairment was carrying mutation in the GTPase domain of MFN2, which was in accordance with the results of Amiott *et al*., (2008). Our data revealed that a potential reason for the observed decreased cytochrome *c* oxidase activity is a twofold decrease in mtDNA copy number (Table 35). mtDNA copy number determination in muscle and fibroblast from the patients showed that

the absolute copy numbers were two-fold reduced in the CMT2A patients in comparison to controls. Only one of the patients had non-significant decrease in the copy number, but was showing high accumulation of deletions (Table 35 and Figure 27). The observed depletion of mtDNA might be due to impaired mtDNA replication as it has been observed in patients carrying mutations in the *OPA1* gene (Amati-Bonneau *et al*., 2008). It was previously described that the rate of oxidative phosphorylation is in linear connection to the mtDNA total amount (Kudin *et al.*, 2002; Rocher *et al*., 2008). Thereafter, the mtDNA depletion is sufficient to explain the observed mitochondrial dysfunction.

The impaired content mixing would suggest accumulation of mtDNA deletions, due to impaired functional complementation of the heteroplasmic molecules (Nakada *et al*., 2009); indeed, muscle and fibroblast samples from all four MFN2 patients show multiple deletions (Figure 27). Although, the deletion amount was higher then in age matched controls, their level was not as high to be responsible for the impaired mitochondrial function (not higher then 0.2 %). However, the patient who did not show mtDNA depletion was harboring 0.18% of deletions and was the only patient caring a deletion in the GTPase domain of MFN2. Our result is in apparent contrast with another study performed by Rouzier *et al.*, 2012, where they have detected 49% deletions in skeletal muscle of one patient. This difference between the results can be due to the advanced age of the patient used in the Rouzier *et al.* study. These results demonstrate the diversity in mitochondrial functional alterations due to different mutations in the *MFN2* gene, which can explain the diversity in the results from previous studies.

The breakpoint analysis by smPCR revealed that some of the deletions observed in the patients were untypical; lacking the heavy strand replication origin or the light strand promoter, or their 3' end breakpoint spans the replication termination site. 13 deletions of that type were detected (Figure 28). Until now deletions erasing DNA above 16,268 np were not described in the literature and only 4 deletions were registered to span the 16,085 np (Samuels *et al.*, 2004). This kind of deletions lack parts of the mtDNA that are important for replication initiation. Accordingly, they cannot be result of clonal expansion, but rather a result from ongoing mutagenesis and impaired mtDNA repair. Out of the 69 mapped deletions, 56 were detected only once in the smPCR reactions, which is in consensus with the absence of clonality. In the MFN2 patients I detected deletions in the small arc of the mtDNA, which might be disease specific (Figure 28). Some of the deletions were spanning the np 16,100 going over the TAS region into the 7S (Figure 28). Deletions expanding over the 16,100 np are rarely described in the literature. To confirm the formation of these deletions, exceeding the TAS region, I checked for the presence of such deletions in fibroblasts treated with high doses of hydrogen peroxide. To follow the impairment of the mtDNA with the increase of hydrogen peroxide dose, I optimized a qPCR which can be used

for determination of the relative amplifiability of the mtDNA and evaluation of its integrity (Figure 29). By applying this method I could confirm the progressive mtDNA damage in linear dependence from the H_2O_2 treatment with increasing concentrations. In the H_2O_2 treated fibroblasts I detected deletions spanning the classical 3' deletion breakpoint at 16,000–16,100 np and entering into the 7S as well as small arc deletions (Table 36), as the ones observed in MFN2 patients. The appearance of such deletions due to oxidative stress, might point to ongoing oxidative stress in MFN2 patients. Furthermore, the impaired content mixing, might explain the absence of clonally expanding deletions and the accumulation of *de novo* mutations.

Impaired mtDNA replication and mtDNA maintenance are most likely the reason for lowered mtDNA content and accumulation of multiple mtDNA deletions in CMT2A patients, with imparied mitochondrial dynamics. The insufficient content mixing would lead as well to insufficient substrates for efficient mtDNA replication and repair of ongoing mtDNA injury.

4. 3 mtDNA deletions in TLE

mtDNA polymerase errors, replication machinery failure and replication fork stalling during the process of mtDNA synthesis can lead to the formation of mtDNA mutations. mtDNA damage can arise as well form different factors such as exposure to environmental mutagens and specifically high vulnerability to ROS activity, due to its endogenous formation during mitochondrial respiration (Shokolenko *et al.*, 2009) (Figure 38). The fate of the damaged mtDNA molecules (marked with a star on Figure 38) is crucial for the fate of the mitochondria and the cell itself. Damaged mtDNA molecules can either undergo repair or be degraded. The repair might end with the complete restoration of the mtDNA in its original state or might end in the formation of stable molecules with altered information, mutant molecules. Mutated molecules that are not missing parts of the DNA important for mtDNA replication can expand clonally, and because of their smaller size they might replicate faster than the wild-type mtDNA molecules. Mutation segregation and clonal expansion lead to the development of a pathological phenotype. However, as mitochondria are very dynamic organelles constantly involved in processes of fusion and fission and balanced mitochondrial content mixing, the damaged or mutated mtDNA is constantly complemented; therefore, the accumulation of deleted mtDNA molecules must reach certain threshold in order to cause pathological changes in the cells.

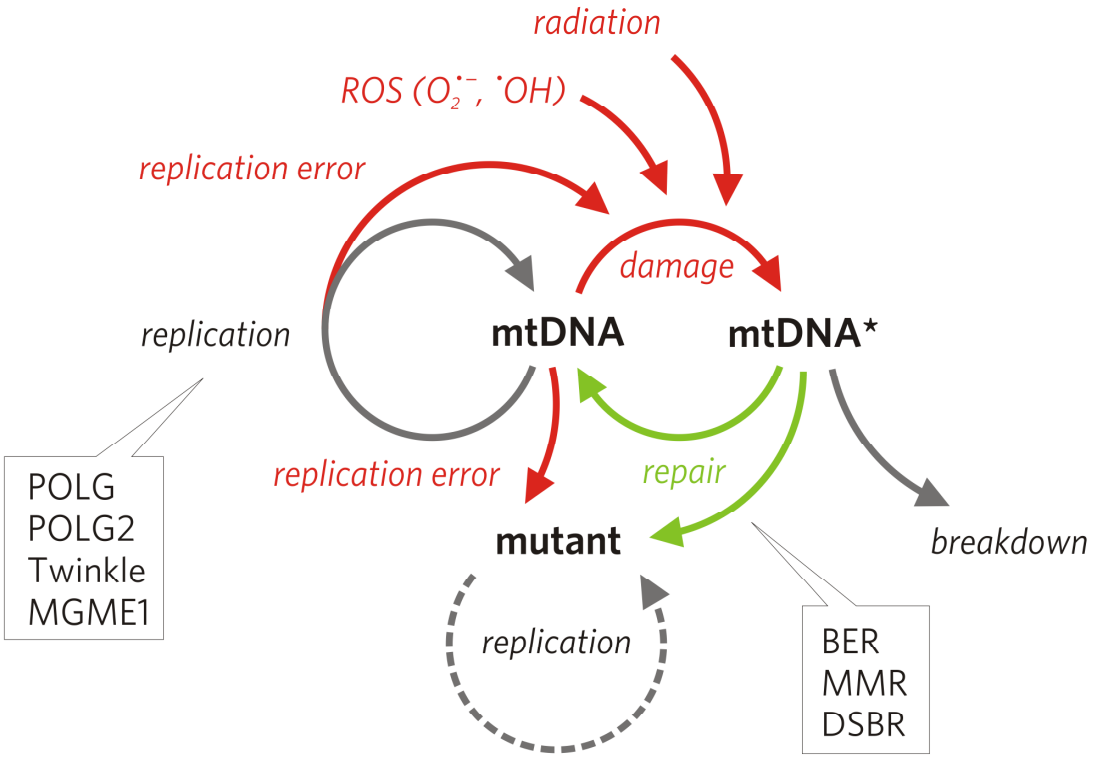

Figure 38 mtDNA mutagenesis. BER, base excision repair; MMR, mismatch repair; DSBR, double-strand break repair; ROS, reactive oxygen species; *, damaged mtDNA molecules, (adapted from Zsurka and Kunz, 2013).

As mitochondria are the main source of ATP in the neurons, failure of their respiratory chain function would lead to neuronal dysfunction and eventually to cell death. Most probably the local insufficiency of ATP in the neurons, for example, in the presynaptic terminal, is causative for the neuronal dysfunction rather then a general energy drop in the cell (Zsurka and Kunz, 2013). Mitochondria were shown to participate in modulating the neuronal excitability and the synaptic transmission (Tang and Zucker, 1997).

Most likely, the local ATP shortage in combination with clonally expanding somatic mtDNA deletions leads to the slow progression of the disease (Zsurka and Kunz, 2013). This mitochondrial dysfunction was shown to play important pathogenic role in the seizure generation and epilepsy, and particularly in temporal lobe epilepsy (TLE) with Ammon's horn sclerosis (AHS) (Kudin *et al*., 2009, Guo *et al*., 2010). mtDNA depletion and accumulation of mtDNA deletions through clonal expansion were described in TLE with AHS (Guo *et al*., 2010). Neuronal cells, such as the interneurons or the pyramidal cells, containing more mitochondria are more prone to damage due to ATP shortage, in comparison to other neuronal cell types, such as the hippocampal granule cells, that have lower amounts of mitochondria (Gulyás *et al*., 2006, Zsurka and Kunz, 2013). These cells being rich of mitochondria are also more vulnerable to injury, due to their dependence on the ATP

production. The hippocampus is having lower seizure threshold and patients with TLE with AHS show segmental neuronal cell loss of pyramidal neurons in the CA1, CA3 and CA4 regions of the hippocampus and almost no injury in the granular cell layer. This cell loss accumulates during the years and is considered as causative for the medicamentation resistance of patients suffering from seizures generated in the temporal lobes and for their severe memory impairment (Kudin *et al*., 2009). Figure 39 shows schematic overview of the pathological mechanisms and a postulated “vicious circle” of mitochondria damage, leading to epilepsy.

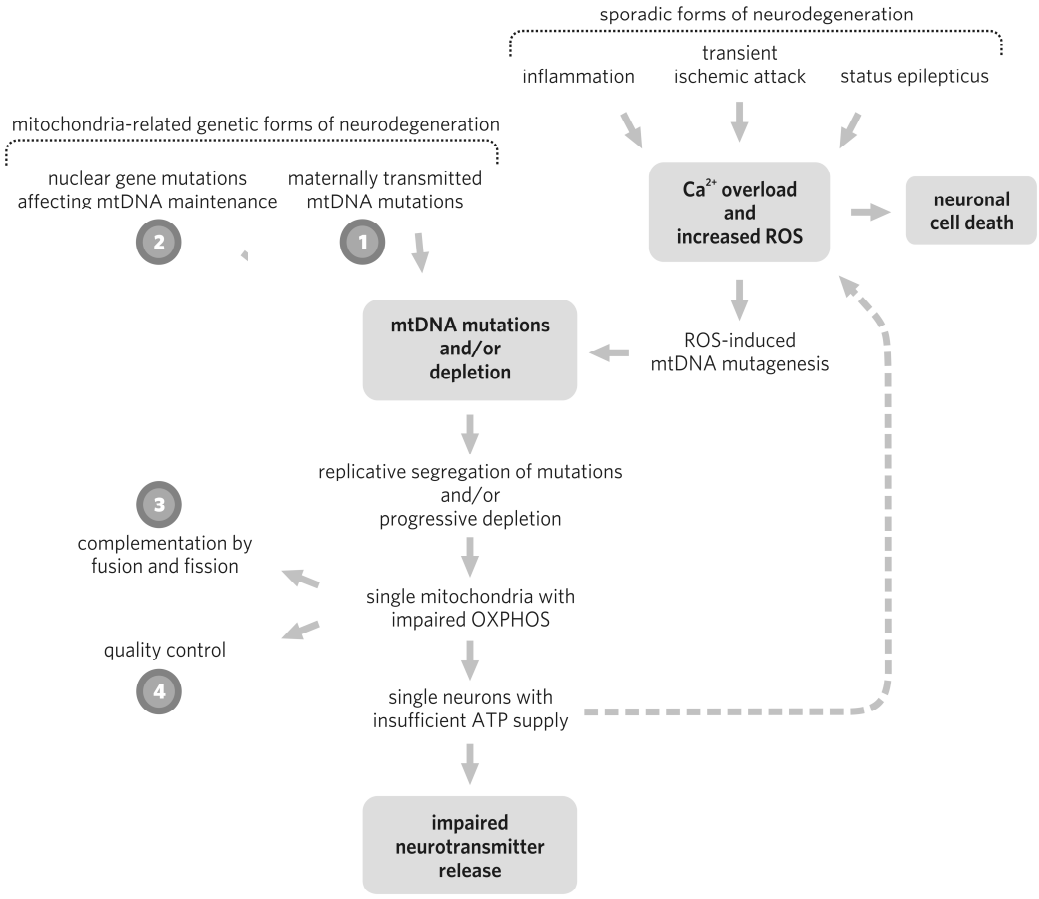

Figure 39 Overview of the accumulation of mutated mtDNA, respiratory failure, and insufficient ATP supply leading to disease (adapted from Zsurka and Kunz, 2013).

Comparison of the amounts of mtDNA rearrangements in the hippocampal brain regions CA1, CA3, AD and PH in samples from TLE patients with AHS, demonstrated that AHS patients show overall higher accumulation of deletions in all four investigated brain regions in comparison to hippocampal brain samples from the same regions in patients with TLE, resulting form brain lesion and with no hippocampal sclerosis, (Figure 30). Significant difference between the two sets of samples, with $p<0.005$ was detected in the CA3 and the

AD hippocampal regions. This finding is in consensus with the literature, as in the AHS pathology the CA3 region is one of the most affected brain regions. In the AD region the differences between the AHS and lesion groups was even more dramatic, with the AHS patients showing 12 fold higher level of deletion accumulation in comparison to the lesion group. The involvement of the AD region in the epileptogenesis is a matter of dispute and our finding of increased amount of deletions in this region in AHS patients might be relevant. It was shown that the AD region is involved in the first steps of the development of the epileptic seizure, by receiving synchronous discharges released due to neuronal cell loss in the cortex, in patients with injury-associated hippocampal epileptogenesis (Sloviter *et al*., 2012). Eventually, the longer survival of the granule cells in the AD region, that are not so prone to the seizure effects might explain the even higher amount of deletions in comparison to the CA3 region (Figure 30). Granule cell dispersion and changes in dendritic orientation and spine distribution were registered in patients with AHS (Freiman *et al*., 2011). Another study from Buckmaster and Dudek in 1997, showed functional abnormalities in the AD region of epileptic kainate-treated rats.

It is not clear whether the hippocampal mtDNA deletions detected in TLE patients with AHS participate in the pathomechanism of the disease, or they are result from it. Our findings showed accumulation of deletions in all regions of the AHS brain samples in 20–30 year old patients (Figure 31), in opposite to aged matched TLE lesion disease controls. Therefore, it is more likely that the mtDNA rearrangements in the AHS hippocampus are not age related and are causative for the disease rather then a consequence of it. These results suggest a different pathological mechanism leading to TLE in AHS patients, and dramatic and fast accumulation of deletions. In young AHS patients, the highest amount of the deletions was detectable in the AD region, whilst the CA3 region deletions accumulation was not significant. Thus, mtDNA perturbations in the AD region might be essential for the early stages of the disease.

Oxidative stress and ROS production are involved in the processes of mtDNA damage and double-strand DNA breakage. Recently, it was suggested that DSB are important for the process of deletion formation (Krishnan *et al*., 2008). They proposed that the 3'→5' activity of an exonuclease, leads to the exposure of single stranded regions of mtDNA that sustain homologous binding to regions of the mtDNA with direct repeats. However, this model is valid only in homologous recombination. In 2009 Fukui and Moraes, have described a novel mouse model, in which they could trigger generation of deletions as consequence of DSB induction at a fixed position on the mtDNA. The model resulted in the formation of various in size deletions, with and without repeats, generated by homologous and non-homologous recombination and representing the situation in aging tissue. It is known that in AHS patients, the 3'-end breakpoints of the deletions cluster at nucleotide

position (np) 16,070–16,090 (Zeviani, 1989; Guo, 2010), that was described as a hotspot for ROS activity (Zeviani *et al.*, 1989; Srivastava and Moraes, 2005) and DSB formation (Bacman *et al.*, 2009), which would suggest that this region might be the 'fixed position' of DSB occurance according to the model proposed from Fukui and Moraes, 2009. In other studies, the DSB generation at that region was described as result from replication fork arrest (Wanrooij *et al.*, 2004) or due to its participation in homologous annealing, based on the single strand nature of the region (Krishnan *et al.*, 2008).

In order to check if deletions with 3' breakpoints within the 16,070–16,090 region, are indeed present in samples included in this study, I performed comparative analysis of the detectable deletions amounts with primer pairs either including or excluding the 16,070–16,090 region. The result showed that in AHS patients, great amount of the deletions seem to have their 3' breakpoints within the 16,070–16,090 region (Figure 32). This result might signify increased ROS production as a causative feature in AHS patients with TLE.

The presence of two specific deletions, with 3' end within the 16,070–16,090 region, 8649–16,084 (7.4 kb) and 5786–16,078 (10.3 kb), was examined in AHS and lesion TLE patients, by applying multiplex PCR. As a reference, the ubiquitous 'common deletion' (4977 bp) was amplified together with the deletions of interest. According to the literatue the 4977 bp deletion is a hallmark of degenerative phenotype, it accumulates with age in normal tissues and is detected at higher frequency in tissues with higher metabolic rate, such as brain and heart tissues (Wallace, 1992a; Bogliolo *et al.*, 1999). In the CA3 region, more then 60% of the AHS samples contained both the 7.4 kb and the 10.3 kb deletions. All samples positive for these specific deletions were containing the common deletion, too. In the lesion set, in 86% of the samples the common deletion was detectable, but in the absence of the two specific deletions. However, the two deletions of 7.4 kb and the 10.3 kb were detectable not only in the CA3 region, but in all four investigated brain regions of the AHS samples, with lowest frequency in the PH region. The detection of these two prominent deletional species in AHS patients supports the hypothesis of deletion formation based on the occurance of DSB at the 16,070–16,090 region.

Appendix I

mtDNA deletions in skeletal muscle biopsies, fibroblasts and urine samples of MGME1 patients.

Sample	Del Start	Del Stop	Repeat length	Count
M2061	262	16,069		2
	461	13,522		
	529	14,382		
	3285	16,069		
	3959	15,737	7	4
	3615	12,986	11	1
M3737	315	16,193	10	
	499	15,028		
	508	14,808		
	512	13,925	6	
	535	14,119		
	873	15,539		5
	886	15,972		4
	3231	13,472		
	3296	16,034		4
	3558	14,816		2
	3578	14,813	8	1
	3743	15,636		3
	4514	14,310		4
	5438	13,792		
	14,287	16,264	7	
M1976	3258	16,070		3
	3846	14,701		
	4490	11,905		
	5240	13,812		
FB1976	84	16,094		
	168	16,222		
	196	15,195		
	399	16,061		
UR1976	3248	15,972		
	3272	15,541		
	3321	15,965		2
	3346	15,971		
	3460	14,389		
	3615	12,986	11	2
	4902	15,848	7	
	8649	16,084	12	
M931	115	12,304		
	308	13,786	5	
	310	15,539		
	462	13,788	6	
	482	14,142	6	

continued

Sample	Del Start	Del Stop	Repeat length	Count
M931	499	14,517		2
	506	14,346	6	
	540	4352		
	541	14,396		
	561	13,785		3
	562	13,462		2
	791	15,515		2
	887	16,079		
	899	16,115	11	2
	3266	16,078		
	3273	16,071		5
	3280	16,032		3
	3572	14,812		
	3578	15,546	10	1
	3586	15,641		
	3603	14,801		
	3611	16,076		2
	3614	14,068		
	4228	14,832		
M4050	539	14,393	10	
	561	15,529	6	5
	1228	14,532		
	3529	15,749		
	4468	14,824		
	5742	14,586		
FB4050	971	15,212		
M4052	453	15,197		5
	461	14,429		4
	482	13,775		
	515	12,562	7	
	899	16,079		
	3333	14,138	9	
	3475	13,626		
	3496	13,039		
	3602	15,272	5	
	3615	12,986	11	1
	3721	15,945		2
	3959	15,737	7	1
	4773	16,320		
FB4052	316	16,193		

Appendix II

mtDNA deletions in skeletal muscle biopsy of a POLG patient carrying the homozygous mutation p.Ala467Thr in the *POLG* gene.

POLG muscle

Del Start	Del Stop	Repeat length	Count
5477	11,061	5	2
5484	11,056	7	2
5491	11,061		2
5623	13,000	11	
5788	13,922		
5788	13,067		2
5789	13,922		
5790	13,922		
5796	13,922		
5830	13,922		
5841	13,649		2
5841	13,923		
5842	13,922		
5918	13,344		
6135	12,302		
6219	15,538	6	
6342	14,004	11	
6366	13,635	5	2
6440	13,841		
6544	13,843	8	
6640	13,240		
6789	14,098		
6930	13,563	10	
7132	14,533	7	2
7515	14,594		
7516	13,799		
7695	15,386		
7752	13,346		2
7818	16,071		2
7819	16,070	6	
7922	16,071		
7946	15,539		
7986	16,072		
8029	15,541	5	
8498	15,612	13	
8533	12,766		
8766	16,068		2
8929	14,530	4	

continued

Start	Stop	Repeat length	Count
9233	15,572		
9233	15,760		
9399	14,603		
9505	14,155		
9582	14,498	6	
9598	15,267	8	
10,292	16,070		
10,477	15,556		2
10,874	15,572		
11,432	16,072		
11,725	15,443	5	

Appendix III

mtDNA deletions in skeletal muscle biopsies and fibroblasts of CMT2A patients.

Sample	Start	Stop
Patient 1 muscle	192	4,195
	502*	3,498*
	1,238*	3,601*
	5,314	16,462
	6,485	15,458
	7,617	14,947
	8,299	15,588
	8,483	13,459
	8,624	15,662
	8,642	16,142
	8,663	16,071
	10,952	15,371
Patient 1 fibroblasts	383	2,989
	6,589	15,799
	10,292	13,632
Patient 2 muscle	464	3,575*
	465	3,802
	5,600	15,851
	5,793	14,599
	6,486	14,500
	6,924*	14,280*
	7,300	14,857
	8,031*	16,069*
	9,891	15,266
	12,134	16,298
Patient 2 fibroblasts	491	4,246
	3,767	15,862
	6,114	15,513
	6,143	15,866
	7,153	15,768
	7,863	14,597
	8,451	16,158
	9,507	16,294
Patient 3 muscle	220	4,570
	561	3,896
	548	4,442
	556	4,001
	790	4,527
	985	4,739
	1,847	4,256
	6,326	11,683
	6,427	11,679

continued

Sample	Start	Stop
Patient 3 muscle	6,541	11,603
	7,815	12,231
	9,033	14,056
	9,098	15,438
	9,450*	14,443*
	9,651*	14,602*
	10,962	15,845
	10,985	16,071
	11,715	15,434
Patient 3 fibroblasts	746	3,290
	694	4,134
	3,578*	15,546*
	3,941	12,886
	6,031*	16,071*
	6,330	13,993
	6,713	12,755
	8,483*	13,459*
	8,900	16,071
Patient 4 fibroblasts	175	3,622
	3,496	16,384
	4,217	15,956
	4,437	16,514
	5,750*	15,613*
	6,231*	15,434*
	6,535*	15,397*
	7,055	16,129
	8,032	16,355

*Repeatedly detected deletion species

In red are listed deletion breakpoints lacking the replication origin O_H or the L-strand promoter (5'-breakpoint below position 441) or with 3'-breakpoint located deep in the replication termination region beyond position 16,100.

List of References:

Aguilera A, García-Muse T (2012) R loops: from transcription byproducts to threats to genome stability. *Mol Cell*, 46: 115–124.

Alam TI, Kanki T, Muta T, Ukaji K, Abe Y, Nakayama H, Takio K, Hamasaki N, Kang D (2003) Human mitochondrial DNA is packaged with TFAM. *Nucleic Acids Res*, 31: 1640–1645.

Alexeyev M, Shokolenko I, Wilson G, LeDoux S (2013) The maintenance of mitochondrial DNA integrity–critical analysis and update. *Cold Spring Harb Perspect Biol*, 5: a012641.

Alexeyev MF (2009) Is there more to aging than mitochondrial DNA and reactive oxygen species? *FEBS J*, 276: 5768–5787.

Altmann R (1890) Die Elementarorganismen und ihre Beziehungen zu den Zellen. *Veit*, Leipzig.

Amati-Bonneau P, Valentino ML, Reynier P, Gallardo ME, Bornstein B, Boissière A, Campos Y, Rivera H, de la Aleja JG, Carroccia R, Iommarini L, Labauge P, Figarella-Branger D, Marcorelles P, Furby A, Beauvais K, Letournel F, Liguori R, La Morgia C, Montagna P, Liguori M, Zanna C, Rugolo M, Cossarizza A, Wissinger B, Verny C, Schwarzenbacher R, Martín MA, Arenas J, Ayuso C, Garesse R, Lenaers G, Bonneau D, Carelli V (2008) OPA1 mutations induce mitochondrial DNA instability and optic atrophy 'plus' phenotypes. *Brain*, 131: 338–351.

Amiott EA, Lott P, Soto J, Kang PB, McCaffery JM, DiMauro S, Abel ED, Flanigan KM, Lawson VH, Shaw JM (2008) Mitochondrial fusion and function in Charcot–Marie–Tooth 2A patient fibroblasts with mitofusin 2 mutations. *Exp Neurol*, 211: 115–127.

Anderson S, Bankier AT, Barrell BG, de Bruijn MH, Coulson AR, Drouin J, Eperon IC, Nierlich DP, Roe BA, Sanger F, Schreier PH, Smith AJ, Staden R, Young IG (1981) Sequence and organization of the human mitochondrial genome. *Nature*, 290: 457–465.

Andersson SG, Karlberg O, Canbäck B, Kurland CG (2003) On the origin of mitochondria: a genomics perspective. *Philos Trans R Soc Lond B Biol Sci*, 358: 165–179.

Andersson SG, Zomorodipour A, Andersson JO, Sicheritz-Pontén T, Alsmark UC, Podowski RM, Näslund AK, Eriksson AS, Winkler HH, Kurland CG (1998) The genome sequence of Rickettsia prowazekii and the origin of mitochondria. *Nature*, 396: 133–40.

Antes A, Tappin I, Chung S, Lim R, Lu B, Parrott AM, Hill HZ, Suzuki CK, Lee CG (2010) Differential regulation of full-length genome and a single-stranded 7S DNA along the cell cycle in human mitochondria. *Nucleic Acids Res*, 38: 6466–6476.

Attardi G, Ojala D (1971) Mitochondrial ribosome in HeLa cells. *Nat New Biol*, 229: 133–136.

Bacman SR, Williams SL, Moraes CT (2009) Intra- and inter-molecular recombination of mitochondrial DNA after in vivo induction of multiple double-strand breaks. *Nucleic Acids Res*, 37: 4218–4226.

Ban-Ishihara R, Ishihara T, Sasaki N, Mihara K, Ishihara N (2013) Dynamics of nucleoid structure regulated by mitochondrial fission contributes to cristae reformation and release of cytochrome c. *Proc Natl Acad Sci U S A*, 110: 11,863–11,868.

Bailey LJ, Cluett TJ, Reyes A, Prolla TA, Poulton J, Leeuwenburgh C, Holt IJ (2009) Mice expressing an error-prone DNA polymerase in mitochondria display elevated replication pausing and chromosomal breakage at fragile sites of mitochondrial DNA. *Nucleic Acids Res*, 37: 2327–2335.

Baron M, Kudin AP, Kunz WS (2007) Mitochondrial dysfunction in neurodegenerative disorders. *Biochem Soc Trans*, 35: 1228–1231.

Barrientos A, Casademont J, Saiz A, Cardellach F, Volpini V, Solans A, Tolosa E, Urbano-Marquez A, Estivill X, Nunes V (1996) Autosomal recessive Wolfram syndrome associated with an 8.5-kb mtDNA single deletion. *Am J Hum Genet*, 58: 963–970.

Baumer A, Zhang C, Linnane AW, Nagley P (1994) Age-related human mtDNA deletions: a heterogeneous set of deletions arising at a single pair of directly repeated sequences. *Am J Hum Genet*, 54: 618–630.

Benda C (1898) Ueber die Spermatogenese der Vertebraten und höheren Evertebraten, II. Theil: Die Histiogenese der Spermien. *Arch Anal Physiol*, 393–398.

Bender A, Krishnan KJ, Morris CM, Taylor GA, Reeve AK, Perry RH, Jaros E, Hersheson JS, Betts J, Klopstock T, Taylor RW, Turnbull DM (2006) High levels of mitochondrial DNA deletions in substantia nigra neurons in aging and Parkinson disease. *Nat Genet*, 38: 515–517.

Benz R (1985) Porin from bacterial and mitochondrial outer membranes. *CRC Crit Rev Biochem*, 19: 145–190.

Benz R (1990) Biophysical properties of porin pores from mitochondrial outer membrane of eukaryotic cells. *Experientia*, 46: 131–137.

Berenberg RA, Pellock JM, DiMauro S, Schotland DL, Bonilla E, Eastwood A, Hays A, Vicale CT, Behrens M, Chutorian A, Rowland LP (1977) Lumping or splitting? "Ophthalmoplegia-plus" or Kearns-Sayre syndrome? *Ann Neurol*, 1: 37–54.

Berk AJ, Clayton DA (1974) Mechanism of mitochondrial DNA replication in mouse L-cells: Asynchronous replication of strands, segregation of circular daughter molecules, aspects of topology and turnover of an initiation sequence. *J Mol Biol*, 86: 801–824.

Berneburg M, Grether-Beck S, Kürten V, Ruzicka T, Briviba K, Sies H, Krutmann J (1999) Singlet oxygen mediates the UVA-induced generation of the photoaging-associated mitochondrial common deletion. *Biol Chem*, 274: 15,345–15,349.

Bestwick ML, Shadel GS (2013) Accessorizing the human mitochondrial transcription machinery. *Trends Biochem Sci*, 38: 283–291.

Blakely EL, Butterworth A, Hadden RD, Bodi I, He L, McFarland R, Taylor RW (2012) MPV17 mutation causes neuropathy and leukoencephalopathy with multiple mtDNA deletions in muscle. *Neuromuscul Disord*, 22: 587–591.

Bogenhagen D, Clayton DA (1977) Mechanism of mitochondrial DNA replication in mouse L-cells: Introduction of superhelical turns into newly replicated molecules. *J Mol Biol*, 119: 69–81.

Bogenhagen D, Clayton DA (1978) Mechanism of mitochondrial DNA replication in mouse L-cells: kinetics of synthesis and turnover of the initiation sequence. *J Mol Biol*, 119: 49–68.

Bogenhagen DF (2012) Mitochondrial DNA nucleoid structure. *Biochim Biophys Acta*, 1819: 914–920.

Bogliolo M, Izzotti A, De Flora S, Carli C, Abbondandolo A, Degan P (1999) Detection of the '4977 bp' mitochondrial DNA deletion in human atherosclerotic lesions. *Mutagenesis*, 14: 77–82.

Bohlega S, Tanji K, Santorelli FM, Hirano M, al-Jishi A, DiMauro S (1996) Multiple mitochondrial DNA deletions associated with autosomal recessive ophthalmoplegia and severe cardiomyopathy. *Neurology*, 46: 1329–1334.

Bowmaker M, Yang MY, Yasukawa T, Reyes A, Jacobs HT, Huberman JA, Holt IJ (2003) Mammalian mitochondrial DNA replicates bidirectionally from an initiation zone. *J Biol Chem*, 278: 50,961–50,969.

Brickley K, Stephenson FA (2011) Trafficking kinesin protein (TRAK)-mediated transport of mitochondria in axons of hippocampal neurons. *J Biol Chem*, 286: 18,079–18,092.

Broers CAM, Meijers HHM, Symens JC, Stumm CK, Vogels GD, Brugerolle G (1993) Symbiotic association of *Psalteriomonas vulgaris*, new species with *Methanobacterium formicicum*. *Eur J Protistol*, 29: 98–105.

Brown GG, Gadaleta G, Pepe G, Saccone C, Sbisà E (1986) Structural conservation and variation in the D-loop-containing region of vertebrate mitochondrial DNA. *J Mol Biol*, 192: 503–11.

Brown TA, Cecconi C, Tkachuk AN, Bustamante C, Clayton DA (2005) Replication of mitochondrial DNA occurs by strand displacement with alternative light-strand origins, not via a strand-coupled mechanism. *Genes Dev*, 19: 2466–2476.

Brown TA, Clayton DA (2002) Release of replication termination controls mitochondrial DNA copy number after depletion with 2′,3′-dideoxycytidine. *Nucleic Acids Res*, 30: 2004–2010.

Brown TA, Clayton DA (2006) Genesis and wanderings: origins and migrations in asymmetrically replicating mitochondrial DNA. *Cell Cycle*, 5: 917–921.

Bua E, Johnson J, Herbst A, Delong B, McKenzie D, Salamat S, Aiken JM (2006) Mitochondrial DNA-deletion mutations accumulate intracellularly to detrimental levels in aged human skeletal muscle fibers. *Am J Hum Genet*, 79: 469–480.

Buckmaster PS, Dudek FE (1997) Network properties of the dentate gyrus in epileptic rats with hilar neuron loss and granule cell axon reorganization. *J Neurophysiol*, 77: 2685–2696.

Budd ME, Campbell JL(1997) A yeast replicative helicase, Dna2 helicase, interacts with yeast FEN-1 nuclease in carrying out its essential function. *Mol Cell Biol*, 17: 2136–2142.

Calvo SE, Compton AG, Hershman SG, Lim SC, Lieber DS, Tucker EJ, Laskowski A, Garone C, Liu S, Jaffe DB, Christodoulou J, Fletcher JM, Bruno DL, Goldblatt J, Dimauro S, Thorburn DR, Mootha VK (2012) Molecular diagnosis of infantile mitochondrial disease with targeted next-generation sequencing. *Sci Transl Med*, 4: 118ra10.

Campbell GR, Ziabreva I, Reeve AK, Krishnan KJ, Reynolds R, Howell O, Lassmann H, Turnbull DM, Mahad DJ (2011) Mitochondrial DNA deletions and neurodegeneration in multiple sclerosis. *Ann Neurol*, 69: 481–492.

Campello S, Lacalle RA, Bettella M, Mañes S, Scorrano L, Viola A (2006) Orchestration of lymphocyte chemotaxis by mitochondrial dynamics. *J Exp Med*, 203: 2879–2886.

Cantatore P, Flagella Z, Fracasso F, Lezza AM, Gadaleta MN, de Montalvo A (1987) Synthesis and turnover rates of four rat liver mitochondrial RNA species. *FEBS Lett*, 213: 144–148.

Carré D, Attardi G (1978) Biochemical and electron microscopic characterization of DNA-RNA complexes from HeLa cell mitochondria. *Biochemistry*, 17: 3263–3273.

Cavalier-Smith T (1981) Eukaryote kingdoms: seven or nine? *Biosystems*, 14: 461–481.

Chabi B, Mousson de Camaret B, Duborjal H, Issartel JP, Stepien G (2003) Quantification of mitochondrial DNA deletion, depletion, and overreplication: application to diagnosis. *Clin Chem*, 49: 1309–1317.

Chan DC (2006) Mitochondria: dynamic organelles in disease, aging, and development. *Cell*, 125: 1241–1252.

Chance B, Sies H, Boveris A (1979) Hydroperoxide metabolism in mammalian organs. *Physiol Rev*, 59: 527–605.

Chang DD, Clayton DA (1985) Priming of human mitochondrial DNA replication occurs at the light-strand promoter. *Proc Natl Acad Sci U S A*, 82: 351–355.

Chen H, Chan DC (2010) Physiological functions of mitochondrial fusion. *Ann N Y Acad Sci*, 1201: 21–25.

Chen H, Chomyn A, Chan DC (2005) Disruption of fusion results in mitochondrial heterogeneity and dysfunction. *J Biol Chem*, 280: 26,185–26,192.

Chen H, Detmer SA, Ewald AJ, Griffin EE, Fraser SE, Chan DC (2003) Mitofusins Mfn1 and Mfn2 coordinately regulate mitochondrial fusion and are essential for embryonic development. *J Cell Biol*, 160: 189–200.

Chen H, McCaffery JM, Chan DC (2007) Mitochondrial fusion protects against neurodegeneration in the cerebellum. *Cell*, 130: 548–562.

Chen H, Vermulst M, Wang YE, Chomyn A, Prolla TA, McCaffery JM, Chan DC (2010) Mitochondrial fusion is required for mtDNA stability in skeletal muscle and tolerance of mtDNA mutations. *Cell*, 141: 280–289.

Chen JX, Yan SS (2010) Role of mitochondrial amyloid-beta in Alzheimer's disease. *J Alzheimers Dis*, 20: 569–578.

Chinnery PF, Brown DT, Andrews RM, Singh-Kler R, Riordan-Eva P, Lindley J, Applegarth DA, Turnbull DM, Howell N (2001) The mitochondrial ND6 gene is a hot spot for mutations that cause Leber's hereditary optic neuropathy. *Brain*, 124: 209–218.

Chinnery PF, Samuels DC (1999) Relaxed replication of mtDNA: A model with implications for the expression of disease. *Am J Hum Genet*, 64: 1158–1165.

Chinnery PF, Schon EA (2003) Mitochondria. *J Neurol Neurosurg Psychiatry*, 74: 1188–1199.

Cipolat S, Martins de Brito O, Dal Zilio B, Scorrano L (2004) OPA1 requires mitofusin 1 to promote mitochondrial fusion. *Proc Natl Acad Sci U S A*, 101: 15,927–15,932.

Clayton DA (1982) Replication of animal mitochondrial DNA. *Cell*, 28: 693–705.

Clayton DA (2003) Mitochondrial DNA replication: what we know. *IUBMB Life*, 55: 213–217.

Copeland WC (2008) Inherited mitochondrial diseases of DNA replication. *Annu Rev Med*, 59: 131–146.

Copeland WC, Longley MJ (2008) DNA2 resolves expanding flap in mitochondrial base excision repair. *Mol Cell*, 32: 457–458.

Crews S, Ojala D, Posakony J, Nishiguchi J, Attardi G (1979) Nucleotide sequence of a region of human mitochondrial DNA containing the precisely identified origin of replication. *Nature*, 277: 192–198.

Cymerman IA, Chung I, Beckmann BM, Bujnicki JM, Meiss G (2008) EXOG, a novel paralog of Endonuclease G in higher eukaryotes. *Nucleic Acids Res*, 36: 1369–1379.

D'Aurelio M, Gajewski CD, Lin MT, Mauck WM, Shao LZ, Lenaz G, Moraes CT, Manfredi G (2004) Heterologous mitochondrial DNA recombination in human cells. *Hum Mol Genet*, 13: 3171–3179.

De Bont R, van Larebeke N (2004) Endogenous DNA damage in humans: A review of quantitative data. *Mutagenesis*, 19: 169–185.

de Brito OM, Scorrano L (2008) Mitofusin 2 tethers endoplasmic reticulum to mitochondria. *Nature*, 456: 605–610.

Debrosse S, Parikh S (2012) Neurologic disorders due to mitochondrial DNA mutations. *Semin Pediatr Neurol*, 19: 194–202.

de Vries DD, van Engelen BG, Gabreëls FJ, Ruitenbeek W, van Oost BA (1993) A second missense mutation in the mitochondrial ATPase 6 gene in Leigh's syndrome. *Ann Neurol*, 34: 410–412.

Diaz F, Bayona-Bafaluy MP, Rana M, Mora M, Hao H, Moraes CT (2002) Human mitochondrial DNA with large deletions repopulates organelles faster than full-length genomes under relaxed copy number control. *Nucleic Acids Res*, 30: 4626–4633.

Doda JN, Wright CT, Clayton DA (1981) Elongation of displacement-loop strands in human and mouse mitochondrial DNA is arrested near specific template sequences. *Proc Natl Acad Sci U S A*, 78: 6116–6120.

Dorn GW 2nd, Maack C (2013) SR and mitochondria: calcium cross-talk between kissing cousins. *J Mol Cell Cardiol*, 55: 42–49.

Dringen R, Pfeiffer B, Hamprecht B (1999) Synthesis of the antioxidant glutathione in neurons: supply by astrocytes of CysGly as precursor for neuronal glutathione. *J Neurosci*, 19: 562–569.

Dunbar DR, Moonie PA, Swingler RJ, Davidson D, Roberts R, Holt IJ (1993) Maternally transmitted partial direct tandem duplication of mitochondrial DNA associated with diabetes mellitus. *Hum Mol Genet*, 2: 1619–1624.

Duxin JP, Dao B, Martinsson P, Rajala N, Guittat L, Campbell JL, Spelbrink JN, Stewart SA (2009) Human Dna2 is a nuclear and mitochondrial DNA maintenance protein. *Mol Cell Biol*, 29*:* 4274–4282.

Eimon PM, Chung SS, Lee CM, Weindruch R, Aiken JM (1996) Age-associated mitochondrial DNA deletions in mouse skeletal muscle: comparison of different regions of the mitochondrial genome. *Dev Genet*, 18: 107–113.

El-Hattab AW, Scaglia F (2013) Mitochondrial DNA depletion syndromes: review and updates of genetic basis, manifestations, and therapeutic options. *Neurotherapeutics*, 10: 186–198.

Elson JL, Samuels DC, Turnbull DM, Chinnery PF (2001) Random intracellular drift explains the clonal expansion of mitochondrial DNA mutations with age. *Am J Hum Genet*, 68: 802–806.

Embley TM, van der Giezen M, Horner DS, Dyal PL, Foster P (2003) Mitochondria and hydrogenosomes are two forms of the same fundamental organelle. *Philos Trans R Soc Lond B Biol Sci*, 358: 191–202.

Emelyanov VV (2003) Mitochondrial connection to the origin of the eukaryotic cell. *Eur J Biochem*, 270: 1599–1618.

Ernster L, Schatz G (1981) Mitochondria: a historical review. *J Cell Biol*, 91: 227–255.

Farge G, Holmlund T, Khvorostova J, Rofougaran R, Hofer A, Falkenberg M (2008) The N-terminal domain of TWINKLE contributes to single-stranded DNA binding and DNA helicase activities. *Nucleic Acids Res*, 36: 393–403.

Fisher RP, Lisowsky T, Parisi MA, Clayton DA (1992) DNA wrapping and bending by a mitochondrial high mobility group-like transcriptional activator protein. *J Biol Chem*, 267: 3358–3367.

Fransson A, Ruusala A, Aspenström P (2003) Atypical Rho GTPases have roles in mitochondrial homeostasis and apoptosis. *Biol Chem*, 278: 6495–6502.

Frazier AE, Kiu C, Stojanovski D, Hoogenraad NJ, Ryan MT (2006) Mitochondrial morphology and distribution in mammalian cells. *Biol Chem*, 387: 1551–1558.

Freiman TM, Eismann-Schweimler J, Frotscher M (2011) Granule cell dispersion in temporal lobe epilepsy is associated with changes in dendritic orientation and spine distribution. *Exp Neurol*, 229: 332–338.

Friedman JR, Lackner LL, West M, DiBenedetto JR, Nunnari J, Voeltz GK (2011) ER tubules mark sites of mitochondrial division. *Science*, 334: 358–362.

Fukui H, Moraes CT (2009) Mechanisms of formation and accumulation of mitochondrial DNA deletions in aging neurons. *Hum Mol Genet*, 18: 1028–1036.

Fusté JM, Wanrooij S, Jemt E, Granycome CE, Cluett TJ, Shi Y, Atanassova N, Holt IJ, Gustafsson CM, Falkenberg M (2010) Mitochondrial RNA polymerase is needed for activation of the origin of light-strand DNA replication. *Mol Cell*, 37: 67–78.

Glater EE, Megeath LJ, Stowers RS, Schwarz TL (2006) Axonal transport of mitochondria requires milton to recruit kinesin heavy chain and is light chain independent. *J Cell Biol*, 173: 545–557.

Gohil VM, Greenberg ML (2009) Mitochondrial membrane biogenesis: phospholipids and proteins go hand in hand. *J Cell Biol*, 184: 469–472.

Götz A, Isohanni P, Pihko H, Paetau A, Herva R, Saarenpää-Heikkilä O, Valanne L, Marjavaara S, Suomalainen A (2008) Thymidine kinase 2 defects can cause multi-tissue mtDNA depletion syndrome. *Brain*, 131: 2841–2850.

Gray H, Wong TW (1992) Purification and identification of subunit structure of the human mitochondrial DNA polymerase. *J Biol Chem*, 267: 5835–5841.

Gray MW, Burger G, Lang BF (2001) The origin and early evolution of mitochondria. *Genome Biol*, 2: REVIEWS1018.

Graziewicz MA, Longley MJ, Bienstock RJ, Zeviani M, Copeland WC (2004) Structure-function defects of human mitochondrial DNA polymerase in autosomal dominant progressive external ophthalmoplegia. *Nat Struct Mol Biol*, 11: 770–776.

Graziewicz MA, Longley MJ, Copeland WC (2006) DNA polymerase gamma in mitochondrial DNA replication and repair. *Chem Rev*, 106: 383–405.

Greaves LC, Reeve AK, Taylor RW, Turnbull DM (2012) Mitochondrial DNA and disease. *J Pathol*, 226: 274–286.

Gredilla R, Garm C, Stevnsner T (2012) Nuclear and mitochondrial DNA repair in selected eukaryotic aging model systems. *Oxid Med Cell Longev*, 2012: 282438.

Gulyás AI, Buzsáki G, Freund TF, Hirase H (2006) Populations of hippocampal inhibitory neurons express different levels of cytochrome c. *Eur J Neurosci*, 23: 2581–2594.

Guo X, Popadin KY, Markuzon N, Orlov YL, Kraytsberg Y, Krishnan KJ, Zsurka G, Turnbull DM, Kunz WS, Khrapko K (2010) Repeats, longevity and the sources of mtDNA deletions: evidence from 'deletional spectra'. *Trends Genet*, 26: 340–343.

Haack TB, Haberberger B, Frisch EM, Wieland T, Iuso A, Gorza M, Strecker V, Graf E, Mayr JA, Herberg U, Hennermann JB, Klopstock T, Kuhn KA, Ahting U,Sperl W, Wilichowski E, Hoffmann GF, Tesarova M, Hansikova H, Zeman J, Plecko B, Zeviani M, Wittig I, Strom TM, Schuelke M, Freisinger P, Meitinger T, Prokisch H (2012) Molecular diagnosis in mitochondrial complex I deficiency using exome sequencing. *J Med Genet*, 49: 277–283.

Hales KG, Fuller MT (1997) Developmentally regulated mitochondrial fusion mediated by a conserved, novel, predicted GTPase. *Cell*, 90: 121–129.

Hanes JW, Thal DM, Johnson KA (2006) Incorporation and replication of 8-oxo-deoxyguanosine by the human mitochondrial DNA polymerase. *J Biol Chem*, 281: 36,241–36,248.

Harvey JN, Barnett D (1992) Endocrine dysfunction in Kearns-Sayre syndrome. *Clin Endocrinol (Oxf)*, 37: 97–103.

Hatefi Y (1985) The mitochondrial electron transport and oxidative phosphorylation system. *Annu Rev Biochem*. 54: 1015–1069.

Henle ES, Luo Y, Linn S (1996) Fe2+, Fe3+, and oxygen react with DNA-derived radicals formed during iron-mediated Fenton reactions. *Biochemistry*, 35: 12,212–12,219.

Hermann GJ, Thatcher JW, Mills JP, Hales KG, Fuller MT, Nunnari J, Shaw JM (1998) Mitochondrial fusion in yeast requires the transmembrane GTPase Fzo1p. *J Cell Biol*, 143: 359–373.

Hjort K, Goldberg AV, Tsaousis AD, Hirt RP, Embley TM (2010) Diversity and reductive evolution of mitochondria among microbial eukaryotes. *Philos Trans R Soc Lond B Biol Sci*, 365: 713–727.

Holland PM, Abramson RD, Watson R, Gelfand DH (1991) Detection of specific polymerase chain reaction product by utilizing the 5'-3' exonuclease activity of Thermus aquaticus DNA polymerase. *Proc Natl Acad Sci U S A*, 88: 7276–7280.

Holt IJ, He J, Mao CC, Boyd-Kirkup JD, Martinsson P, Sembongi H, Reyes A, Spelbrink JN (2007) Mammalian mitochondrial nucleoids: organizing an independently minded genome. *Mitochondrion*, 7: 311–321.

Holt IJ, Lorimer HE, Jacobs HT (2000) Coupled leading- and lagging-strand synthesis of mammalian mitochondrial DNA. *Cell*, 100: 515–524.

Honda S, Aihara T, Hontani M, Okubo K, Hirose S (2005) Mutational analysis of action of mitochondrial fusion factor mitofusin-2. *J Cell Sci*, 118: 3153–3161.

Honigberg BM, Volkmann D, Entzeroth R, Scholtyseck E (1984) A freeze-fracture electron microscope study of Trichomonas vaginalis Donné and Tritrichomonas foetus (Riedmüller). *J Protozool*, 31: 116–131.

Huoponen K, Vilkki J, Aula P, Nikoskelainen EK, Savontaus ML (1991) A new mtDNA mutation associateed with Leber hereditary optic neuroretinopathy. *Am J Hum Genet*, 48: 1147–1153.

Huttenlocher PR, Solitare GB, Adams G (1976) Infantile diffuse cerebral degeneration with hepatic cirrhosis. *Arch Neurol*, 33: 186–192.

Imlay JA, Linn S (1988) DNA damage and oxygen radical toxicity. *Science*, 240: 1302–1309.

Ishihara N, Eura Y, Mihara K (2004) Mitofusin 1 and 2 play distinct roles in mitochondrial fusion reactions via GTPase activity. *J Cell Sci*, 117: 6535–6546.

Jastroch M, Divakaruni AS, Mookerjee S, Treberg JR, Brand MD (2010) Mitochondrial proton and electron leaks. *Essays Biochem*, 47: 53–67.

Johns DR, Neufeld MJ, Park RD (1992) An ND-6 mitochondrial DNA mutation associated with Leber hereditary optic neuropathy. *Biochem Biophys Res Commun*, 187: 1551–1557.

Kai Y, Miyako K, Muta T, Umeda S, Irie T, Hamasaki N, Takeshige K, Kang D (1999) Mitochondrial DNA replication in human T lymphocytes is regulated primarily at the H-strand termination site. *Biochim Biophys Acta*, 1446: 126–134.

Kajander OA, Rovio AT, Majamaa K, Poulton J, Spelbrink JN, Holt IJ, Karhunen PJ, Jacobs HT (2000) Human mtDNA sublimons resemble rearranged mitochondrial genoms found in pathological states. *Hum Mol Genet*, 9: 2821–2835.

Kang D, Miyako K, Kai Y, Irie T, Talzeshige K (1997) In vivo determination of replication origins of human mitochondrial DNA by ligation-mediated polymerase chain reaction. *J Biol Chem*, 272: 15,275–15,279.

Kasamatsu H, Robberson DL, Vinograd J (1971) A Novel Closed-Circular Mitochondrial DNA with Properties of a Replicating Intermediate. *Proc Natl Acad Sci U S A*, 68: 2252–2257.

Kasiviswanathan R, Collins TR, Copeland WC (2012) The interface of transcription and DNA replication in the mitochondria. *Biochim Biophys Acta*, 1819: 970–978.

Kaufman BA, Durisic N, Mativetsky JM, Costantino S, Hancock MA, Grutter P, Shoubridge EA (2007) The mitochondrial transcription factor TFAM coordinates the assembly of multiple DNA molecules into nucleoid-like structures. *Mol Biol Cell*, 18: 3225–3236.

Kaukonen J, Juselius JK, Tiranti V, Kyttälä A, Zeviani M, Comi GP, Keränen S, Peltonen L, Suomalainen A (2000) Role of adenine nucleotide translocator 1 in mtDNA maintenance. *Science*, 289: 782–785.

Kazak L, Reyes A, He J, Wood SR, Brea-Calvo G, Holen TT, Holt IJ (2013) A cryptic targeting signal creates a mitochondrial FEN1 isoform with tailed R-Loop binding properties. *PLoS One*, 8: e62340.

Khrapko K, Bodyak N, Thilly WG, van Orsouw NJ, Zhang X, Coller HA, Perls TT, Upton M, Vijg J, Wei JY (1999) Cell-by-cell scanning of whole mitochondrial genomes in aged human heart reveals a significant fraction of myocytes with clonally expanded deletions. *Nucleic Acids Res*, 27: 2434–2441.

Kirschner RH, Wolstenholme DR, Gross NJ (1968) Replicating molecules of circular mitochondrial DNA. *Proc Natl Acad Sci U S A*, 60: 1466–1472.

Koike K, Wolstenholme DR (1974) Evidence for discontinuous replication of circular mitochondrial DNA molecules from Novikoff rat ascites hepatoma cells. *J Cell Biol*, 61: 14–25.

Koirala S, Guo Q, Kalia R, Bui HT, Eckert DM, Frost A, Shaw JM (2013) Interchangeable adaptors regulate mitochondrial dynamin assembly for membrane scission. *Proc Natl Acad Sci U S A*, 110: E1342–1351.

Kolesar JE, Wang CY, Taguchi YV, Chou SH, Kaufman BA (2013) Two-dimensional intact mitochondrial DNA agarose electrophoresis reveals the structural complexity of the mammalian mitochondrial genome. *Nucleic Acids Res*, 41: e58.

Korhonen JA, Pham XH, Pellegrini M, Falkenberg M (2004) Reconstitution of a minimal mtDNA replisome in vitro. *EMBO J*, 23: 2423–2429.

Kornblum C, Nicholls TJ, Haack TB, Schöler S, Peeva V, Danhauser K, Hallmann K, Zsurka G, Rorbach J, Iuso A, Wieland T, Sciacco M, Ronchi D, Comi GP, Moggio M, Quinzii CM, DiMauro S, Calvo SE, Mootha VK, Klopstock T, Strom TM, Meitinger T, Minczuk M, Kunz WS, Prokisch H (2013) Loss-of-function mutations in MGME1 impair mtDNA replication and cause multisystemic mitochondrial disease. *Nat Genet*, 45: 214–219.

Koshiba T, Detmer SA, Kaiser JT, Chen H, McCaffery JM, Chan DC (2004) Structural basis of mitochondrial tethering by mitofusin complexes. *Science*, 305: 858–862.

Kowald A, Dawson M, Kirkwood TB (2014) Mitochondrial mutations and ageing: can mitochondrial deletion mutants accumulate via a size based replication advantage? *J Theor Biol*, 340: 111–118.

Kraytsberg Y, Kudryavtseva E, McKee AC, Geula C, Kowall NW, Khrapko K (2006) Mitochondrial DNA deletions are abundant and cause functional impairment in aged human substantia nigra neurons. *Nat Genet*, 38: 518–520.

Kraytsberg Y, Nicholas A, Caro P, Khrapko K (2008) Single molecule PCR in mtDNA mutational analysis: Genuine mutations vs. damage bypass-derived artifacts. *Methods*, 46: 269–73.

Krebs H, Henseleit K (1932a) Untersuchungen über die Harnstoffbildung im Tierkörper I. *Klinische Wochenschrift*, 11: 757–759.

Krebs H, Henseleit K (1932b) Untersuchungen über die Harnstoffbildung im Tierkörper II. *Klinische Wochenschrift*, 11: 1137–1139.

Krebs H, Henseleit K (1932c) Untersuchungen über die Harnstoffbildung im Tierkörper. *Hoppe-Seyler's Zeitschrift für physiologische Chemie*, 210: 33–66.

Krebs HA, Johnson WA (1937) Metabolism of ketonic acids in animal tissues. *Biochem J*, 31: 645–660.

Krishnan KJ, Reeve AK, Samuels DC, Chinnery PF, Blackwood JK, Taylor RW, Wanrooij S, Spelbrink JN, Lightowlers RN, Turnbull DM (2008) What causes mitochondrial DNA deletions in human cells? *Nat Genet*, 40: 275–279.

Kudin AP, Bimpong-Buta NY, Vielhaber S, Elger CE, Kunz WS (2004) Characterization of superoxide-producing sites in isolated brain mitochondria. *J Biol Chem*, 279: 4127–4135.

Kudin AP, Debska-Vielhaber G, Kunz WS (2005) Characterization of superoxide production sites in isolated rat brain and skeletal muscle mitochondria. *Biomed Pharmacother*, 59: 163–168.

Kudin AP, Kudina TA, Seyfried J, Vielhaber S, Beck H, Elger CE, Kunz WS (2002) Seizure-dependent modulation of mitochondrial oxidative phosphorylation in rat hippocampus. *Eur J Neurosci*, 15: 1105–1114.

Kudin AP, Zsurka G, Elger CE, Kunz WS (2009) Mitochondrial involvement in temporal lobe epilepsy. *Exp Neurol*, 218: 326–332.

Kukat A, Trifunovic A (2009) Somatic mtDNA mutations and aging-facts and fancies. *Exp Gerontol*, 44: 101–105.

Kukat C, Larsson NG (2013) mtDNA makes a U-turn for the mitochondrial nucleoid. *Trends Cell Biol*, 23: 457–463.

Kukat C, Wurm CA, Spåhr H, Falkenberg M, Larsson NG, Jakobs S (2011) Super-resolution microscopy reveals that mammalian mitochondrial nucleoids have a uniform size and frequently contain a single copy of mtDNA. *Proc Natl Acad Sci USA*, 108: 13,534–13,539.

Lakshmanan LN, Gruber J, Halliwell B, Gunawan R (2012) Role of direct repeat and stem-loop motifs in mtDNA deletions: cause or coincidence? *PLoS One*, 7: e35271.

Larsson NG, Wang J, Wilhelmsson H, Oldfors A, Rustin P, Lewandoski M, Barsh GS, Clayton DA (1998) Mitochondrial transcription factor A is necessary for mtDNA maintenance and embryogenesis in mice. *Nat Genet*, 18: 231–236.

Lazarow A, Cooperstein SJ (1953) Studies on the mechanism of Janus green B staining of mitochondria. I. Review of the literature. *Exp Cell Res*, 5: 56–69.

Leanza L, Ferraro P, Reichard P, Bianchi V (2008) Metabolic interrelations within guanine deoxynucleotide pools for mitochondrial and nuclear DNA maintenance. *J Biol Chem*, 283: 16,437–16,445.

Lee CM, Lopez ME, Weindruch R, Aiken JM (1998) Association of age-related mitochondrial abnormalities with skeletal muscle fiber atrophy. *Free Radic Biol Med*, 25: 964–972.

Lee CW, Peng HB (2008) The function of mitochondria in presynaptic development at the neuromuscular junction. *Mol Biol Cell*, 19: 150–158.

Lee DY, Clayton DA (1997) RNase mitochondrial RNA processing correctly cleaves a novel R loop at the mitochondrial DNA leading-strand origin of replication. *Gene Dev*, 11: 582–592.

Lee DY, Clayton DA (1998) Initiation of mitochondrial DNA replication by transcription and R-loop processing. *J Biol Chem*, 273: 30,614–30,621.

Lee HC, Wei YH (2007) Oxidative stress, mitochondrial DNA mutation, and apoptosis in aging. *Exp Biol Med (Maywood)*, 232: 592–606.

Lee YS, Kennedy WD, Yin YW (2009) Structural insight into processive human mitochondrial DNA synthesis and disease-related polymerase mutations. *Cell*, 139: 312–324.

Lehninger AL (1945) The Relationship of the Adenosine Polyphosphates to Fatty Acid Oxidation in Homogenized Liver Preparations. *J Biol Chem*, 157: 363–382.

Leigh D (1951) Subacute necrotizing encephalomyelopathy in an infant. *J Neurol Neurosurg Psychiatry*, 14: 216–221.

Li Z, Okamoto K, Hayashi Y, Sheng M (2004) The importance of dendritic mitochondria in the morphogenesis and plasticity of spines and synapses. *Cell*, 119: 873–887.

Lindmark DG, Müller M (1973) Hydrogenosome, a cytoplasmic organelle of the anaerobic flagellate Tritrichomonas foetus, and its role in pyruvate metabolism. *J Biol Chem*, 248: 7724–7728.

Linnane AW, Marzuki S, Ozawa T, Tanaka M (1989) Mitochondrial DNA mutations as an important contributor to ageing and degenerative diseases. *Lancet*, 1: 642–645.

Liu P, Qian L, Sung JS, de Souza-Pinto NC, Zheng L, Bogenhagen DF, Bohr VA, Wilson DM 3rd, Shen B, Demple B (2008) Removal of oxidative DNA damage via FEN1-dependent long-patch base excision repair in human cell mitochondria. *Mol Cell Biol*, 28: 4975–4987.

Liu X, Hajnóczky G (2009) Ca2+-dependent regulation of mitochondrial dynamics by the Miro-Milton complex. *Int J Biochem Cell Biol*, 41: 1972–1976.

Liu Y, Fiskum G, Schubert D (2002) Generation of reactive oxygen species by the mitochondrial electron transport chain. *J Neurochem*, 80: 780–787.

Longley MJ, Clark S, Yu Wai Man C, Hudson G, Durham SE, Taylor RW, Nightingale S, Turnbull DM, Copeland WC, Chinnery PF (2006) Mutant POLG2 disrupts DNA polymerase gamma subunits and causes progressive external ophthalmoplegia. *J Hum Genet*, 78: 1026–1034.

Longley MJ, Humble MM, Sharief FS, Copeland WC (2010) Disease variants of the human mitochondrial DNA helicase encoded by C10orf2 differentially alter protein stability, nucleotide hydrolysis, and helicase activity. *J Biol Chem*, 285: 29,690–29,702.

Magnusson J, Orth M, Lestienne P, Taanman JW (2003) Replication of mitochondrial DNA occurs throughout the mitochondria of cultured human cells. *Exp Cell Res*, 289: 133–142.

Manfredi G, Vu T, Bonilla E, Schon EA, DiMauro S, Arnaudo E, Zhang L, Rowland LP, Hirano M (1997) Association of myopathy with large-scale mitochondrial DNA duplications and deletions: which is pathogenic? *Ann Neurol*, 42: 180–188.

Mao CC, Holt IJ (2009) Clinical and molecular aspects of diseases of mitochondrial DNA instability. *Chang Gung Med J*, 32: 354–369.

Margerison JH, Corsellis JA (1966) Epilepsy and the temporal lobes: a clinical, electroencephalographic and neuropathological study of the brain in epilepsy, with particular reference to the temporal lobes. *Brain*, 89: 499–530.

Margulis L, Sagan D (2001) Marvellous microbes. *Resurgence*, 206: 10–12.

Martin IV, MacNeill SA (2002) ATP-dependent DNA ligases. *Genome Biol*, 3: REVIEWS3005.

Marzuki S, Berkovic SF, Saifuddin Noer A, Kapsa RM, Kalnins RM, Byrne E, Sasmono T, Sudoyo H (1997) Developmental genetics of deleted mtDNA in mitochondrial oculomyopathy. *J Neurol Sci*, 145: 155–162.

Mathews CK (2006) DNA precursor metabolism and genomic stability. *FASEB J*, 20: 1300–1314.

Mereschkowsky KS (1905) Über Natur und Ursprung der Chromatophoren im Pflanzenreiche. *Biol. Centralbl*, 25: 593–604, 689–691.

Michaelis L (1900) Die vitale Farbung, eine Darstellungs methode der Zellgranula. *Arch Mikrosk Anal*, 55: 558–575.

Miquel J (1992) An update on the mitochondrial-DNA mutation hypothesis of cell aging. *Mutat Res*, 275: 209–216.

Misko A, Jiang S, Wegorzewska I, Milbrandt J, Baloh RH (2010) Mitofusin 2 is necessary for transport of axonal mitochondria and interacts with the Miro/Milton complex. *J Neurosci*, 30: 4232–4240.

Mita S, Rizzuto R, Moraes CT, Shanske S, Arnaudo E, Fabrizi GM, Koga Y, DiMauro S, Schon EA (1990) Recombination via flanking direct repeats is a major cause of large-scale deletions of human mitochondrial DNA. *Nucleic Acids Res*, 18: 561–567.

Mitchell P (1961) Coupling of phosphorylation to electron and hydrogen transfer by a chemi-osmotic type of mechanism. *Nature*, 191: 144–148.

Mitsuya H, Jarrett RF, Matsukura M, Di Marzo Veronese F, DeVico AL, Sarngadharan MG, Johns DG, Reitz MS, Broder S (1987) Long-term inhibition of human T-lymphotropic virus type III/lymphadenopathy-associated virus (human immunodeficiency virus) DNA synthesis and RNA expression in T cells protected by 2',3'-dideoxynucleosides in vitro. *Proc Natl Acad Sci U S A*, 84: 2033–2037.

Miyabayashi S, Hanamizu H, Endo H, Tada K, Horai S (1991) A new type of mitochondrial DNA deletion in patients with encephalomyopathy. *J Inherit Metab Dis*, 14: 805–812.

Moraes CT(2001) What regulates mitochondrial DNA copy number in animal cells? *Trends Genet*, 17: 199–205.

Moraes CT, Ricci E, Petruzzella V, Shanske S, DiMauro S, Schon EA, Bonilla E (1992) Molecular analysis of the muscle pathology associated with mitochondrial DNA deletions. *Nat Genet*, 1: 359–367.

Morris RL, Hollenbeck PJ (1995) Axonal transport of mitochondria along microtubules and F-actin in living vertebrate neurons. *J Cell Biol*, 131: 1315–1326.

Moslemi AR, Lindberg C, Oldfors A (1997) Analysis of multiple mitochondrial DNA deletions in inclusion body myositis. *Hum Mutat*, 10: 381–386.

Müller M (1993)The hydrogenosome. *J Gen Microbiol*, 139: 2879–2889.

Nakada K, Sato A, Hayashi J (2009) Mitochondrial functional complementation in mitochondrial DNA-based diseases. *Int J Biochem Cell Biol*, 41: 1907–1913.

Nangaku M, Sato-Yoshitake R, Okada Y, Noda Y, Takemura R, Yamazaki H, Hirokawa N (1994) KIF1B, a novel microtubule plus end-directed monomeric motor protein for transport of mitochondria. *Cell*, 79: 1209–1220.

Nass MM (1966) The circularity of mitochondrial DNA. *Proc Natl Acad Sci U S A*, 56: 1215–1222.

Nass MM, Nass S (1963) Intramitochondrial fibers with DNA characteristics. I. Fixation and electron staining reactions. *J Cell Biol*, 19: 593–611.

Naviaux RK, Nyhan WL, Barshop BA, Poulton J, Markusic D, Karpinski NC, Haas RH (1999) Mitochondrial DNA polymerase gamma deficiency and mtDNA depletion in a child with Alpers' syndrome. *Ann Neurol*, 45: 54–58.

Ngo HB, Kaiser JT, Chan DC (2011) Tfam, a mitochondrial transcription and packaging factor, imposes a U-turn on mitochondrial DNA. *Nat Struct Mol Biol*, 18: 1290–1296.

Nicolino M, Ferlin T, Forest M, Godinot C, Carrier H, David M, Chatelain P, Mousson B (1997) Identification of a large-scale mitochondrial deoxyribonucleic acid deletion in endocrinopathies and deafness: report of two unrelated cases with diabetes mellitus and adrenal insufficiency, respectively. *J Clin Endocrinol Metab*, 82: 3063–3067.

Nishino I, Spinazzola A, Hirano M (1999) Thymidine phosphorylase gene mutations in MNGIE, a human mitochondrial disorder. *Science*, 283: 689–692.

Ostergaard E, Christensen E, Kristensen E, Mogensen B, Duno M, Shoubridge EA, Wibrand F (2007) Deficiency of the alpha subunit of succinate-coenzyme A ligase causes fatal infantile lactic acidosis with mitochondrial DNA depletion. *Am J Hum Genet*, 81: 383–387.

Palade GE (1952) The fine structure of mitochondria. *Anat Rec*, 114: 427–451.

Palade GE (1953) An electron microscope study of the mitochondrial structure. *J Histochem Cytochem*, 1: 188–211.

Perier C, Bender A, García-Arumí E, Melià MJ, Bové J, Laub C, Klopstock T, Elstner M, Mounsey RB, Teismann P, Prolla T, Andreu AL, Vila M (2013) Accumulation of mitochondrial DNA deletions within dopaminergic neurons triggers neuroprotective mechanisms. *Brain*, 136: 2369–2378.

Pham XH, Farge G, Shi Y, Gaspari M, Gustafsson CM, Falkenberg M (2006) Conserved sequence box II directs transcription termination and primer formation in mitochondria. *J Biol Chem*, 281: 24,647–24,652.

Picard M, Taivassalo T, Ritchie D, Wright KJ, Thomas MM, Romestaing C, Hepple RT (2011) Mitochondrial structure and function are disrupted by standard isolation methods. *PLoS One*, 6: e18317.

Pikó L, Bulpitt KJ, Meyer R (1984) Structural and replicative forms of mitochondrial DNA in tissues from adult and senescent BALB/c mice and Fischer 344 rats. *Mech Ageing Dev*, 26: 113–131.

Pohjoismäki JL, Goffart S, Taylor RW, Turnbull DM, Suomalainen A, Jacobs HT, Karhunen PJ (2010) Developmental and pathological changes in the human cardiac muscle mitochondrial DNA organization, replication and copy number. *PLoS One*, 5:e10426.

Pohjoismäki JL, Goffart S, Tyynismaa H, Willcox S, Ide T, Kang D, Suomalainen A, Karhunen PJ, Griffith JD, Holt IJ, Jacobs HT (2009) Human heart mitochondrial DNA is organized in complex catenated networks containing abundant four-way junctions and replication forks. *J Biol Chem*, 284: 21,446–21,457.

Quintana A, Schwindling C, Wenning AS, Becherer U, Rettig J, Schwarz EC, Hoth M (2007) T cell activation requires mitochondrial translocation to the immunological synapse. *Proc Natl Acad Sci U S A*, 104: 14,418–14,423.

Rahman S, Blok RB, Dahl HH, Danks DM, Kirby DM, Chow CW, Christodoulou J, Thorburn DR (1996) Leigh syndrome: clinical features and biochemical and DNA abnormalities. *Ann Neurol*, 39: 343–351.

Ray PD, Huang BW, Tsuji Y (2012) Reactive oxygen species (ROS) homeostasis and redox regulation in cellular signaling. *Cell Signal*, 24: 981–990.

Rebelo AP, Williams SL, Moraes CT (2009) In vivo methylation of mtDNA reveals the dynamics of protein-mtDNA interactions. *Nucleic Acids Res*, 37: 6701–6715.

Reyes A, Kazak L, Wood SR, Yasukawa T, Jacobs HT, Holt IJ (2013) Mitochondrial DNA replication proceeds via a 'bootlace' mechanism involving the incorporation of processed transcripts. Nucleic Acids Res, 41: 5837–5850.

Robberson DL, Clayton DA (1972) Replication of Mitochondrial DNA in Mouse L Cells and Their Thymidine Kinase-Derivatives: Displacement Replication on a Covalently-Closed Circular Template. *Proc Natl Acad Sci U S A*, 69: 3810–3814.

Rocher C, Taanman JW, Pierron D, Faustin B, Benard G, Rossignol R, Malgat M, Pedespan L, Letellier T (2008) Influence of mitochondrial DNA level on cellular energy metabolism: implications for mitochondrial diseases. *J Bioenerg Biomembr*, 40: 59–67.

Roger AJ, Silberman JD (2002) Cell evolution: mitochondria in hiding. *Nature*, 418: 827–829.

Rojo M, Legros F, Chateau D, Lombès A (2002) Membrane topology and mitochondrial targeting of mitofusins, ubiquitous mammalian homologs of the transmembrane GTPase Fzo. *J Cell Sci*, 115: 1663–1674.

Ronchi D, Di Fonzo A, Lin W, Bordoni A, Liu C, Fassone E, Pagliarani S, Rizzuti M, Zheng L, Filosto M, Ferrò MT, Ranieri M, Magri F, Peverelli L, Li H, Yuan YC, Corti S, Sciacco M, Moggio M, Bresolin N, Shen B, Comi GP (2013) Mutations in DNA2 link progressive myopathy to mitochondrial DNA instability. *Am J Hum Genet*, 92: 293–300.

Ropp PA, Copeland WC (1996) Cloning and characterization of the human mitochondrial DNA polymerase, DNA polymerase gamma. *Genomics*, 36: 449–458.

Rossignol R, Faustin B, Rocher C, Malgat M, Mazat JP, Letellier T (2003) Mitochondrial threshold effects. *Biochem J*, 370: 751–762.

Rouzier C, Bannwarth S, Chaussenot A, Chevrollier A, Verschueren A, Bonello-Palot N, Fragaki K, Cano A, Pouget J, Pellissier JF, Procaccio V, Chabrol B, Paquis-Flucklinger V (2011) The MFN2 gene is responsible for mitochondrial DNA instability and optic atrophy 'plus' phenotype. *Brain*, 135: 23–34.

Rouzier C, Bannwarth S, Chaussenot A, Chevrollier A, Verschueren A, Bonello-Palot N, Fragaki K, Cano A, Pouget J, Pellissier JF, Procaccio V, Chabrol B, Paquis-Flucklinger V (2012) The MFN2 gene is responsible for mitochondrial DNA instability and optic atrophy 'plus' phenotype. *Brain*, 135: 23–34.

Ruhanen H, Ushakov K, Yasukawa T (2011) Involvement of DNA ligase III and ribonuclease H1 in mitochondrial DNA replication in cultured human cells. *Biochim Biophys Acta*, 1813: 2000–2007.

Saada A, Shaag A, Mandel H, Nevo Y, Eriksson S, Elpeleg O (2001) Mutant mitochondrial thymidine kinase in mitochondrial DNA depletion myopathy. *Nat Genet*, 29: 342–344.

Salinas S, Bilsland LG, Schiavo G (2008) Molecular landmarks along the axonal route: axonal transport in health and disease. *Curr Opin Cell Biol*, 20: 445–453.

Samuels DC, Schon EA, Chinnery PF (2004) Two direct repeats cause most human mtDNA deletions. *Trends Genet*, 20: 393–398.

Sandbank U, Lerman P (1972) Progressive cerebral poliodystrophy—Alpers' disease. Disorganized giant neuronal mitochondria on electron microscopy. *J Neurol Neurosurg Psychiatry*, 35: 749–755.

Saraste M (1999) Oxidative phosphorylation at the fin de siècle. *Science*, 283: 1488–1493.

Schon EA, Rizzuto R, Moraes CT, Nakase H, Zeviani M, DiMauro S (1989) A direct repeat is a hotspot for large-scale deletion of human mitochondrial DNA. *Science*, 244: 346–349.

Seligmann H (2009) Mitochondrial tRNAs as light strand replication origins: similarity between anticodon loops and the loop of the light strand replication origin predicts initiation of DNA replication. *Biosystems*, 99: 85–93.

Shadel GS, Clayton DA (1997) Mitochondrial DNA maintenance in vertebrates. *Annu Rev Biochem*, 66: 409–435.

Sheng ZH, Cai Q (2012) Mitochondrial transport in neurons: impact on synaptic homeostasis and neurodegeneration. *Nat Rev Neurosci*, 13: 77–93.

Shi P, Wei Y, Zhang J, Gal J, Zhu H (2010) Mitochondrial dysfunction is a converging point of multiple pathological pathways in amyotrophic lateral sclerosis. *J Alzheimers Dis*, 20: 311–324.

Shiflett AM, Johnson PJ (2010) Mitochondrion-related organelles in eukaryotic protists. *Annu Rev Microbiol*, 64: 409–429.

Shoffner JM, Lott MT, Voljavec AS, Soueidan SA, Costigan DA, Wallace DC (1989) Spontaneous Kearns-Sayre/chronic external ophthalmoplegia plus syndrome associated with a mitochondrial DNA deletion: a slip-replication model and metabolic therapy. *Proc Natl Acad Sci U S A*, 86: 7952–7956.

Shokolenko I, Venediktova N, Bochkareva A, Wilson GL, Alexeyev MF (2009) Oxidative stress induces degradation of mitochondrial DNA. *Nucleic Acids Res*, 37: 2539–2548.

Shoshan-Barmatz V, Mizrachi D (2012) VDAC1: from structure to cancer therapy. *Front Oncol*, 2:164.

Shutt T, Geoffrion M, Milne R, McBride HM (2012) The intracellular redox state is a core determinant of mitochondrial fusion. *EMBO Rep*, 13: 909–915.

Sian J, Dexter DT, Lees AJ, Daniel S, Agid Y, Javoy-Agid F, Jenner P, Marsden CD (1994) Alterations of glutathione levels in Parkinson's disease and other neurodegenerative disorders affecting basal ganglia. *Ann Neurol*, 36: 348–355.

Siddiqui A, Rivera-Sánchez S, Castro Mdel R, Acevedo-Torres K, Rane A, Torres-Ramos CA, Nicholls DG, Andersen JK, Ayala-Torres S (2012) Mitochondrial DNA damage is associated with reduced mitochondrial bioenergetics in Huntington's disease. *Free Radic Biol Med*, 53: 1478–1488.

Sitarz KS, Yu-Wai-Man P, Pyle A, Stewart JD, Rautenstrauss B, Seeman P, Reilly MM, Horvath R, Chinnery PF (2012) MFN2 mutations cause compensatory mitochondrial DNA proliferation. *Brain*, 135: e219, 1–3; author reply e220, 1–3.

Skladal D, Halliday J, Thorburn DR (2003) Minimum birth prevalence of mitochondrial respiratory chain disorders in children. *Brain*, 126: 1905–1912.

Smeitink J, van den Heuvel L, DiMauro S (2001) The genetics and pathology of oxidative phosphorylation. *Nat Rev Genet*, 2: 342–352.

Sohl CD, Kasiviswanathan R, Copeland WC, Anderson KS (2013) Mutations in human DNA polymerase γ confer unique mechanisms of catalytic deficiency that mirror the disease severity in mitochondrial disorder patients. *Hum Mol Genet*, 22: 1074–1085.

Solano A, Gámez J, Carod FJ, Pineda M, Playán A, López-Gallardo E, Andreu AL, Montoya J (2003) Characterisation of repeat and palindrome elements in patients harbouring single deletions of mitochondrial DNA. *J Med Genet*, 40: e86.

Song S, Pursell ZF, Copeland WC, Longley MJ, Kunkel TA, Mathews CK (2005) DNA precursor asymmetries in mammalian tissue mitochondria and possible contribution to mutagenesis through reduced replication fidelity. *Proc Natl Acad Sci U S A*, 102: 4990–4995.

Song Z, Cao Y, Samuels DC (2011) Replication pauses of the wild-type and mutant mitochondrial DNA polymerase gamma: a simulation study. *PLoS Comput Biol*, 7: e1002287.

Spelbrink JN, Li FY, Tiranti V, Nikali K, Yuan QP, Tariq M, Wanrooij S, Garrido N, Comi G, Morandi L, Santoro L, Toscano A, Fabrizi GM, Somer H, Croxen R, Beeson D, Poulton J, Suomalainen A, Jacobs HT, Zeviani M, Larsson C (2001) Human mitochondrial DNA deletions associated with mutations in the gene encoding Twinkle, a phage T7 gene 4-like protein localized in mitochondria. *Nat Genet*, 28: 223–231.

Spinazzola A, Viscomi C, Fernandez-Vizarra E, Carrara F, D'Adamo P, Calvo S (2006) MPV17 encodes an inner mitochondrial membrane protein and is mutated in infantile hepatic mitochondrial DNA depletion. *Nat Genet*, 38: 570–575.

Spinazzola A, Zeviani M (2005) Disorders of nuclear-mitochondrial intergenomic signaling. *Gene*, 354:162–168.

Spitz DR, Sullivan SJ (2010) The generation of stable oxidative stress-resistant phenotypes in Chinese hamster fibroblasts chronically exposed to hydrogen peroxide or hyperoxia. *Methods Mol Biol*, 610: 83–19.

Srivastava S, Moraes CT (2005) Double-strand breaks of mouse muscle mtDNA promote large deletions similar to multiple mtDNA deletions in humans. *Hum Mol Genet*, 14: 893–902.

Stewart JD, Schoeler S, Sitarz KS, Horvath R, Hallmann K, Pyle A, Yu-Wai-Man P, Taylor RW, Samuels DC, Kunz WS, Chinnery PF (2011) POLG mutations cause decreased mitochondrial DNA repopulation rates following induced depletion in human fibroblasts. *Biochim Biophys Acta*, 1812: 321–325.

Stowers RS, Megeath LJ, Górska-Andrzejak J, Meinertzhagen IA, Schwarz TL (2002) Axonal transport of mitochondria to synapses depends on milton, a novel Drosophila protein. *Neuron*, 36: 1063–1077.

Stumpf JD, Copeland WC (2011) Mitochondrial DNA replication and disease: insights from DNA polymerase γ mutations. *Cell Mol Life Sci*, 68: 219–233.

Sung JY, Engmann O, Teylan MA, Nairn AC, Greengard P, Kim Y (2008) WAVE1 controls neuronal activity-induced mitochondrial distribution in dendritic spines. *Proc Natl Acad Sci U S A*, 105: 3112–3116.

Suzuki T, Nagao A, Suzuki T (2011) Human mitochondrial tRNAs: biogenesis, function, structural aspects, and diseases. *Annu Rev Genet*, 45: 299–329.

Svirbely JL, Szent-Györgyi A (1933) The chemical nature of vitamin C. *Biochem J*, 27: 279–285.

Swerdlow RH, Khan SM (2004) A "mitochondrial cascade hypothesis" for sporadic Alzheimer's disease. *Med Hypotheses*, 63: 8–20.

Sykora P, Wilson DM 3rd, Bohr VA (2012) Repair of persistent strand breaks in the mitochondrial genome. *Mech Ageing Dev*, 133: 169–175.

Szczesny B, Tann AW, Longley MJ, Copeland WC, Mitra S (2008) Long patch base excision repair in mammalian mitochondrial genomes. *J Biol Chem*, 283: 26,349–26,356.

Szczesny RJ, Hejnowicz MS, Steczkiewicz K, Muszewska A, Borowski LS, Ginalski K, Dziembowski A (2013) Identification of a novel human mitochondrial endo-/exonuclease Ddk1/c20orf72 necessary for maintenance of proper 7S DNA levels. *Nucleic Acids Res*, 41: 3144–3161.

Taanman JW (1999) The mitochondrial genome: structure, transcription, translation and replication. *Biochim Biophys Acta*, 1410: 103–123.

Takamatsu C, Umeda S, Ohsato T, Ohno T, Abe Y, Fukuoh A, Shinagawa H, Hamasaki N, Kang D (2002) Regulation of mitochondrial D-loops by transcription factor A and single-stranded DNA-binding protein. *EMBO Rep*, 3: 451–456.

Tanaka Y, Kanai Y, Okada Y, Nonaka S, Takeda S, Harada A, Hirokawa N (1998) Targeted disruption of mouse conventional kinesin heavy chain, kif5B, results in abnormal perinuclear clustering of mitochondria. *Cell*, 93: 1147–1158.

Tang Y, Zucker RS (1997) Mitochondrial involvement in post-tetanic potentiation of synaptic transmission. *Neuron*, 18: 483–491.

Tann AW, Boldogh I, Meiss G, Qian W, Van Houten B, Mitra S, Szczesny B (2011) Apoptosis induced by persistent single-strand breaks in mitochondrial genome: critical role of EXOG (5'-EXO/endonuclease) in their repair. *J Biol Chem*, 286: 31,975–31,983.

Tapper DP, Clayton DA (1981) Mechanism of replication of human mitochondrial DNA. Localization of the 5’ ends of nascent daughter strands. *J Biol Chem*, 256: 5109–5115.

Tauber J, Dlasková A, Šantorová J, Smolková K, Alán L, Špaček T, Plecitá-Hlavatá L, Jabůrek M, Ježek P (2013) Distribution of mitochondrial nucleoids upon mitochondrial network fragmentation and network reintegration in HEPG2 cells. *Int J Biochem Cell Biol*, 45: 593–603.

Taylor RW, Turnbull DM (2005) Mitochondrial DNA mutations in human disease. *Nat Rev Genet*, 6: 389–402.

Terzioglu M, Ruzzenente B, Harmel J, Mourier A, Jemt E, López MD, Kukat C, Stewart JB, Wibom R, Meharg C, Habermann B, Falkenberg M, Gustafsson CM, Park CB, Larsson NG (2013) MTERF1 binds mtDNA to prevent transcriptional interference at the light-strand promoter but is dispensable for rRNA gene transcription regulation. *Cell Metab*, 17: 618–626.

Thorsness PE, Weber ER (1996) Escape and migration of nucleic acids between chloroplasts, mitochondria, and the nucleus. *Int Rev Cytol*, 165: 207–234.

Tiranti V, Rocchi M, DiDonato S, Zeviani M (1993) Cloning of human and rat cDNAs encoding the mitochondrial single-stranded DNA-binding protein (SSB). *Gene*, 126: 219–225.

Tiranti V, Savoia A, Forti F, D'Apolito MF, Centra M, Rocchi M, Zeviani M (1997) Identification of the gene encoding the human mitochondrial RNA polymerase (h-mtRPOL) by cyberscreening of the Expressed Sequence Tags database. *Hum Mol Genet*, 6: 615–625.

Tovar J, Fischer A, Clark CG (1999) The mitosome, a novel organelle related to mitochondria in the amitochondrial parasite Entamoeba histolytica. *Mol Microbiol*, 32: 1013–1021.

Vafai SB, Mootha VK (2012) Mitochondrial disorders as windows into an ancient organelle. *Nature*, 491: 374–383.

Van Goethem G, Dermaut B, Löfgren A, Martin JJ, Van Broeckhoven C (2001) Mutation of POLG is associated with progressive external ophthalmoplegia characterized by mtDNA deletions. *Nat Genet*, 28: 211–212.

Vermulst M, Wanagat J, Kujoth GC, Bielas JH, Rabinovitch PS, Prolla TA, Loeb LA (2008) DNA deletions and clonal mutations drive premature aging in mitochondrial mutator mice. *Nat Genet*, 40: 392–394.

Verstreken P, Ly CV, Venken KJ, Koh TW, Zhou Y, Bellen HJ (2005) Synaptic mitochondria are critical for mobilization of reserve pool vesicles at Drosophila neuromuscular junctions. *Neuron*, 47: 365–378.

Vielhaber S, Debska-Vielhaber G, Peeva V, Schoeler S, Kudin AP, Minin I, Schreiber S, Dengler R, Kollewe K, Zuschratter W, Kornblum C, Zsurka G, Kunz WS (2013) Mitofusin 2 mutations affect mitochondrial function by mitochondrial DNA depletion. *Acta Neuropathol*, 125: 245–256.

Wallace DC (1992a) Diseases of the mitochondrial DNA. *Annu Rev Biochem*, 61: 1175–212.

Wallace DC (1992b) Mitochondrial genetics: a paradigm for aging and degenerative diseases? *Science*, 256: 628–632.

Wallace DC, Singh G, Lott MT, Hodge JA, Schurr TG, Lezza AM, Elsas LJ, Nikoskelainen EK (1988) Mitochondrial DNA mutation associated with Leber's hereditary optic neuropathy. *Science*, 242: 1427–1430.

Walter MC, Czermin B, Muller-Ziermann S, Bulst S, Stewart JD, Hudson G, Schneiderat P, Abicht A, Holinski-Feder E, Lochmüller H, Chinnery PF, Klopstock T, Horvath R (2010) Late-onset ptosis and myopathy in a patient with a heterozygous insertion in POLG2. *J Neurol*, 257: 1517–1523.

Wang D, Kreutzer DA, Essigmann JM (1998) Mutagenicity and repair of oxidative DNA damage: Insights from studies using defined lesions. *Mutat Res*, 400: 99–115.

Wang X, Su B, Zheng L, Perry G, Smith MA, Zhu X (2009) The role of abnormal mitochondrial dynamics in the pathogenesis of Alzheimer's disease. *J Neurochem*, 1: 153–159.

Wanrooij PH, Uhler JP, Simonsson T, Falkenberg M, Gustafsson CM (2010) G-quadruplex structures in RNA stimulate mitochondrial transcription termination and primer formation. *Proc Natl Acad Sci U S A*, 107: 16,072–16,077.

Wanrooij S, Falkenberg M (2010) The human mitochondrial replication fork in health and disease. *Biochim Biophys Acta*, 1797: 1378–1388.

Wanrooij S, Fusté JM, Farge G, Shi Y, Gustafsson CM, Falkenberg M (2008) Human mitochondrial RNA polymerase primes lagging-strand DNA synthesis in vitro. *Proc Natl Acad Sci U S A*, 105: 11,122–11,127.

Wanrooij S, Goffart S, Pohjoismäki JL, Yasukawa T, Spelbrink JN (2007) Expression of catalytic mutants of the mtDNA helicase Twinkle and polymerase POLG causes distinct replication stalling phenotypes. *Nucleic Acids Res*, 35: 3238–3251.

Wanrooij S, Luoma P, van Goethem G, van Broeckhoven C, Suomalainen A, Spelbrink JN (2004) Twinkle and POLG defects enhance age-dependent accumulation of mutations in the control region of mtDNA. *Nucleic Acids Res*, 32: 3053–3064.

Wanrooij S, Miralles Fusté J, Stewart JB, Wanrooij PH, Samuelsson T, Larsson NG, Gustafsson CM, Falkenberg M (2012) In vivo mutagenesis reveals that OriL is essential for mitochondrial DNA replication. *EMBO Rep*, 13: 1130–1137.

Waqar MA, Evans MJ, Manly KF, Hughes RG, Huberman JA (1984) Effects of 2',3'-dideoxynucleosides on mammalian cells and viruses. *J Cell Physiol*, 121: 402–408.

Wei YH, Pang CY, You BJ, Lee HC (1996) Tandem duplications and large-scale deletions of mitochondrial DNA are early molecular events of human aging process. *Ann N Y Acad Sci*, 786: 82–101.

Werth JL, Thayer SA (1994) Mitochondria buffer physiological calcium loads in cultured rat dorsal root ganglion neurons. *J Neurosci*, 14: 348–356.

Wiesner RJ, Zsurka G, Kunz WS (2006) Mitochondrial DNA damage and the aging process: facts and imaginations. *Free Radic Res*, 40: 1284–1294.

Williams AJ, Kaguni LS (1995) Stimulation of Drosophila mitochondrial DNA polymerase by single-stranded DNA-binding protein. *J Biol Chem*, 270: 860–865.

Williams BA, Hirt RP, Lucocq JM, Embley TM (2002) A mitochondrial remnant in the microsporidian Trachipleistophora hominis. *Nature*, 418: 865–869.

Williams SL, Huang J, Edwards YJ, Ulloa RH, Dillon LM, Prolla TA, Vance JM, Moraes CT, Züchner S (2010) The mtDNA mutation spectrum of the progeroid Polg mutator mouse includes abundant control region multimers. *Cell Metab*, 12: 675–682.

Williams TB, Daniels M, Puthenveetil G, Chang R, Wang RY, Abdenur JE (2012) Pearson syndrome: unique endocrine manifestations including neonatal diabetes and adrenal insufficiency. *Mol Genet Metab*, 106: 104–107.

Wong TW, Clayton DA (1985) In vitro replication of human mitochondrial DNA: accurate initiation at the origin of light-strand synthesis. *Cell*, 42: 951–958.

Yakubovskaya E, Chen Z, Carrodeguas JA, Kisker C, Bogenhagen DF (2006) Functional human mitochondrial DNA polymerase gamma forms a heterotrimer. *J Biol Chem*, 281: 374–382.

Yamamoto H, Tanaka M, Katayama M, Obayashi T, Nimura Y, Ozawa T (1992) Significant existence of deleted mitochondrial DNA in cirrhotic liver surrounding hepatic tumor. *Biochem Biophys Res Commun*, 182: 913–920.

Yang C, Curth U, Urbanke C, Kang C (1997) Crystal structure of human mitochondrial single-stranded DNA binding protein at 2.4 A resolution. *Nat Struct Biol*, 4: 153–157.

Yang MY, Bowmaker M, Reyes A, Vergani L, Angeli P, Gringeri E, Jacobs HT, Holt IJ (2002) Biased incorporation of ribonucleotides on the mitochondrial L-strand accounts for apparent strand-asymmetric DNA replication. *Cell*, 111: 495–505.

Yasukawa T, Reyes A, Cluett TJ, Yang MY, Bowmaker M, Jacobs HT, Holt IJ (2006) Replication of vertebrate mitochondrial DNA entails transient ribonucleotide incorporation throughout the lagging strand. *EMBO J*, 25: 5358–5371.

Yasukawa T, Yang MY, Jacobs HT, Holt IJ (2005) A bidirectional origin of replication maps to the major noncoding region of human mitochondrial DNA. *Mol Cell*, 18: 651–662.

Youle RJ, Karbowski M (2005) Mitochondrial fission in apoptosis. *Nat Rev Mol Cell Biol*, 6: 657–663.

Young MJ, Longley MJ, Li FY, Kasiviswanathan R, Wong LJ, Copeland WC (2011) Biochemical analysis of human POLG2 variants associated with mitochondrial disease. *Hum Mol Genet*, 20: 3052–3066.

Zeviani M, Servidei S, Gellera C, Bertini E, DiMauro S, DiDonato S (1989) An autosomal dominant disorder with multiple deletions of mitochondrial DNA starting at the D-loop region. *Nature*, 339: 309–311.

Zhang H, Pommier Y (2008) Mitochondrial topoisomerase I sites in the regulatory D-loop region of mitochondrial DNA. *Biochemistry*, 47: 11,196–11,203.

Zhao S, Fernald RD (2005) Comprehensive algorithm for quantitative real-time polymerase chain reaction*. J Comput Biol*, 12: 1047–1064.

Zheng L, Shen B (2011) Okazaki fragment maturation: nucleases take centre stage. *J Mol Cell Biol*, 3: 23–30.

Zheng L, Zhou M, Guo Z, Lu H, Qian L, Dai H, Qiu J, Yakubovskaya E, Bogenhagen DF, Demple B, Shen B (2008) Human DNA2 is a mitochondrial nuclease/helicase for efficient processing of DNA replication and repair intermediates. *Mol Cell*, 32: 325–36.

Zsurka G, Baron M, Stewart JD, Kornblum C, Bös M, Sassen R, Taylor RW, Elger CE, Chinnery PF, Kunz WS (2008) Clonally expanded mitochondrial DNA mutations in epileptic individuals with mutated DNA polymerase gamma. *J Neuropathol Exp Neurol*, 67: 857–866.

Zsurka G, Kunz WS (2013) Mitochondrial involvement in neurodegenerative diseases. *IUBMB Life*, 65: 263–272.

Zubáčová Z, Novák L, Bublíková J, Vacek V, Fousek J, Rídl J, Tachezy J, Doležal P, Vlček C, Hampl V (2013) The Mitochondrion-Like Organelle of Trimastix pyriformis Contains the Complete Glycine Cleavage System. *PLoS One*, 8: e55417.

Züchner S, Mersiyanova IV, Muglia M, Bissar-Tadmouri N, Rochelle J, Dadali EL, Zappia M, Nelis E, Patitucci A, Senderek J, Parman Y, Evgrafov O, Jonghe PD, Takahashi Y, Tsuji S, Pericak-Vance MA, Quattrone A, Battaloglu E, Polyakov AV, Timmerman V, Schröder JM, Vance JM (2004) Mutations in the mitochondrial GTPase mitofusin 2 cause Charcot–Marie–Tooth neuropathy type 2A, *Nat Genet*, 36: 449–451.

Zucker RS (1999) Calcium- and activity-dependent synaptic plasticity. *Curr Opin Neurobiol*, 9: 305–313.

Bibliography:

Fenchel T, Finlay BJ. Ecology and Evolution in Anoxic Worlds, Oxford University Press, Oxford, UK, 1995.

Clayton DA. 'Mitochondrial DNA replication'. DNA *Replication* in Eukaryotic Cells, Cold Spring Harbor Laboratory Press, 31: 1015–1027, 1996.

Lane RJM, Johnson MA, Barron MJ. 'Muscle biopsy analysis'. Handbook of muscle disease, editor Lane RJM, Marcel Dekker, New York: Marcel Dekker Inc., 1996.

Lodish H, Berk A, Kaiser CA, Krieger M, Bretscher A, Ploegh H, Amon A, Scott MP. Textbook of Molecular Cell Biology, 7th Edition, WH Freeman and Co, NY, USA, 2012.

Morfini GA, Burns MR, Stenoien DL, Brady ST. 'Chapter 8, Axonal transport'. Basic Neurochemistry, 8th edition, American society for Neurochemistry, Elsevier Inc, 2012.

Nelson DL, Cox MM. Textbook of Lehninger Principles of Biochemistry, 3rd edition, Worth Publishers: New York, 2000.

Peters A, Palay SL, Webster H. The Fine Structure of the Nervous System: Neurons and Their Supporting Cells, New York: Oxford University Press, 1991.

Sachs J. Vorlesungen über Pflanzen-Physiologie, Verlag W. Engelmann, Leipzig, 1882.

Scheffler IE. MITOCHONDRIA, 2nd edition, J Wiley and Sons, Inc., Hoboken, New Jersey, 2008.

Sloviter RS, Bumanglag AV, Schwarcz R, Frotscher M. 'Abnormal dentate gyrus network circuitry in temporal lobe epilepsy'. Jasper's Basic Mechanisms of the Epilepsies. 4th edition., editors: Noebels JL, Avoli M, Rogawski MA, Olsen RW, Delgado-Escueta AV, Bethesda National Center for Biotechnology Information (US), 2012.

Wallin IE. Symbionticism and the Origin of Species, Bailliere, Tindall & Cox, London, 1927.

Watson JD, Baker TA, Bell SP, Gann A, Levine M, Losick R. Molecular Biology of the Gene, 5th edition, Peason Benjamin Cummings, CSHL Press, 2004.

Declaration

I, hereby confirm that this work is my own. This thesis has been written independently and with no other sources and aids than stated. The presented thesis has not been submitted to another university and I have not applied for a doctorate procedure so far.

Hiermit versichere ich, dass die vorgelegte Arbeit – abgesehen von den ausdrücklich bezeichneten Hilfsmitteln – persönlich, selbständig und ohne Benutzung anderer als der angegebenen Hilfsmittel angefertigt wurde. Aus anderen Quellen direkt oder indirekt übernommenen Daten und Konzepte sind unter Angabe der Quelle kenntlich gemacht worden.
Die vorliegende Arbeit wurde an keiner anderen Hochschule als Dissertation eingereicht. Ich habe früher noch keinen Promotionsversuch unternommen.

_____ _____

Ort, Datum Unterschrift

List of Publications:

Nicholls TJ*, Zsurka G*, **Peeva V**, Schöler S, Szczesny RJ, Cysewski D, Reyes A, Kornblum C, Sciacco M, Moggio M, Dziembowski A, Kunz WS, Minczuk M (2014) Altered 5'-end DNA processing causes accumulation of linear mitochondrial DNA fragments in MGME1 exonuclease deficient human mitochondria. *In preparation*

Baris OR, Ederer S, Neuhaus JFG, von Kleist-Retzow JC, Wunderlich CM, Martin Pal M, Wunderlich TF, **Peeva V**, Zsurka G, Kunz WS, Stöckigt F, Schrickel JW, Wiesner RJ (2014) Mosaic respiratory chain deficiency in the aged heart - few cardiomyocytes with mitochondrial dysfunction are sufficient to cause ventricular arrhythmias. *In preparation*

Kornblum C, Nicholls TJ, Haack TB, Schöler S, **Peeva V**, Danhauser K, Hallmann K, Zsurka G, Rorbach J, Iuso A, Wieland T, Sciacco M, Ronchi D, Comi GP, Moggio M, Quinzii CM, DiMauro S, Calvo SE, Mootha VK, Klopstock T, Strom TM, Meitinger T, Minczuk M, Kunz WS, Prokisch H (2013) Loss-of-function mutations in MGME1 impair mtDNA replication and cause multisystemic mitochondrial disease. *Nat Genet*, 45: 214–219.

Vielhaber S*, Debska-Vielhaber G*, **Peeva V***, Schoeler S, Kudin AP, Minin I, Schreiber S, Dengler R, Kollewe K, Zuschratter W, Kornblum C, Zsurka G, Kunz WS (2013) Mitofusin 2 mutations affect mitochondrial function by mitochondrial DNA depletion. *Acta Neuropathol*, 125: 245–256.

Zsurka G, Kudina T, **Peeva V**, Hallmann K, Elger CE, Khrapko K, Kunz WS (2010) Distinct patterns of mitochondrial genome diversity in bonobos (Pan paniscus) and humans. *BMC Evol Biol*, 10: 270.

** equal author contribution*

Abstracts:

C Kornblum, T Nicholls, TB Haack, S Schoeler, **V Peeva**, K Danhauser, K Hallmann, G Zsurka, J Rorbach, A Iuso, T Wieland, M Sciacco, D Ronchi, GP Comi, M Moggio, CM Quinzii, S DiMauro, SE Calvo, VK Mootha, T Klopstock, TM Strom, T Meitinger, M Minczuk, WS Kunz, H Prokisch (2013) O.24 Loss of function of MGME1, a novel player in mitochondrial DNA replication, causes a distinct autosomal recessive mitochondrial disorder. *Neuromuscular Disorders*, 23: 852.

WS Kunz, G Zsurka, **V Peeva** (2012) Characterization of multiple mitochondrial DNA deletions in sclerotic hippocampus of patients with temporal lobe epilepsy. *EPILEPSIA*, 53: 23.

V Peeva, G Zsurka, S Schöler, AP Kudin, S Vielhaber, G Debska-Vielhaber, WS Kunz (2012) Disrupted mitochondrial fusion affects oxidative phosphorylation by mtDNA depletion. *Biochimica et Biophysica Acta (BBA)-Bioenergetics*, 1817: 73–74.

VM Peeva, G Zsurka, WS Kunz (2010) Analysis of mitochondrial DNA deletions in epileptic hippocampus. *Biochimica et Biophysica Acta (BBA)-Bioenergetics*, 1797: 76.